CHAOTIC DYNAMICS IN MODEL HAMILTONIAN AND DISSIPATIVE SYSTEMS

A thesis submitted to the University of Calicut
for the partial fulfilment of the degree of
Doctor of Philosophy
in Physics

RAJAN NAMBIAR A.

DEPARTMENT OF PHYSICS
UNIVERSITY OF CALICUT

2003

Dedicated to
My parents
Late Sri.T. Padmanabhan Nair
And
Smt. A. Saraswathi Amma.

DECLARATION.

Certified that this thesis **Chaotic Dynamics in Model Hamiltonian and Dissipative Systems** is a bonafiede record of the research work carried out by me during the period 1996-2003 in the Department of Physics, University of Calicut, under the supervision of Prof. P. Rameshan, and that no part of this thesis has been presented earlier for the award of any degree, diploma, title or recognition.

Calicut University.
05-05-2003.

Rajan Nambiar A.

UNIVERSITY OF CALICUT
COMPUTER CENTRE

Dr. P. RAMESHAN
Professor of Physics

Calicut University P.O.
Kerala – India – 673635
Phone off: 0494-401144 - 417
Res: 0494-401347
E-mail: ramrah@sify.com

CERTIFICATE.

I hereby certify that this thesis submitted by Sri. Rajan Nambiar A. is a bonafiede record of the research work carried out by him in the Department of Physics, University of Calicut, during the period 1996-2003, under the guidance and supervision of me.

Calicut University
05-05-2003

Dr. P.Rameshan

ACKNOWLEDGEMENTS.

I express my most sincere thanks to Prof. P. Rameshan for his inspiring guidance and constant help during my research. I am also thankful to him for his support in using the infrastructures of the Computer Centre, University of Calicut.

I am out of words when recollecting the help rendered to me by Shri. M.C.Valsakumar, IGCAR, Kalpakkam. He made me to understand the basics of theoretical Physics and essence of Non-linear dynamics. Without his constant help and support this work would not have been possible.

I express my gratitude to Prof. K. Neelakandan, Head, Dept. of Physics, University of Calicut for his support during my research work.

I am grateful to Dr. K.P.N. Murthy, IGCAR, Kalpakkam, for the fruitful discussions and critical reading of the thesis and valuable suggestions. Dr. S.V.M. Sathyanarayana, IGCAR, Kalpakkam also need special acknowledgement for the discussions in the early phase of my work. Prof. F.Haake, University of Essen, Germany, Prof. G.Casati, University degli studi dell' Insurbria, Italy, also are acknowledged for their comments.

I am also grateful to Dr. K.M. Varier, Dr. Antony Joseph, Dr. Vishnu Mayya Bannur, Smt. Mini P. Balakrishnan, Sri, Viswanatha Pillai, Sri. Ramakrishnan, Smt. Geetha, Sri, V.T. Madhu, Sri. T.P. Ajithkumar, and all other staff members and friends of Dept. of Physics for their encouragements during my work.

I am grateful to my wife Mrs. Geeta Rajan and sons Adith and Udith for their patience in bearing me during my research.

I acknowledge University Grants Commission for granting me the fellowship under Faculty Improvemt Programme and Govt. Of Kerala for granting me leave for my F.I.P. period.

Calicut University.
05-05-2003.

Rajan Nambiar. A.

CONTENTS

-1

CHAPTER 1

Part I

INTRODUCTION

The discovery that determinism need not necessarily imply predictability has had a major impact on many fields of science, engineering and mathematics. Several nonlinear systems have been found to exhibit regular and unpredictable dynamical behaviour. They are called chaotic systems. The central character of a chaotic system is that it does not repeat its past behaviour even approximately. The unpredictability has its origin in its sensitive dependence on the initial conditions. The system started with arbitrarily close initial conditions evolve entirely differently. In particular, the trajectories diverge exponentially and hence predictability is lost. This is in contrast to a regular system for which predictability is possible. The divergence of the trajectories is characterized by the Lyapunov exponent. If this exponent is negative or zero the system behaves regularly and if positive, the system evolves chaotically. For a regular system, during the evolution, the phase space points are attracted to a fixed point (as in damped oscillations) or to a limit cycle (as in the van der Pol oscillator) or settles on a torus (as in higher dimensional Hamiltonian systems). The Lyapunov exponent gives a measure of the predictability. More precisely the inverse of the Lyapunov exponent gives a time scale beyond which the dynamics becomes unpredictable.

It was Henri Poincare who, towards the end of nineteenth century, was the first to recognize this phenomenon of chaos, while studying the orbits of the outer planets of our solar system. But we had to wait for several decades, for the subject of chaos to be rediscovered in the pioneering work of Lorenz; the advent of computers made possible the rebirth and the subsequent phenomenal growth of the subject.

When predictions become impossible, a chaotic system resembles a stochastic system - a system subject to random external forces. However, there are differences. The

irregularity in a deterministic chaotic system is part of its intrinsic dynamics, while in stochastic system it is due to noise, external or internal. In stochastic processes no predictions, short term or long term are possible. But in chaotic processes short time predictions are possible, but long term forecasting is impossible.

Ever since chaos was found in a model for weather forecasting, proposed and studied by Lorenz in the sixties, several real and model systems have been found that exhibit a rich variety of chaotic dynamics. These come under two broad classes- dissipative systems and Hamiltonian. These include the forced pendulum, iteration over non-linear maps like the Henon map, the kicked rotator, kicked oscillator, the Henon-Heiles system, etc. These are briefly introduced and discussed in the next few sections.

In this thesis we propose a new model that exhibit regular as well as a rich variety of chaotic dynamical behaviour. These are discussed in chapter 2. A quantum mechanical treatment is discussed in chapter 3.

Besides, we investigate the intriguing connections between non linear maps and the ordinary differential equations derived through Taylor expansions. This work discussed in chapter 4 provides new and useful insights on maps and dynamical equations.

The model proposed in chapter 2, is a Hamiltonian system describing the dynamics of a charged particle in a medium having a dielectric discontinuity. This problem shares several of its features with the anisotropic Kepler problem described in Gutzwiller [28]. In the model of Gutzwiller, chaos arises from the anisotropy of the mass which can be transformed to anisotropy of the potential through an appropriate canonical transformation. In our problem, the chaos has its origin in the force due to image charge, which renders the potential anisotropic. This is briefly discussed below.

We derive the Hamiltonian of our model system by considering all the forces acting on the moving charge, including those due to image charges. Then solving

Hamilton's equations of motion, the dynamical trajectory of the system is calculated for different initial conditions and for different relative values of the dielectric constants. Let δ denote the ratio of the dielectric constants. We find that for certain specific values of the control parameter δ and initial conditions, the system exhibits chaotic behaviour. We also find that for the same value of δ, we have regular dynamics for some initial conditions and chaotic behaviour for some others. This type of behaviour - different initial conditions in phase space leading to invariant tori (representing regular regions) and submerged tori (representing chaotic motion) - is expected of an Hamiltonian system. A typical example is the Henon-Heiles system, which becomes chaotic for certain energies.

We have investigated the system described above employing standard techniques like stability analysis, time series analysis, Lyapunov spectrum, power spectrum, Poincare sections etc. The time series analysis clearly shows the sensitive dependence on initial conditions. The trajectories from two nearby initial conditions exhibit exponential divergence. We have also calculated the Lyapunov spectrum which confirms emergence of chaos. For calculating Lyapunov exponents we have employed the recently proposed QR algorithm [34], which is superior to the Wolf's algorithm [33]. The QR algorithm is described briefly in the appendix.

Further, we have investigated the dynamical evolution of the system using Poincare sections for different initial conditions with same energy. We get a number of invariant tori corresponding to regular motion and a patch corresponding to chaos. In fact, from this plot, we could identify the initial conditions that lead to regular dynamics and those that result in chaos. The distribution of Poincare return times for regular and chaotic dynamics are plotted. We find the distribution of return times for regular motion to be noticeably different from that for chaotic motion. To the best of our knowledge such a study has not been reported in the context of Hamiltonian chaos.

The power spectrum for chaotic and regular trajectories also give distinctly differing characteristic features for Hamiltonian systems, even though these differences are not as dramatic as one finds for the dissipative systems.

We study the quantum mechanical formulation of this system in chapter 3. In literature we see two different approaches in the quantum mechanical treatment of classically chaotic systems. One is the study of the statistics of the energy level spacings. The level spacing obeys Poissonian statistics for classically regular systems and Wigner distribution for classically chaotic systems. This change in distributions is attributed to the level repulsions which is a characteristic feature of quantum chaos. Simple systems like Sinai billiards were studied and their eigenvalue spectrum were investigated for signature of quantum chaos. However calculation of sufficiently large number of eigenvalues is rather difficult for our model system. Hence we have opted for the second method based on the Bohmian mechanics. In chapter 3 we have employed this method for our quantum calculations, which gives a correspondence between a classical trajectory and a Bohmian trajectory. The wave functions also play an important role in these calculation. Within the Bohmian frame work, we construct an effective potential as the sum of the classical potential and a state dependent quantum potential. The particle moves in this effective potential, guided by the quantum wave. In this method, we can define a trajectory (for the particle) which is not possible in the conventional quantum frame work. This means that a comparison of trajectories from two nearby initial conditions is possible, as in classical case, and chaotic behaviour, if present, can be characterized.

The trajectories calculated using this method show a clear difference between chaotic and regular motion. The distance of separation between two trajectories started from nearby initial conditions diverges exponentially in chaotic case; in contrast, there is no such divergence in regular motion. We have tested this method and the algorithm

developed by us for the known case of the Henon-Heiles system. Our results exactly match with those reported by Senguptha and Chattaraj [52]. Besides, our algorithm is found to be more accurate than that of Senguptha and Chattaraj [52].

In chapter 4 we begin with a discussion on the Taylor expansion $x(t+1) = \sum_{j=0}^{\infty} \frac{1}{j!} \frac{d^j x(t)}{dt^j}$ in the discrete map x (t+1) = f (x (t)). Such an expansion should represent the original dynamical system. We consider truncating this series at finite order N to get a new dynamical system $\sum_{j=0}^{N} \frac{1}{j!} \frac{d^j x(t)}{dt^j} = f(x(t))$. The behaviour of this dynamical system is entirely different from that of the map for all finite N. As is evident from the stability analysis, truncation up to second order does not give any chaotic behaviour, irrespective of the nature of the map. Considering the stability of the solution about an arbitrary reference point and using Routh-Hurwitz theorem, we show that for truncation of the order five or greater, the system is unstable. Numerical calculations performed on a few model systems corroborate this finding. For the specific case of the logistic map, third and fourth order truncations show regular, chaotic and unstable behaviour. However, these are remarkably different from the behaviour of the original map. For the case of the logistic map, we have further explored the Taylor series expansion up to third and fourth orders. By a suitable transformation we get two-parameter differential equations with a riddled parameter space- an unmistakable signature of structural instability. We thus demonstrate that even very simple systems behave in a complicated manner.

The new findings reported in the thesis are briefly summarized in the fifth chapter. In the next few sections, we briefly review some important nonlinear systems and maps which exhibit chaotic behaviour.

Part II

SECTION A

DISSIPATIVE SYSTEMS.

Over the last two or three decades a number of dynamical systems have been identified, which exhibit chaos. There are a lot of monographs appeared on the subject[1-6]. During the seventies R.M. May gave a beatuful account of a very simple model (Logistic map) which shows very complicated behaviour [7]. A decade before this, E.N. Lorenz had put forward a model while trying to simulate the atmospheric dynamics, which shows complicated behaviour[8]. This complicated behaviour lead to the introduction of strange attractor[9], which is basin of attraction of a chaotic system. Later Feigenbaum discovered universality in some non-linear systems[10]. The study of chaos also started throwing light on the unsolved problem of turbulence [11]. A large number of experimental work were also started during this period in Physics, Chemistry, Fluid dynamics, Electronics, Biology, Medicine etc.[12-20]

Some models exhibiting chaos are described below.

1.1.Forced pendulum.

A forced pendulum is given by the equation

$$\frac{d^2\theta}{dt^2} + r\frac{d\theta}{dt} + \sin\theta = f\sin(2\pi\nu t) \qquad (1.1.1)$$

where the first term represents inertia, the second, friction at the pivot, the third, gravity and the term on the right hand side represents a sinusoidal torque applied at the pivot.(This equation also describes the behaviour of a simple Josephson junction circuit). Here the equation have three degrees of freedom which is a necessary condition for getting chaos in a system represented by differential equations.The non linearity in equation (1.1.1) is coming from the term Sin θ. If we do a simple transformation as

$$x^{(1)} = \theta \qquad (1.1.2a)$$

$$x^{(2)} = d\theta/dt \qquad (1.1.2b)$$

$$x^{(3)} = 2\pi\nu\, t \qquad (1.1.2c)$$

Equation (1.1.1) can be written as three autonomous first order equations and since the dimensionality of the system is now 3 (N=3), the system exhibits chaos for particular choice of parameters r, F and ν

The phase plot of the above system (with $2\pi\nu = \omega_D$) for $\omega_D = 2/3$, r=0.5 and f=1.2 is given in the fig.1.1.1. It clearly shows the chaotic nature of the trajectories. For a regular oscillatory motion, the phase plot would have been a closed curve, either an ellipse or a circle. Here, instead we are getting a number of curves showing irregular motion of the pendulum.

The time series for the forced pendulum plotted for two nearby initial conditions (for the parameter values $\omega_D = 2/3$, r=0.5 and f=1.2) of the variable $x^{(2)}$ is given in fig.1.1.2. Here the two trajectories initially superimpose, and later they diverge and are widely separated. This sensitive dependence on initial conditions is the characteristic feature of a chaotic system.

The power spectra for two different cases are given in fig.1.1.3. Fig.1.1.3a is for $\omega_D = 2/3$, r=0.5 and f=0.9, which corresponds to regular behaviour. Here we have only one frequency and its higher harmonics. But in fig 1.1.3b, which is for $\omega_D = 2/3$, r=0.5 and f=1.2, we get a broadband spectrum. Here we get all possible frequencies up to a range, which is an indication of chaos. The power spectrum initially falls exponentially and the fall near the tail is much slower.

The bifurcation diagram given in fig.1.1.4 shows period doubling, chaos, periodic windows, intermittency, reverse bifurcation etc. Comparing this with the bifurcation of logistic map, the features like periodic windows etc. are not as clear as that in logistic map.

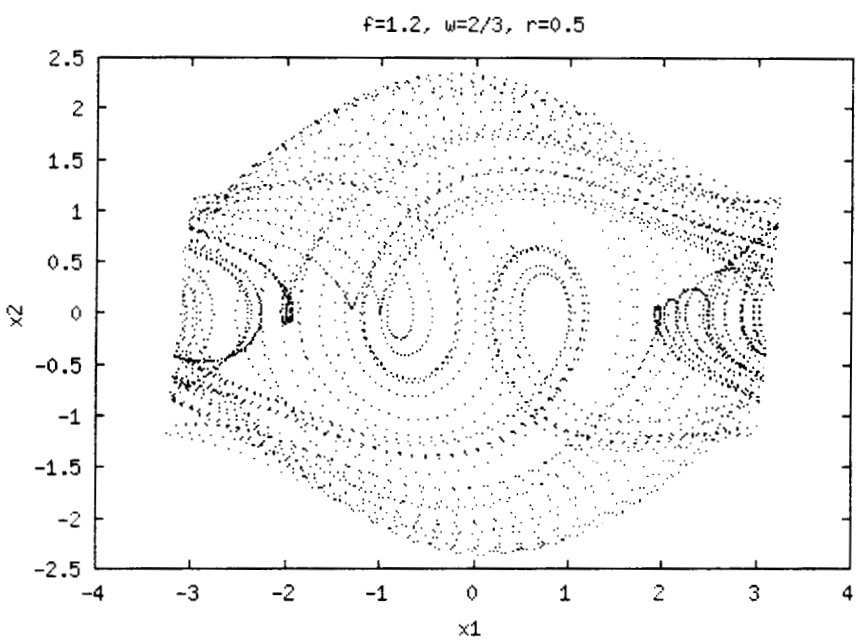

Fig.1.1.1.The Phase plot (θ vs. dθ/dt) for the forced pendulum for ω_D =2/3,r=0.5 and f=1.2

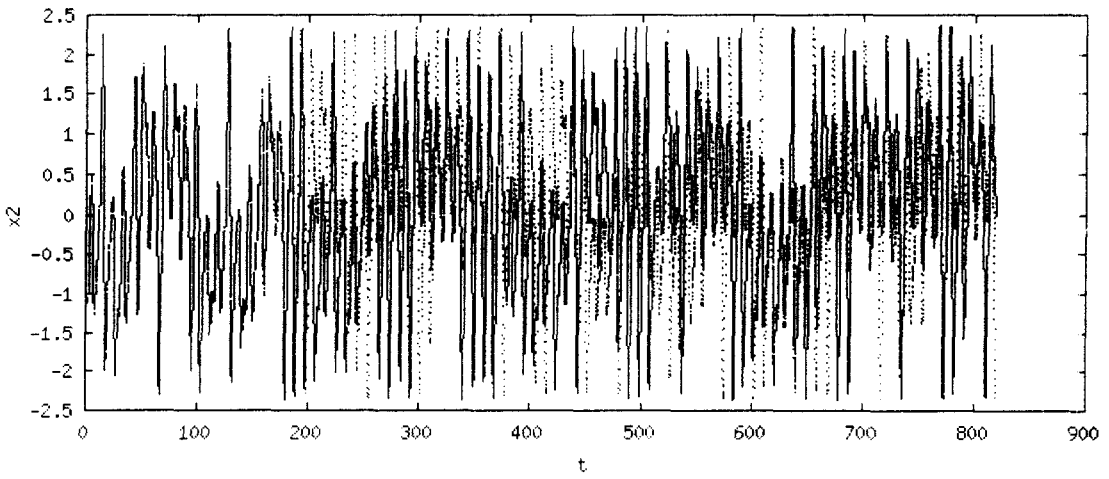

Fig.1.1.2.The time series for the forced pendulum for ω_D =2/3, r=0.5 and f=1.2. Solid line and dotted line are for two initial conditions separated by 10^{-6} units.

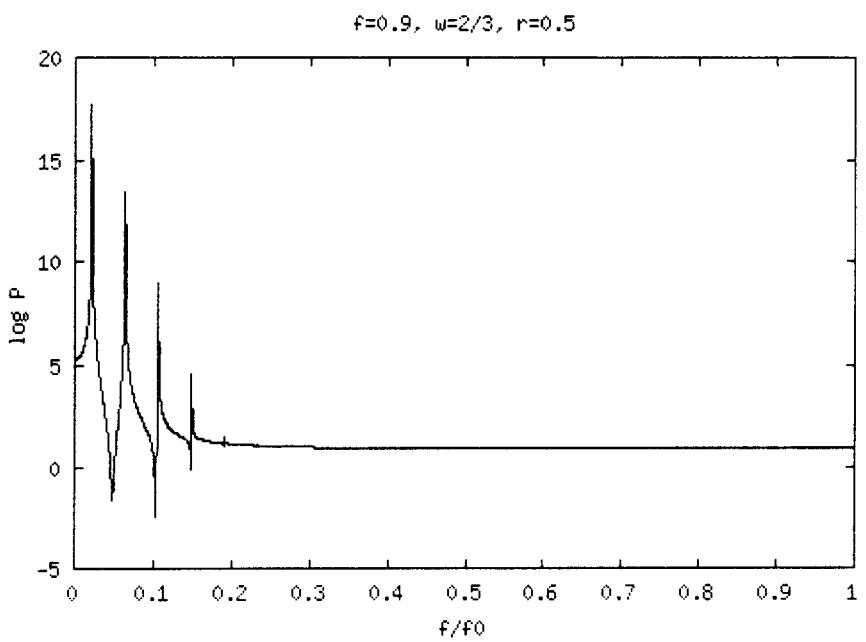

Fig.1.1.3a. The power spectra for the pendulum for ω_D =2/3, r=0.5 and f=0.9(regular)

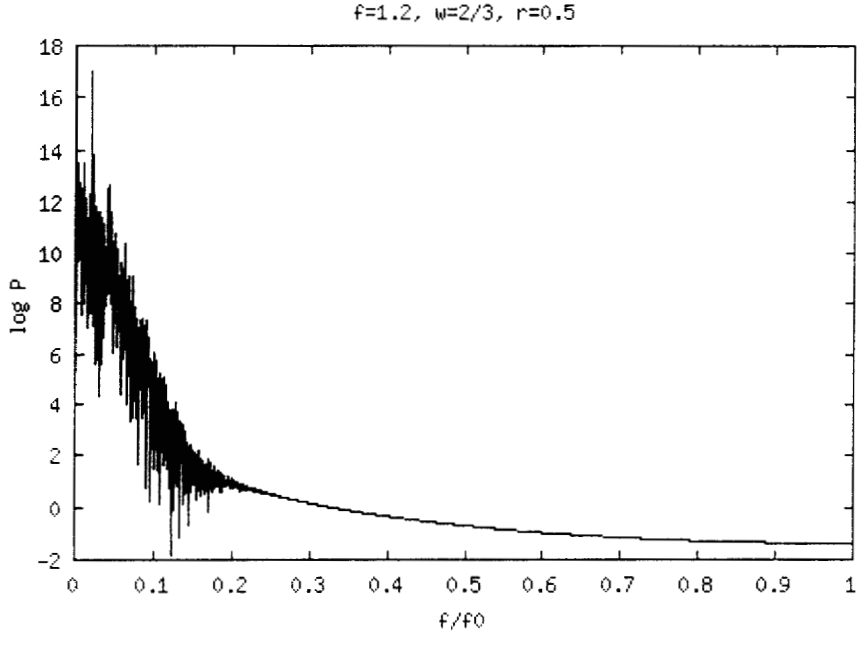

Fig.1.1.3b The power spectra for the pendulum for ω_D =2/3, r=0.5 and f=1.2(chaotic)

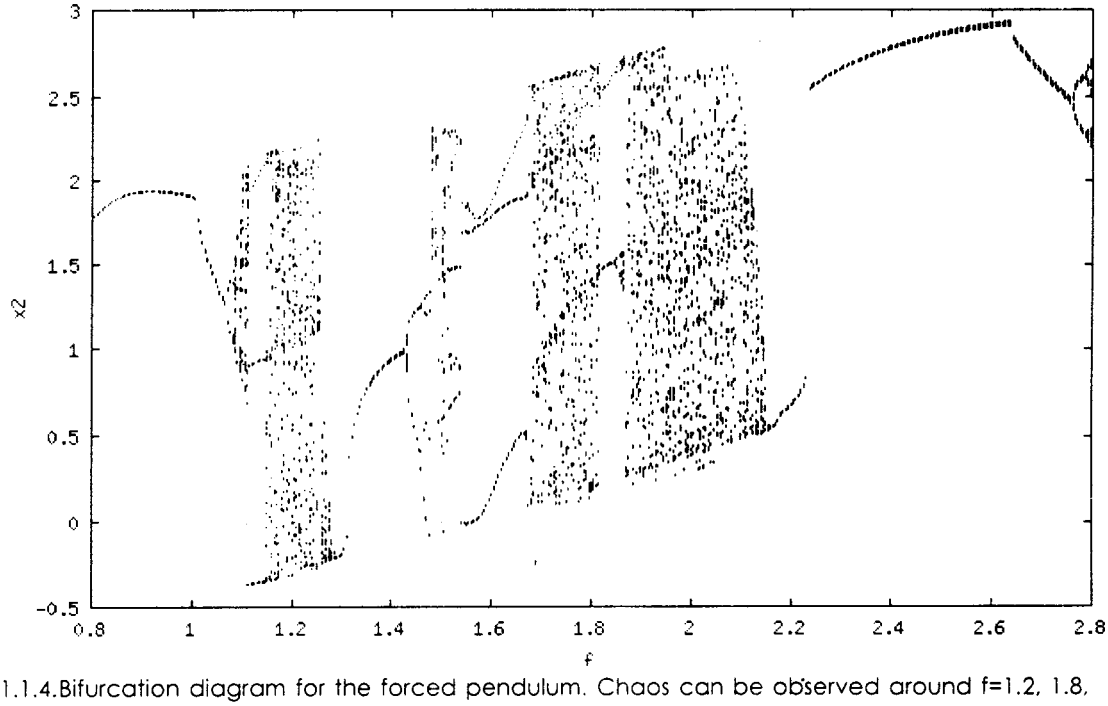

Fig.1.1.4.Bifurcation diagram for the forced pendulum. Chaos can be observed around f=1.2, 1.8, 2.0 etc.

1.2.Lorenz model

In fact chaotic systems of low dimensions were known even before 1970. The present activities in the study of chaos started after the publication of a paper by E.N.Lorenz in 1963. He was trying to model the dynamics of the atmosphere by approximating the equations governing fluid dynamics using three variables[8]. The Lorenz model is given by the equations

$$\left.\begin{aligned} dx/dt &= -\sigma x + \sigma y \\ dy/dt &= -x z + r x - y \\ dz/dt &= x y - b z \end{aligned}\right\} \qquad (1.2.1)$$

where σ, r and b are dimensionless parameters. Here x is proportional to the circulatory fluid flow velocity, y characterizes the temperature difference between rising and falling fluid regions, and z chracterizes the distortion of the vertical temperature profile from its linear-with-height equilibrium variation. For a choice of parameters σ=10, b = 8/3 and r= 28, the system shows chaotic behaviour. The phase plot for the above parameter values gives a strange attractor.(see Fig.1.2.1). The Lorenz attractor in 2-Dimensional space and 3-Dimensional space are given in fig. 1.2.1a. and fig. 1.2.1b.

The time series and power spectrum for the Lorenz model for the parameters given above are plotted in fig .1.2.2. and fig.1.2.3. The sensitive dependence on initial condition, which is a signature of chaos is seen from fig. 1.2.2. The power spectrum (fig.1.2.3) depicts a continuous band at lower frequencies which also is an indication of chaos.

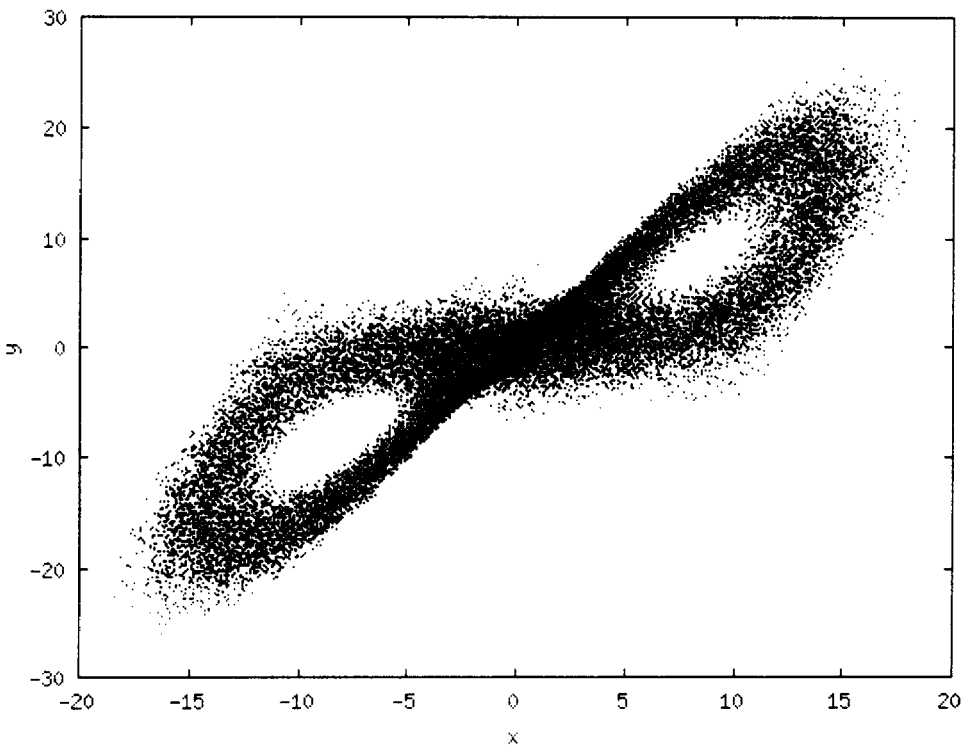

Fig.1.2.1a. Lorenz attractor in 2-D for the parameters σ=10, b = 8/3 and r= 28.

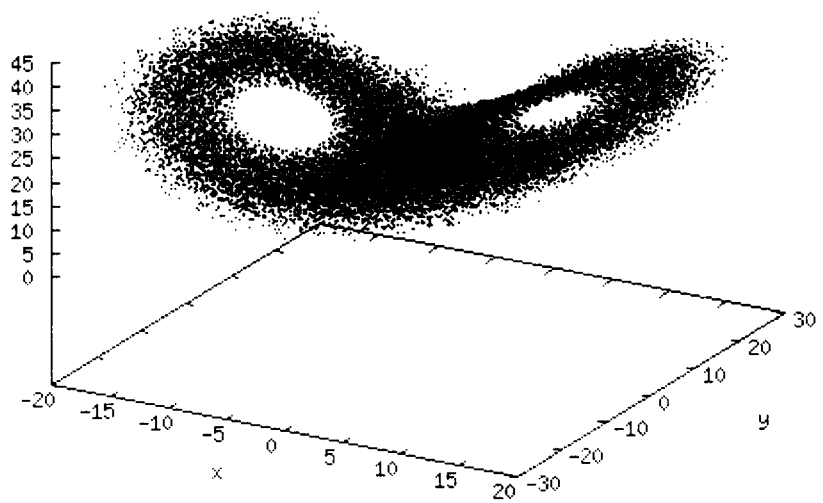

Fig.1.2.1b. Lorenz attractor in 3-D for the parameters σ=10, b = 8/3 and r= 28.

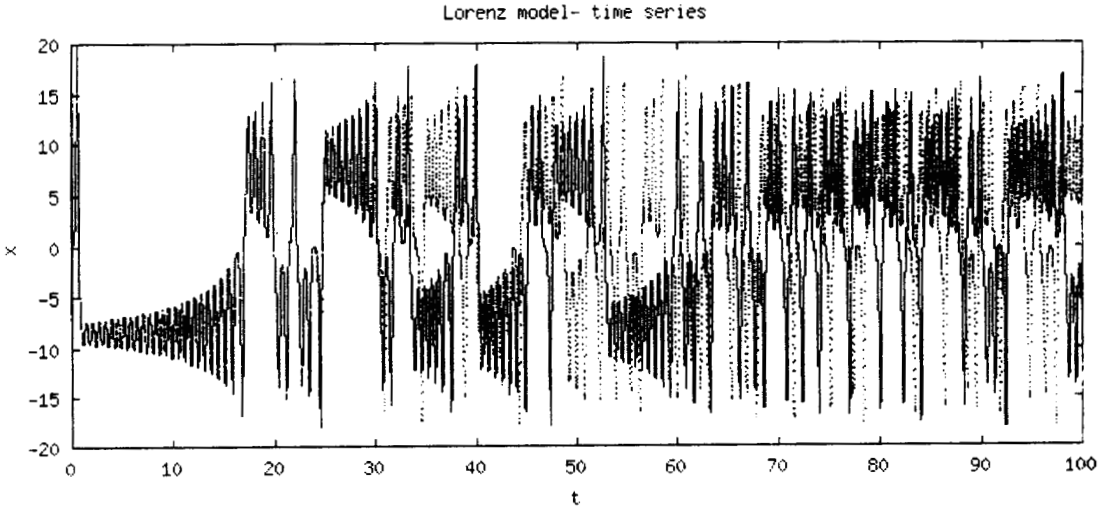

Fig.1.2.2.The time series for Lorenz model for two nearby initial conditions (seperated by 10^{-6}) for the parameters σ=10, b = 8/3 and r= 28.

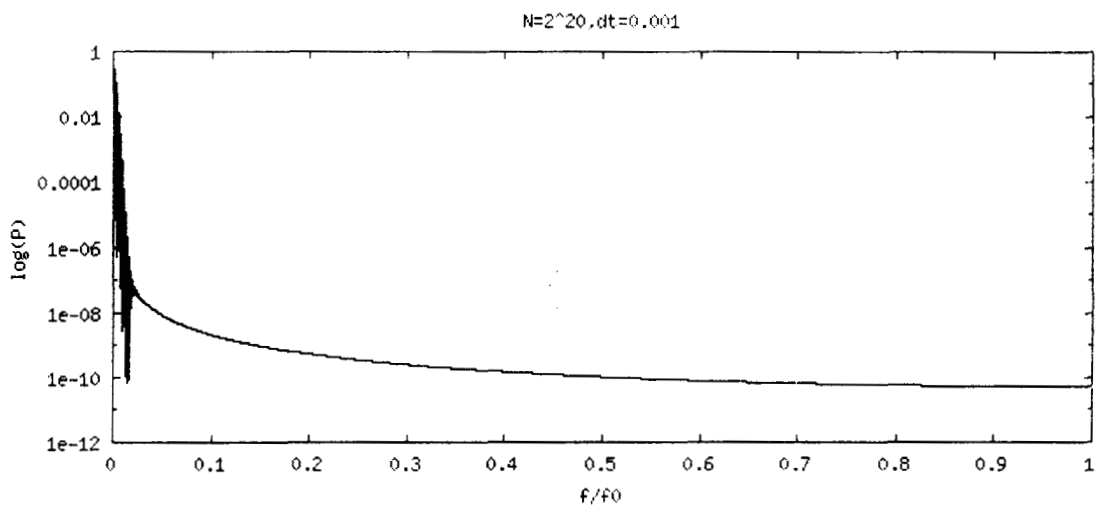

Fig.1.2.3.The power spectrum for Lorenz model for the parametrers given in fig.1.2.2.

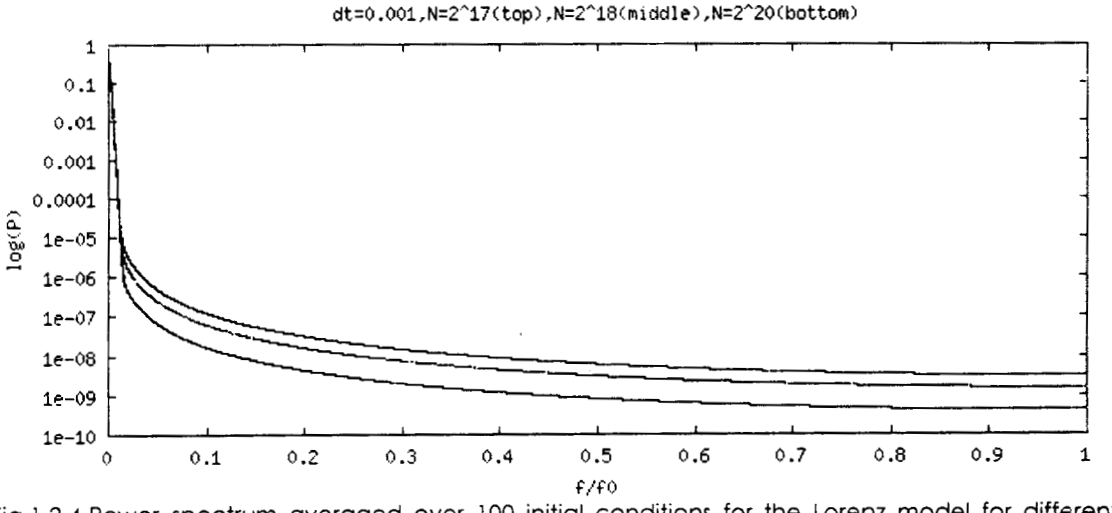

Fig.1.2.4.Power spectrum averaged over 100 initial conditions for the Lorenz model for different number of evolution steps (N).

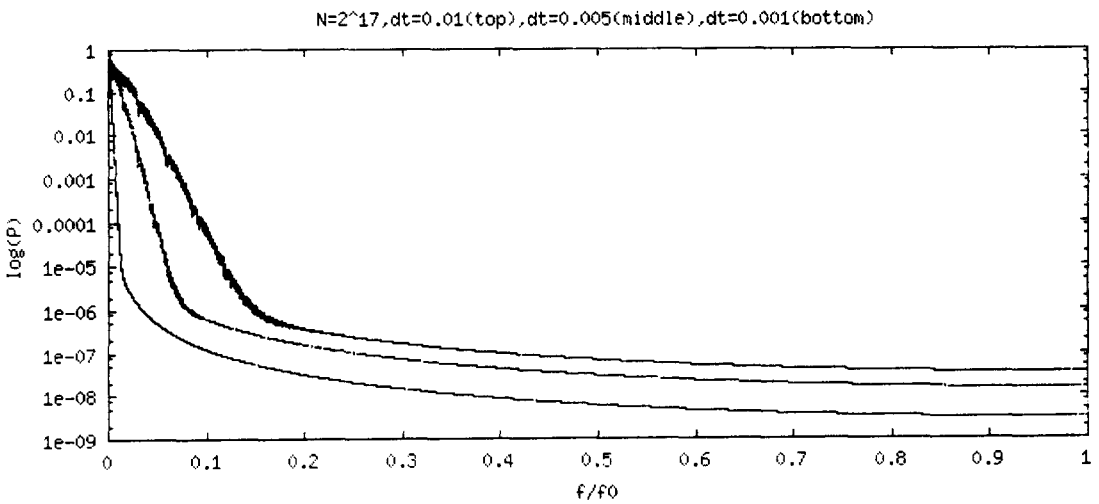

Fig.1.2.5. Averaged Power spectra for Lorenz model for different sampling interval (dt) or different Nyquist frequency.(a)top for dt=0.01 (b) middle for dt=0.005 (c) bottom for dt=0.001.

The power spectrum is averaged over various initial values and is plotted in fig.1.2.4. for different N(number of data) values. The power spectrum is found to depend on N (the tail region scales as 1/N). (This is due to the finite size effect). Also the power spectrum seems to be dependent on the Nyquist frequency (or sampling time interval dt) (see fig. 1.2.5). The power spectra calculated numerically will be always *aliased*. In otner words, the effect of frequencies beyond $f_c=1/2(dt)$ will be folded back into the power spectrum calculated [21].

1.3. Maps or Difference equations.

Since study of differential equations (flow) is quite an involved work, people started concentrating on difference equations (or maps).

One of such maps which shows chaotic behaviour is a piecewise linear one-dimensional map given by,

$$x_{n+1} = 1 - 2\left|x_n - \frac{1}{2}\right| \qquad (1.3.1)$$

For $x_n < ½$ the above equation is

$$x_{n+1} = 2x_n \qquad \text{and}$$

for $x_n > ½$,

$$x_{n+1} = 2(1 - x_n)$$

This map called tent map shows the behaviour of stretching (which leads to exponential divergence of nearby trajectories) and folding (which keeps the orbit bounded) [22]

Another simple map closely related to the tent map is

$$x_{n+1} = 2\,x_n \text{ modulo } 1 \qquad (1.3.2)$$

A third system which shows chaos and well studied by various people is the Logistic map which is used by R.M. May for modeling yearly variations in the population

of an insect species [7]. The logistic map can be derived from the Logistic differential equation, which describes the population dynamics.

The rate of change of population (say, of any insect, in limited conditions) is given by[23]

$$\dot{x} = rx(1 - \frac{x}{k}) = rx - \frac{rx^2}{k} = rx - sx^2. \qquad (1.3.3)$$

In the above the first term represents exponential increase of the population and the second term represent the decrease of population due to limited resources.

The difference equation corresponding to (1.3.3) is

$$\begin{aligned} & N_{n+1} - N_n = rN_n - sN_n^2 \\ \text{Or } & N_{n+1} = (r+1)N_n - sN_n^2 \\ & N_{n+1} = r'N_n - sN_n^2 \end{aligned} \qquad (1.3.4)$$

Where r' = r+1.

Normalizing N by taking x = N/(r'/s) in equation (1.3.4), we get

$x_{n+1} = r' x_n - r' x_n^2$ or

$$x_{n+1} = r' x_n (1 - x_n) \qquad (1.3.5)$$

with $x \in [0,1]$ and $0 < r' \leq 4$

This map is rich in its dynamics with period doubling, chaos, intermittency etc. Later Mitchell J. Feigenbaum used this model to show some universal characters for quadratic maps exhibiting chaos [10].

In Chapter 4 we give a new way of treating maps, namely, equating them to finite series differential equations.

1.4.Two-dimensional map - Henon map.

A well known example for a 2-dimensional map is the Henon map. It is given by the difference equation [22,24]

$$\begin{aligned} x_{n+1} &= a - x_n^2 + by_n \\ y_{n+1} &= x_n \end{aligned} \qquad (1.4.1)$$

In this map they describe a model, which is simple, yet exhibit the same essential properties of a non-linear differential equation like Lorenz system. Instead of considering the whole trajectories in 3-dimensional space, they used only successive intersections with a 2-dimensional surface of section. For a=1.3 and b=0.3, the result of plotting successive points obtained by iterating equation (1.4.1) is given in fig.1.4.1. The attractor in the figure is a strange attractor corresponding to chaos. The self-similarity is clearly seen from it by taking a blow up of a small portion of it. The dimension of the attractor is fractional (D = 1.26) and hence it is a fractal.

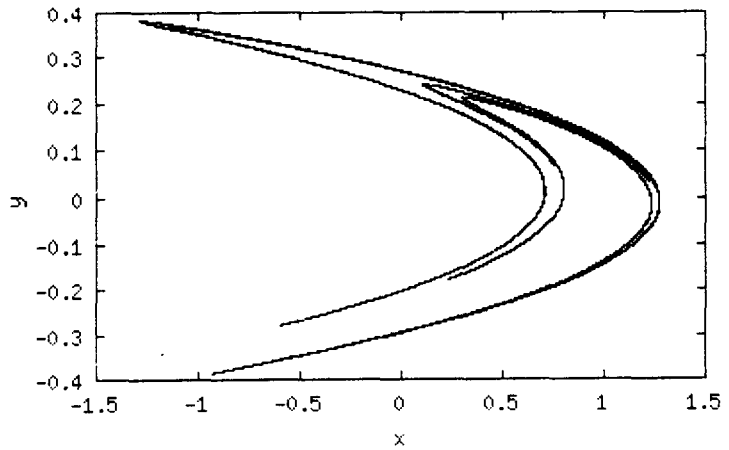

Fig.1.4.1. Plot of Henon attractor for a=1.3 and b=0.3

Chaos has been observed in some chemical reactions also. One of such well studied examples is the Bolouzov- Zhabotinskii (B-Z) reaction.[17]

In chapter 4 we have studied the Logistic equivalent of differential equation, which shows very interesting results.

In the next section we give a brief review of Hamiltonian systems and how chaos in such systems are characterized.

SECTION B

HAMILTONIAN SYSTEMS

Hamiltonian systems are a class of dynamical systems that occur in a variety of circumstances. The special properties of Hamilton's equations endow these systems with attributes that differ qualitatively and fundamentally from other systems. For example, Hamilton's equations do not possess *attractors*.

Some of the Hamiltonian systems are, the well known case of mechanical systems without friction, paths followed by magnetic field lines in a plasma, the mixing of fluids, the ray equations describing the trajectories of propagating waves etc. In all of these situations chaos can be an important issue. Also, chaos in Hamiltonian systems may throw light on issues like foundations of statistical mechanics and stability of the solar system. In addition, Hamiltonian mechanics and its structure are reflected in quantum mechanics.

1.5. The dynamics of Hamiltonian systems.

The dynamics of a Hamiltonian system is completely specified by a simple function, the Hamiltonian, H (**p**, **q**, **t**). If the number of degrees of freedom of the system is N (N=3n, for n particles interacting in 3-D space), then the trajectory (**p** (t), **q** (t)) of the system in 2N-dimensional phase-space can be determined by solving the Hamilton's equations of motion, viz,

$$\left.\begin{aligned} d\mathbf{p}/dt &= -\,\partial H(\mathbf{p}, \mathbf{q}, t)/\partial \mathbf{q} \\ d\mathbf{q}/dt &= \partial H(\mathbf{p}, \mathbf{q}, t)/\partial \mathbf{p} \end{aligned}\right\} \qquad (1.5.1)$$

If H does not have any explicit time dependence (i.e., H=H (**p**, **q**)), then

$$\left.\begin{aligned} \frac{dH}{dt} &= \frac{dq}{dt}\frac{\partial H}{\partial q} + \frac{dp}{dt}\frac{\partial H}{\partial p} \\ &= \frac{\partial H}{\partial p}\frac{\partial H}{\partial q} - \frac{\partial H}{\partial q}\frac{\partial H}{\partial p} \\ &= 0 \end{aligned}\right\} \qquad (1.5.2)$$

Identifying H as the energy E, of the system, we see that the energy is conserved.

i.e., $E = H(\mathbf{p}, \mathbf{q})$ = a constant of motion. (1.5.3)

One of the basic properties of Hamilton's equations is that they preserve 2N-dimensional volumes in the phase space. Thus, if we consider an initial closed surface S_0 in the 2N-dimensional phase space and evolve each point on the surface forward with time, we obtain at each instant of time t a new closed surface S_t which contains within it precisely the same 2N-dimensional volume as does S_0. As a consequence of this result, Hamiltonian systems do not have attractors in the usual sense. This incompressibility of phase space volume for Hamiltonian systems is called *Liouville's* theorem.

For an integrable system, the trajectory in phase space will remain on the constant energy surface. Since there are N constants of motion for an integrable system with N degrees of freedom, the trajectories are confined on an N-dimensional torus in the 2N dimensional phase space. Even if we give slight perturbation to this integrable Hamiltonian, the tori are not destroyed. Only for very large perturbations, the tori get destroyed and the system goes from regular to chaotic motion. For a not enough strong perturbation, we may observe some regular tori and some other destroyed ones. The idea of transition from integrability to non-integrability is given by KAM theorem [22]. Also it is observed that, the trajectories can wander from one torus to another in phase space within constant energy surface.

1.6. A few examples of Hamiltonian systems.

A classical example of a non-integrable Hamiltonian system is the *three-body problem* (say, in celestial mechanics or atomic physics). A number of non-integrable Hamiltonian systems have been identified and studied for their chaotic behaviour. It includes differential equations and difference equation (maps) representing Hamiltonian systems. The standard map, kicked oscillator, kicked rotator; Henon-Heils systems etc. are some of the well-studied chaotic systems.

1.6.1.The standard map (Kicked rotator)

Let us consider a rotator with a moment of inertia I and length L, fastened to a frictionless pivot subjected to a periodic impulse of strength k/L . Let P_θ be the angular momentum and θ the angular position at any instant. Then the Hamiltonian can be written as [22,25].

$$H = \frac{P_\theta^2}{2I} - kCos\theta \sum_{n=-\infty}^{\infty} \delta(\frac{t}{T} - n) \qquad (1.6.1)$$

Here $\frac{P_\theta^2}{2I}$ is the unperturbed Hamiltonian.

The Hamiltonian (1.6.1) corresponds to a particle motion in a periodic wave packet with an infinite number of harmonics of equal amplitude.

The equations of motion derived from (1.6.1) are

$$\dot{P}_\theta = -\frac{\partial H}{\partial \theta} = -kSin\theta \sum_{n=-\infty}^{\infty} \delta(\frac{t}{T} - n) \qquad (1.6.2)$$

$$\dot{\theta} = \frac{\partial H}{\partial P_\theta} = \frac{P_\theta}{I} \qquad (1.6.3)$$

If (P_n, θ_n) are the values of the variables just before n^{th} kick, and (P_{n+1}, θ_{n+1}) are the values of the same variables before the next $(n+1)^{th}$ kick, then from (1.6.2) and (1.6.3) we get the mapping equations as

$$\left.\begin{aligned} P_{n+1} &= P_n - k \sin \theta_n \\ \theta_{n+1} &= \theta_n + P_{n+1} \end{aligned}\right\} \qquad (1.6.4)$$

when k= 0, the system will be integrable, and the trajectory can be put on a *torus* P (mod 2π), θ(mod 2π) and the corresponding phase portrait will be a closed curve. But when $k > 0$, the phase portrait will be complicated (see ref .25).

This map, also called as Chirikov-Taylor map, offers a simplified model of the onset of chaos by retaining the typical complex features of the problem. When the value of k is increased above zero, the system becomes non-integrable. The fig.1.6.1 shows (θ,P) plot for various initial conditions. If the initial condition is on an invariant torus it traces out the closed curve corresponding to the torus. If the initial condition yields a chaotic orbit, then it will wander through out an area densely filling that area. For small perturbation (k=0.5) there are many KAM tori. (See fig.1.6.1). When k is increased, more and more KAM tori disappear and the chaotic orbit fills almost the phase space. Phase plot for k=1.0 and 2.5 are also given in fig.1.6.2 and fig. 1.6.3.

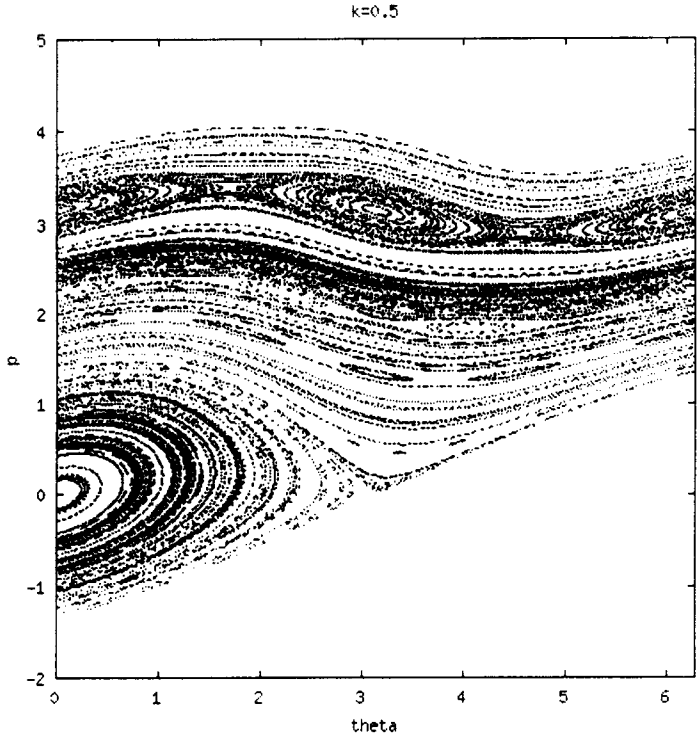

Fig.1.6.1 The phase portrait of the standard map (k=0.5)

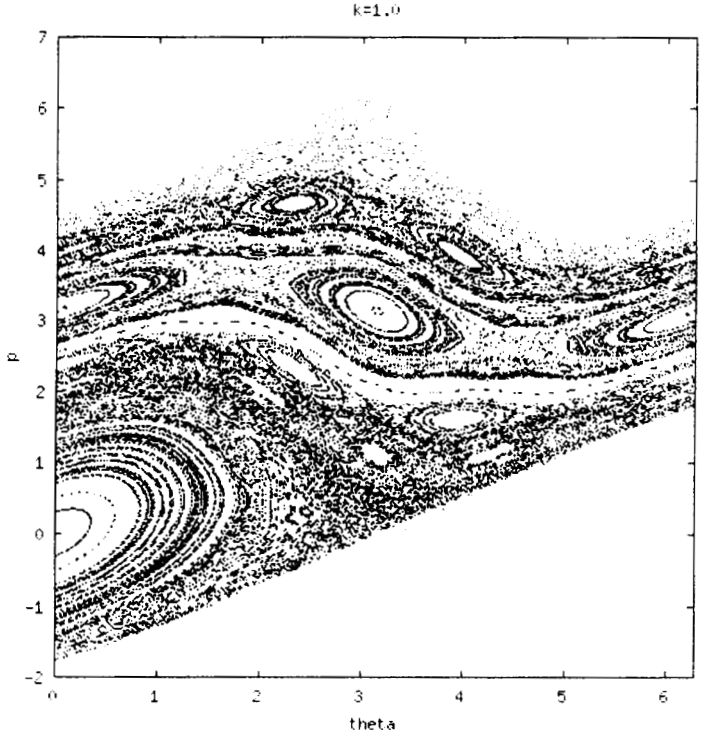

Fig: 1.6.2. The phase portrait of the standard map (k=1.0)

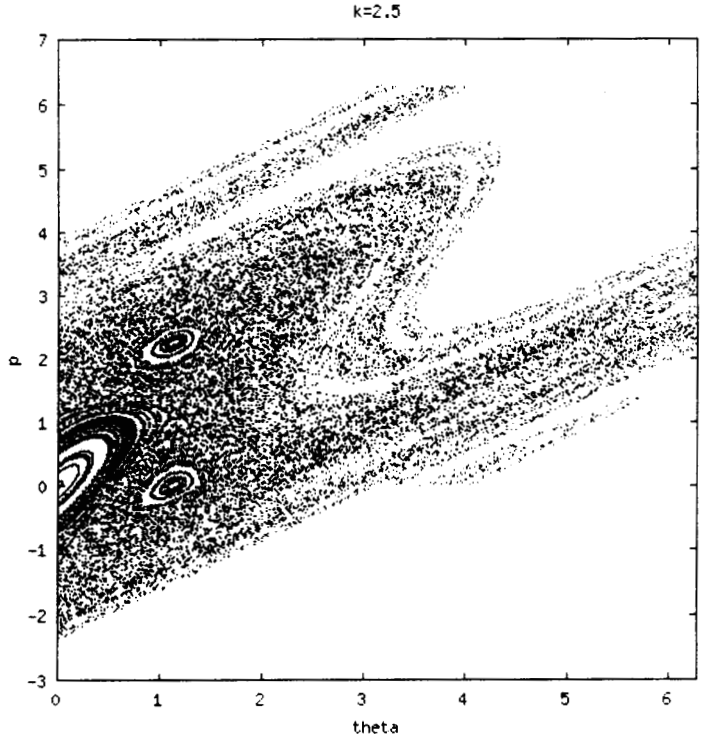

Fig: 1.6.3. The phase portrait of the standard map (k=2.5)

1.6.2.The Web – Map (Kicked Oscillator)

The Web-Map is a result of the consideration of particle motion in a constant magnetic field and an electrostatic wave packet propagating perpendicular to the magnetic field. The Hamiltonian of the system is

$$H = \frac{1}{2}(p^2 + \omega_0^2 x^2) - \frac{\omega_0 k}{T} Cosx \sum_{n=-\infty}^{\infty} \delta(\frac{t}{T} - n) \qquad (1.6.5)$$

The equation of motion obtained from (1.6.5) can be written as a difference equation and by a suitable transformation we obtain the map [25]

$$\begin{aligned} u_{n+1} &= (u_n + KSinv_n)Cos\alpha + v_n Sin\alpha \\ v_{n+1} &= -(u_n + KSinv_n)Sin\alpha + v_n Cos\alpha \end{aligned} \qquad (1.6.6)$$

where $u = \frac{\dot{x}}{\omega_0}$, v= - x , $\alpha = \omega_0 T$

The most interesting case involving map (1.6.6) is that of the resonance between sequences of kicks and oscillator frequency ω_0

i.e., when $\alpha = \omega_0 T = 2\pi/q$ (1.6.7)

This map can be considered as a dynamical generator of the q-fold symmetry for the resonance condition (1.6.7), which is of the crystalline type for

$q \in \{q_c\} = \{1,2,3,4,6\}$ (1.6.8)

and the quasi-crystal type for $q \notin \{q_c\}$

Examples of a phase plane with narrow stochastic layers are given in fig. (1.6.4) for q=4,5,6,7

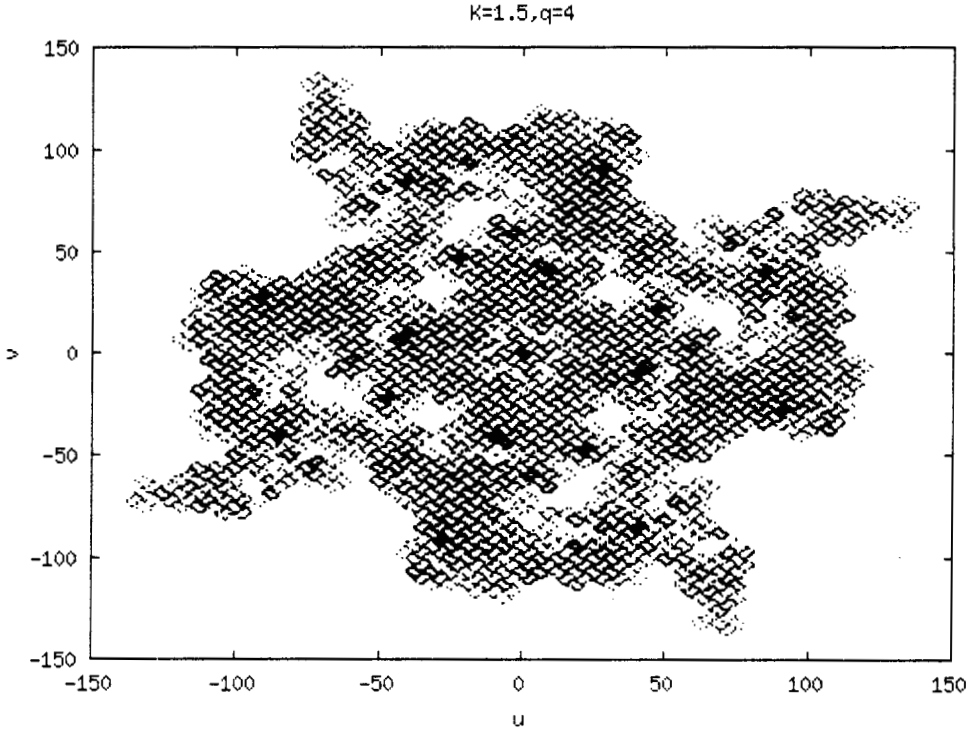

Fig.1.6.4 a. The phase plot for the web-map (eq.1.6.6) for q=4 and k=1.5

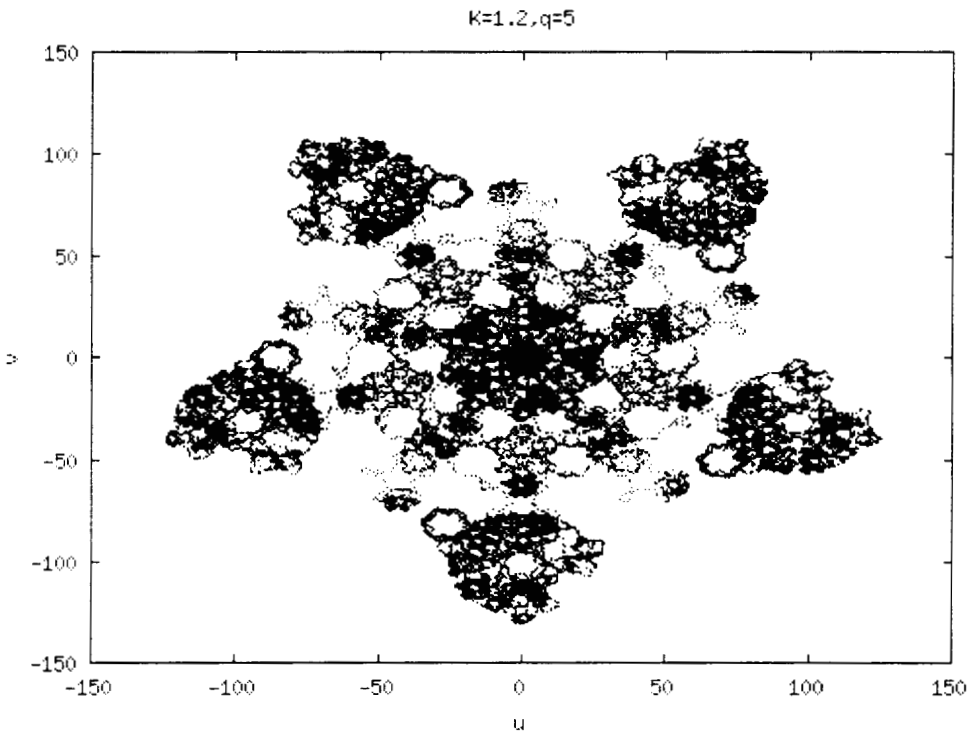

Fig.1.6.4 b. The phase plot for the web-map (eq.1.6.6) for q=5 and k=1.2

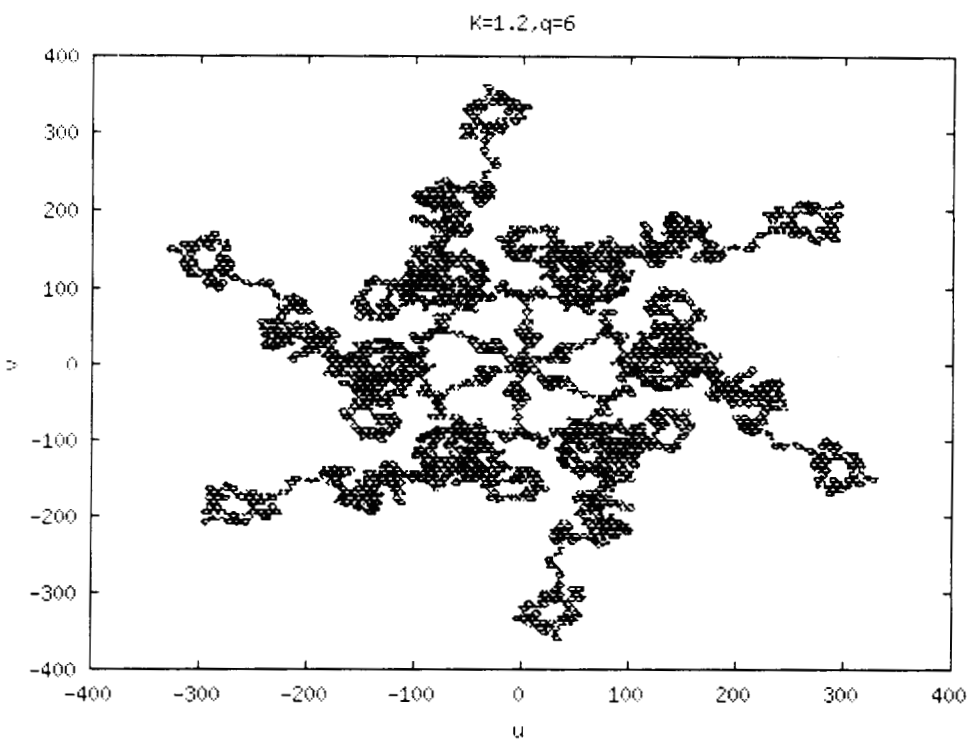

Fig.1.6.4 c. The phase plot for the web-map (eq.1.6.6) for q=6 and k=1.2

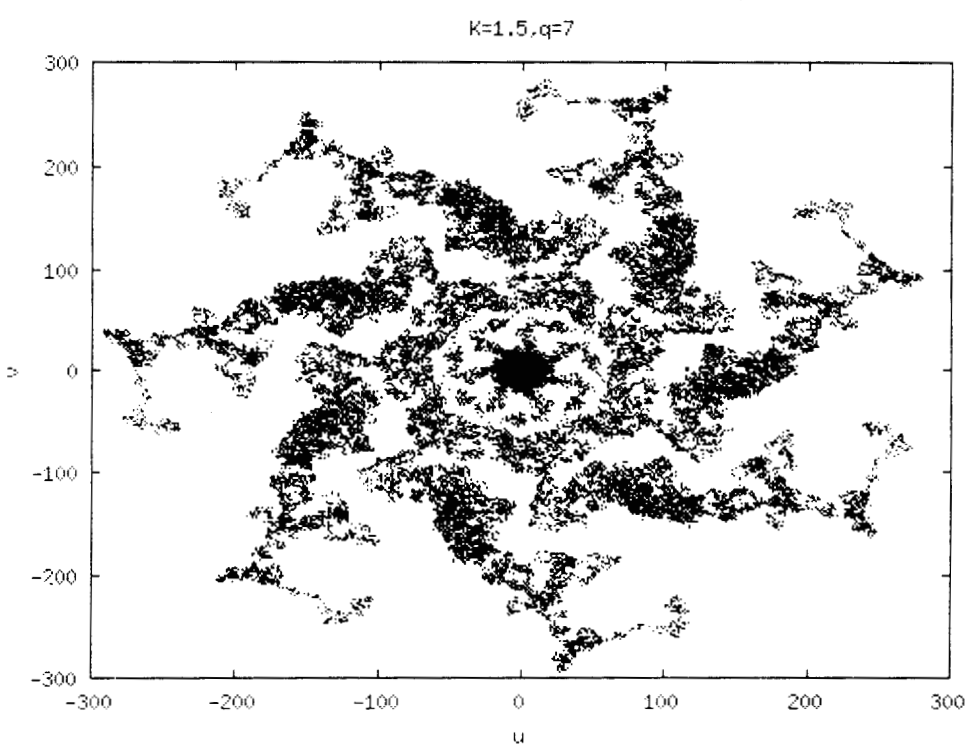

Fig.1.6.4 d. The phase plot for the web-map (eq.1.6.6) for q=7 and k=1.5.

These illustrations demonstrate the existence of the *stochastic web* of a corresponding symmetry in the phase plane. The stochastic web is a net with each part being a stochastic layer. One can say that the net of channels, which constitute the stochastic web, provides particle transport along the web (fig.1.6.4)

1.6.3.The Henon- Heils system.

One of the simplest and well studied non-integrable systems is the Henon-Heils system [26,27]. The equations of motion of the Henon-Heils system are

$$\ddot{x} = -x - 2xy$$
$$\ddot{y} = -y + y^2 - x^2 \qquad (1.6.9)$$

The potential is given by

$$V(x,y) = \tfrac{1}{2}(x^2 + y^2) + x^2 y - y^3/3 \qquad (1.6.10)$$

This system has not been solved using any analytical method. Here we have a 4-D phase space x, $\dot{x}$, y, $\dot{y}$ and it in this space is not possible to visualize. If we restrict the initial conditions to one value of the energy, E, there are only three independent co-ordinates left over, due to the constraint H (x, $\dot{x}$, y, $\dot{y}$) =E. Since 3-D space is still difficult to draw, we only plot the intersection points of the orbit x (t), y (t), $\dot{y}$ (t) with a 2-D plane, y vs. $\dot{y}$ (at x = 0). If the system were integrable this *(poincare) surface of section* would look like that of Fig.1.6.5.

But when the system is non-integrable, the surface of section becomes complicated, and these are plotted in Fig.1.6.6. for the Henon-Heils system for various energies E. At E = 1/12, the phase plot does look like a dotted deformed version of the one for an integrable system (fig.1.6.6a). At E = 1/8 the seperatrices seems to be disappeared (fig.1.6.6b) (see Fig.1.6.5. also), replaced by a chaotic collection of dots (from one orbit) through which it would be difficult to draw a nice simple curve. At a higher energy,

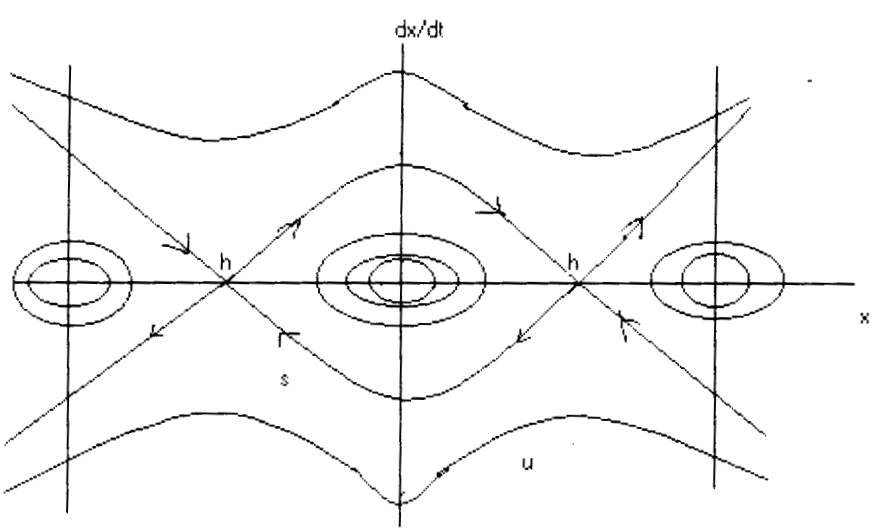

Fig.1.6.5. Phase plane plot for the pendulum. (Schematic)

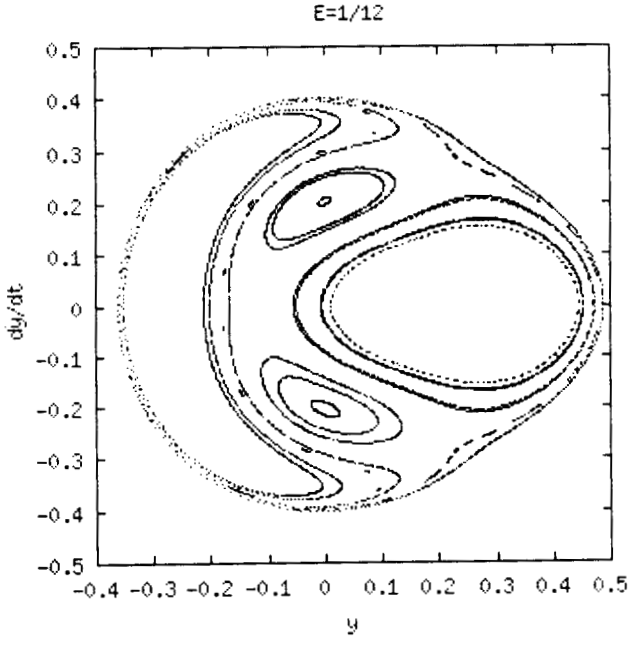

Fig 1.6 6a: Phase plot for Henon-Heils system for E=1/12

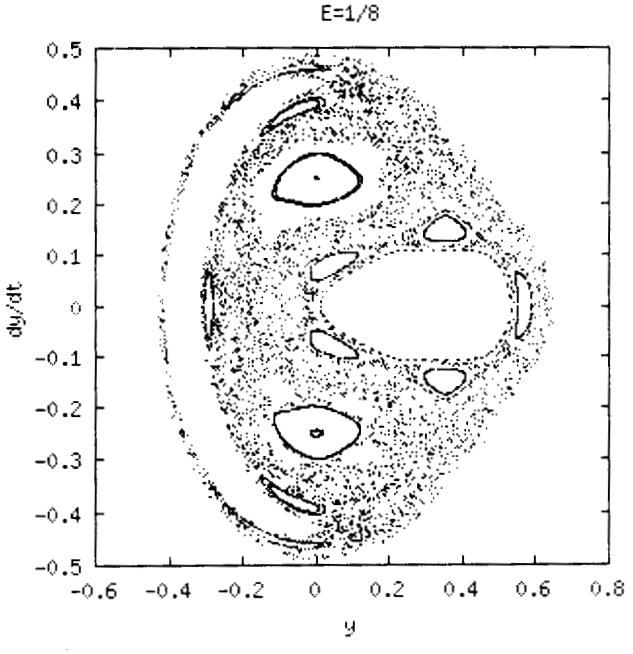

Fig 1.6 6b: Phase plot for Henon-Heils system for E=1/8.

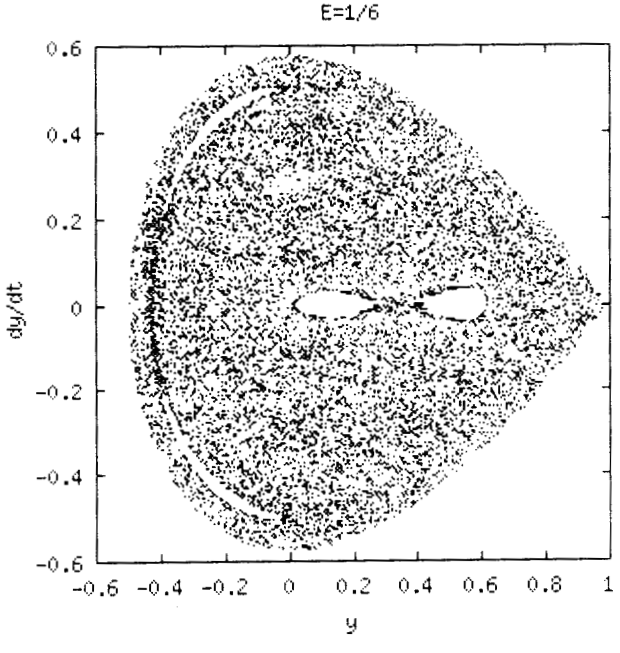

Fig 1.6 6c. Phase plot for Henon-Heils system for E=1/6

E= 1/6, nearly all of the available phase plane seems chaotically *filled* with the intersection dots of just one orbit (fig.1.6.6c). Yet some small *islands*, with an *elliptic* (linearly stable) points at their center, can still be seen. Those orbits do not wander. The time series for Henon-Heils for the energy E=1/12 and E=1/6 for nearby initial conditions is shown in fig.1.6.7. Fig 1.6.7a which corresponds to the energy E=1/12 gives a time series, for two arbitrarily close initial conditions. The two time series exactly superimposes and we cannot distinguish the two. For this energy we get regular motion. The Poincare section for this energy gives invariant tori (fig.1.6.6a), which also suggest regular motion. In fig.1.6.7b the time series for the energy E=1/6 for two arbitrarily close initial conditions are plotted. The divergence of trajectories as seen from the plot clearly suggests the sensitive dependence on initial conditions. The Poincare section plotted for this energy (fig.1.6.6c) give scattered points which is the indication of destroyed torus. Thus chaos is confirmed for the system for the energy E=1/6.

The power spectrum for the case E=1/12 (fig.1.6.8a) show a few prominent frequencies and their higher harmonics. This can be treated as characteristics of regular system with periodic behaviour. But the power spectrum for E=1/6 (fig.1.6.8b) show a spectrum of frequencies which can be interpreted as the behaviour of an irregular system. But the frequency component vanishes beyond a range, which makes a difference between stochastic process and a chaotic system.

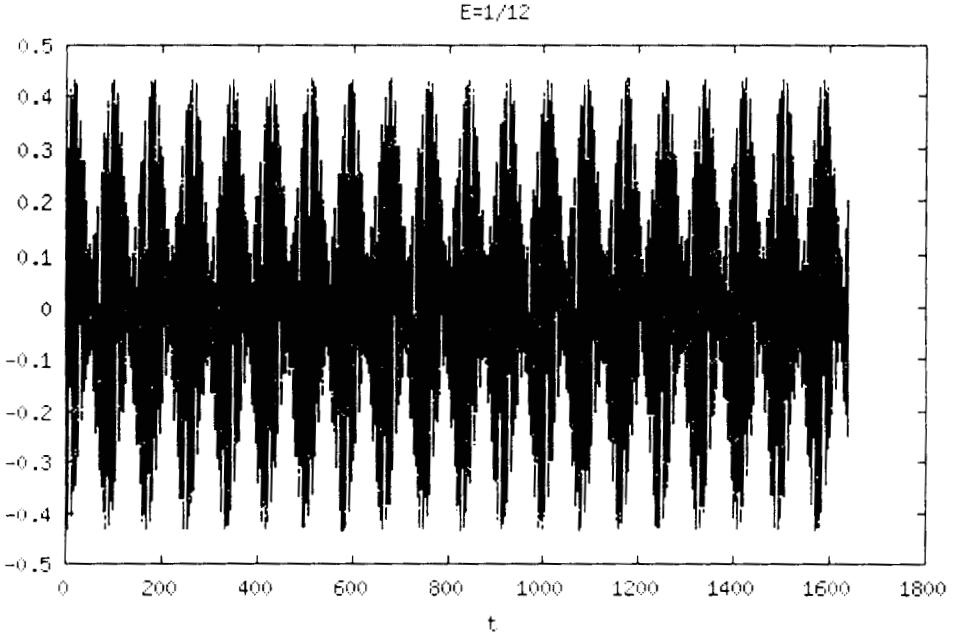

Fig.1.6.7a. The time series for the Henon-Heils model for E=1/12

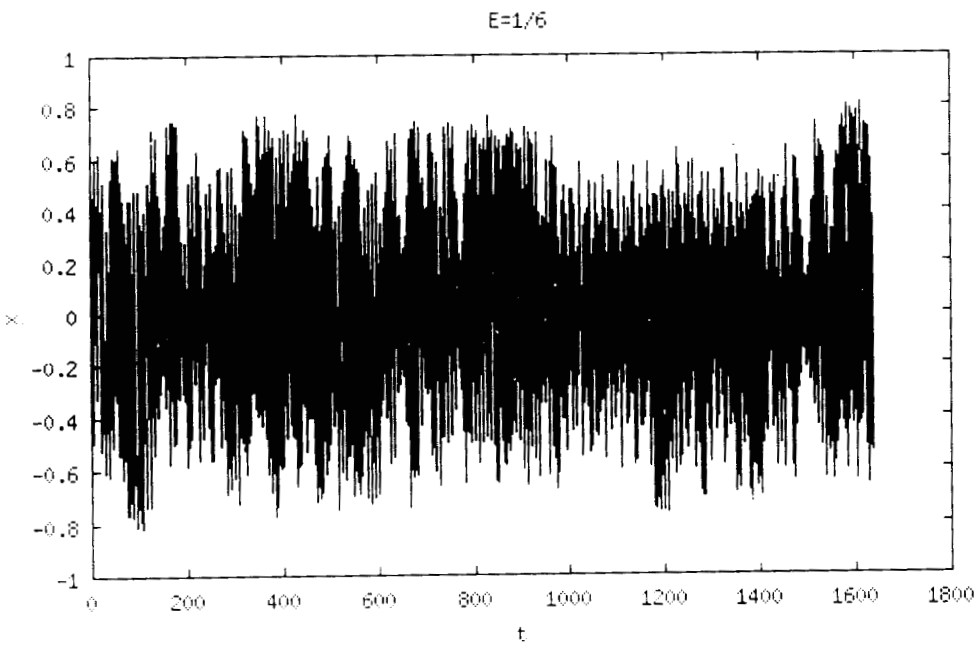

Fig.1.6.7b. The time series for the Henon-Heils model for E=1/6.

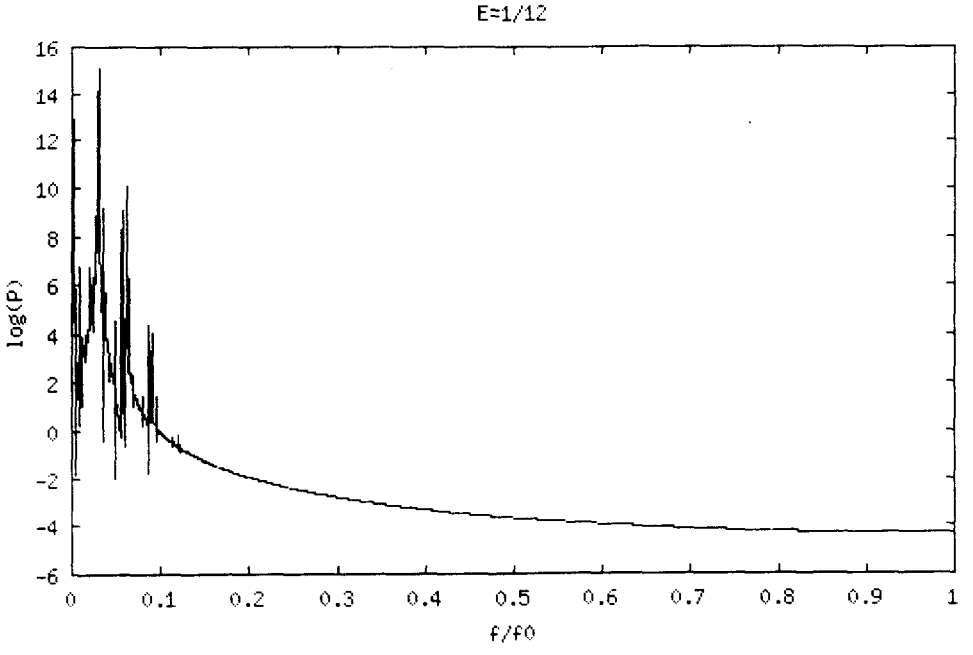

Fig.1.6.8a. The power spectrum for the Henon-Heils model for E= 1/12

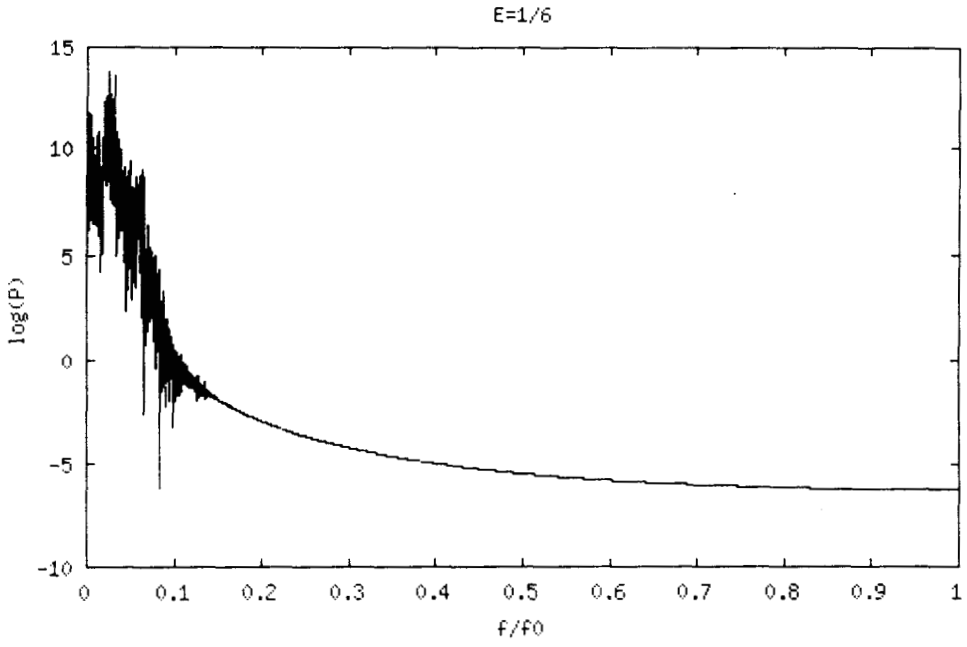

Fig.1.6.8b. The power spectrum for the Henon-Heils model for E=1/6.

We could go on to cite many examples of mechanical systems displaying the type of behaviour seen in the example of Kicked rotor. It is perhaps; somewhat more surprising that these same phenomena apply to situations in which one is not dealing with straightforward problems of mechanics. The point is that these problems are also described by Hamilton's equations. Three examples of this type are the following.

1.Non-turbulent mixing.

2.The trajectories of magnetic field lines in plasmas.

3.The equations for the propagation of short wavelength waves in inhomogeneous media.

In chapter 2 we introduce a new Hamiltonian system, which shows chaotic behaviour for certain parameter values and initial conditions.

CHAPTER 2

MOTION OF A CHARGED PARTICLE AROUND A FIXED OPPOSITE CHARGE NEAR A DIELECTRIC DISCONTINUITY.

2.1.Introduction.

In this chapter we study a model, which is a simple Hamiltonian system, yet exhibiting complicated behaviour, including chaos. We have already discussed the well-known Hamiltonian system, which shows chaos as well as regular features for different energy values, namely Henon-Heils system [26]. The model we describe here is hydrogen like system kept in a dielectric medium near a discontinuity. Precisely, we have a charged particle moving around a fixed opposite charge kept in a medium with a dielectric discontinuity, We are inspired from the Anisotropic Kepler Problem (AKP) described by Gutzwiller [28], which also shows regular as well as chaotic behaviour. In AKP the chaos is coming from the anisotropy in mass of the charged particle moving in the medium. In our model instead of mass anisotropy, we introduced a discontinuity in the medium, which causes image charges for moving as well as stationary charges. If we include the contribution to the force due to all the charges and image charges, the equation of motion will become non linear. (see sec. 2.2.). During the development of the model, we came across similar models, though slightly different, which shows chaos. Some of them are, Hydrogen atom near a metal surface [29], Hydrogen atom interacting with different external fields like magnetic field, electric field, crossed electric and magnetic field [30]. In models given in ref.29 the chaos is due to the image charges and that given in ref 30, it is due to the external fields. In our model we have seen that, the system becomes chaotic, for certain parameters ($\delta=\varepsilon_1/\varepsilon_2$, the ratio of dielectric constants of the two media) and initial conditions. The mathematical model is developed, by considering all the forces on the moving charge, including that due to the image charges. The Hamiltonian thus derived is used for getting Hamilton's equations

of motion. We have scaled the equations for eliminating the terms like charge, mass etc. so that we get simple looking equation. Now the problem is six dimensional one, since we require three co-ordinates and three momenta to get the trajectory of the system in a six dimensional phase space. Since to view the trajectory in six dimension is almost impossible, and even to get a Poincare surface of section becomes a tough job for such a model, we tried to reduce the dimensionality of the problem. Since it has a cylindrical symmetry the angular momentum is conserved, and hence the six dimensional problem is reduced to a four dimensional one. Now we could take a Poincare surface of section by reducing one more dimension by keeping the energy constant. Thus a plane cutting an energy surface in three dimensions can be defined. By looking at various planes and for different parameter values and initial conditions, we could see that the system shows regular as well as chaotic behaviour. Thus we could identify different initial conditions showing chaotic or regular behaviour. In addition the stability analysis of the model shows that, for a range of parameter value δ, it can have fixed points showing center or quasiperiodic solutions (regular) and we could as well imagine that for these values of δ itself, there may be points in phase space which are unstable and may be chaotic. On the other hand, in dissipative systems, we get either fixed points (for regular case) or strange attractors (for chaotic case). Since phase space volume does not contract in case of Hamiltonian systems like our model, we cannot expect strange attractors. At the same time, for Hamiltonian systems, different initial conditions may lead to regular as well as chaotic motion. This assumption made us to search for initial conditions comparatively far away from the stable points for any chaotic region, and in fact we obtained some. We have investigated the system extensively using the standard numerical techniques, like the time series analysis, calculation of Lyapunov exponents, plotting the trajectory, taking the power spectrum, the Poincare surface of section etc. Plotting the time series for two nearby initial conditions shows the sensitive dependence on initial conditions

(SIC) for the initial condition corresponding to chaotic solution. The trajectories plotted also gave a clear evidence of SIC. The distance between the trajectories during the evolution also confirms this. The power spectrum for the time series, which can be used to characterize chaos in dissipative system, also indicate a difference between chaotic and regular motion of our model, even though not as convincing as in the dissipative systems.

The model, which we have described here, shows chaos classically, and may be relevant in the context of electron motion in semiconductors, organization of particles in charged colloids etc. This part of the work is reported in [31].

A quantum mechanical treatment of the problem is discussed in chapter 3.

2.2. Derivation of the Model

Consider a charged particle +Q frozen at $\mathbf{r}_0(x_0,y_0,z_0)$ and a charge –Q which is free to move any where in the medium with a dielectric discontinuity and having the instantaneous state vector r (x, y,z).

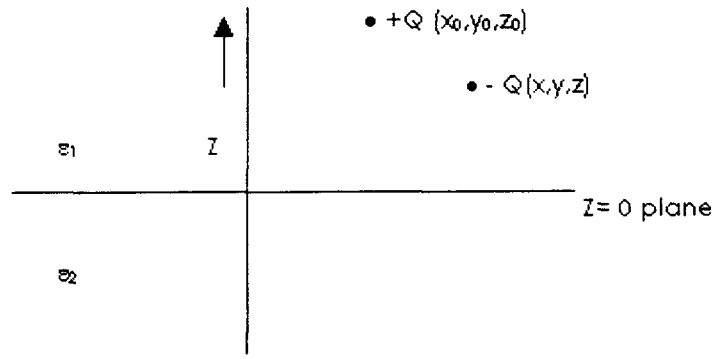

Fig. 2.2.1. Schematic diagram showing the positions of charges.

We can calculate the field **E** in the region z > 0 when physical charge is placed in the region z > 0 as follows by the method of images [32].

We know that whenever a charge in one medium is close to another dielectric, there will be induced charge on the dielectric. This induced charge is distributed through out the dielectric medium and will influence the original charge also. The effect due to the entire charge distribution due to induction can be taken as the effect of a point charge in the dielectric located at an appropriate place. This virtual point charge is called image charge. Whenever we are dealing with forces on a charge in a dielectric, we have to take the effect due to image charge also into account.

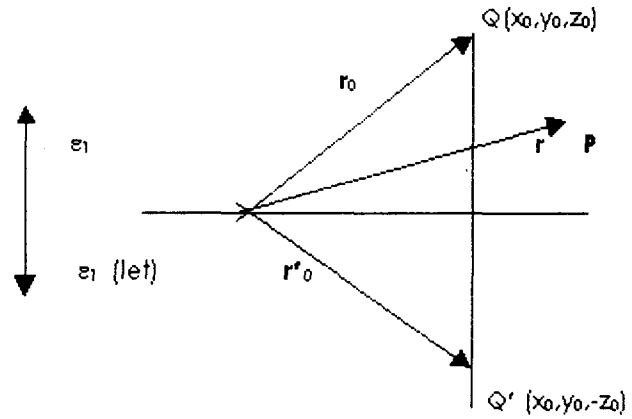

Fig.2.2.2. Vectors representing real charge and image charge.

Let Q' be the image charge of +Q when looking from the medium 1 (with dielectric constant ε_1). Now the entire region can be assumed to be filled with medium 1 (with dielectric constant ε_1). Then the electric field **E** in this region (say at P) can be calculated as follows,

$$E^{>} = \frac{Q}{4\pi\varepsilon_1}\frac{(r-r_0)}{|(r-r_0)|^3} + \frac{Q'}{4\pi\varepsilon_1}\frac{(r-r_0')}{|r-r_0'|^3} \qquad (2.2.1)$$

The charge density at point z > 0 is given by

$$\nabla \cdot E^{>} = \frac{Q}{\varepsilon_1}\delta(r-r_0) + \frac{Q'}{\varepsilon_1}\delta(r-r_0') \qquad (2.2.2)$$

$$= \frac{Q}{\varepsilon_1}\delta(r - r_0) \qquad \text{for } z > 0 \quad (2.2.3)$$

(Since the second term in 2.2.2 becomes zero for z > 0)

If the charge is placed in the region z > 0 we calculate the field at z<0, as described below, see fig.2.2.3.

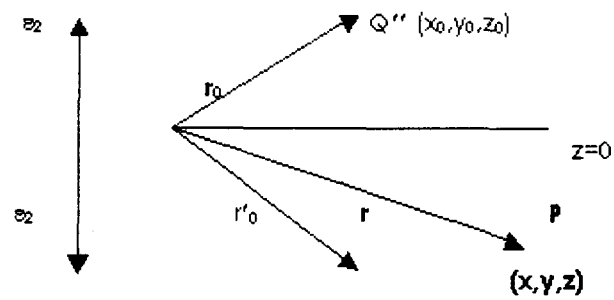

Fig.2.2.3. Position vectors of effective charge (Q") and the moving charge -Q

We consider that the entire medium is replaced by medium 2 (with dielectric constant ε_2) and let the effective charge when looking from a point z < 0 be Q".

$$E^{<} = \frac{Q''}{4\pi\varepsilon_2}\frac{(r - r_0)}{|r - r_0|^3} \qquad (2.2.4)$$

$$\nabla \cdot E^{<} = \frac{Q''}{\varepsilon_2}\delta(r - r_0) = 0, \text{ for } z < 0 \qquad (2.2.5)$$

We have

$$\mathbf{D} = \varepsilon\,\mathbf{E} \qquad (2.2.6)$$

Normal component of D is continuous and so D_z is continuous.

$$\varepsilon_1 E_z^{>}\Big|_{z\to 0} = \varepsilon_2 E_z^{<}\Big|_{z\to 0} \qquad (2.2.7)$$

As $z \to 0$ $r = \rho = (x\hat{i} + y\hat{j})$

So $$(r - r_0) = (\rho - \rho_0) - z_0\hat{k} \quad \text{(2.2.8a)}$$

$$(r - r_0') = (\rho - \rho_0) + z_0\hat{k} \quad \text{(2.2.8b)}$$

$$|(r - r_0)|^2 = |(\rho - \rho_0)|^2 + z_0^2 \quad \text{(2.2.9a)}$$

$$\left|(r - r_0')\right|^2 = |(\rho - \rho_0)|^2 + z_0^2 \quad \text{(2.2.9b)}$$

But tangential component of E is continuous.

i.e., $$E_{x>}\Big|_{z\to 0} = E_{x<}\Big|_{z\to 0} \quad \text{(2.2.10a)}$$

$$E_{y>}\Big|_{z\to 0} = E_{y<}\Big|_{z\to 0} \quad \text{(2.2.10b)}$$

From (2.2.7) (using (2.2.1), (2.2.4), 2.2.8) and 2.2.9) we get

$$\frac{Q}{4\pi}\frac{(\rho - \rho_0) - z_0\hat{k}}{\left[|\rho - \rho_0|^2 + z_0^2\right]^{3/2}}\Bigg|_z + \frac{Q'}{4\pi}\frac{(\rho - \rho_0) + z_0\hat{k}}{\left[|\rho - \rho_0|^2 + z_0^2\right]^{3/2}}\Bigg|_z$$

$$= \frac{Q''}{4\pi}\frac{(\rho - \rho_0) - z_0\hat{k}}{\left[|\rho - \rho_0|^2 + z_0^2\right]^{3/2}}\Bigg|_z \quad \text{(2.2.11)}$$

i.e., $$-Q + Q' = -Q'' \quad \text{(2.2.12a)}$$

or $$Q'' = Q - Q' \quad \text{(2.2.12b)}$$

From equations (2.2.10a) and (2.2.10b) we get,

$$\frac{Q}{4\pi\varepsilon_1}\frac{(\rho - \rho_0) - z_0\hat{k}}{\left[|\rho - \rho_0|^2 + z_0^2\right]^{3/2}}\Bigg|_{x-y} + \frac{Q'}{4\pi\varepsilon_1}\frac{(\rho - \rho_0) + z_0\hat{k}}{\left[|\rho - \rho_0|^2 + z_0^2\right]^{3/2}}\Bigg|_{x-y}$$

$$= \frac{Q''}{4\pi\varepsilon_2}\frac{(\rho - \rho_0) - z_0\hat{k}}{\left[|\rho - \rho_0|^2 + z_0^2\right]^{3/2}}\Bigg|_{x-y} \quad \text{(2.2.13)}$$

$$\text{i.e.,}\quad \frac{Q}{\varepsilon_1}+\frac{Q'}{\varepsilon_1}=\frac{Q''}{\varepsilon_2} \tag{2.2.14}$$

Then using (2.2.12) we get,

$$Q'=\frac{\varepsilon_1-\varepsilon_2}{\varepsilon_1+\varepsilon_2}Q \tag{2.2.15}$$

and

$$Q''=\frac{2\varepsilon_2}{\varepsilon_1+\varepsilon_2}Q \tag{2.2.16}$$

Equations (2.2.15) and (2.2.16) gives the image charges at z < 0 and z>0 respectively.

2.3.The Equation of motion for the model

Let us put $a=\frac{\varepsilon_1-\varepsilon_2}{\varepsilon_1+\varepsilon_2}=\frac{\delta-1}{\delta+1}$ and $b=\frac{2\varepsilon_2}{\varepsilon_1+\varepsilon_2}=\frac{2}{\delta+1}$ where $\delta=\frac{\varepsilon_1}{\varepsilon_2}$. The situation when the particle is at z>0 is shown in the fig2.3.1. (Let O be the origin of co-ordinate system)

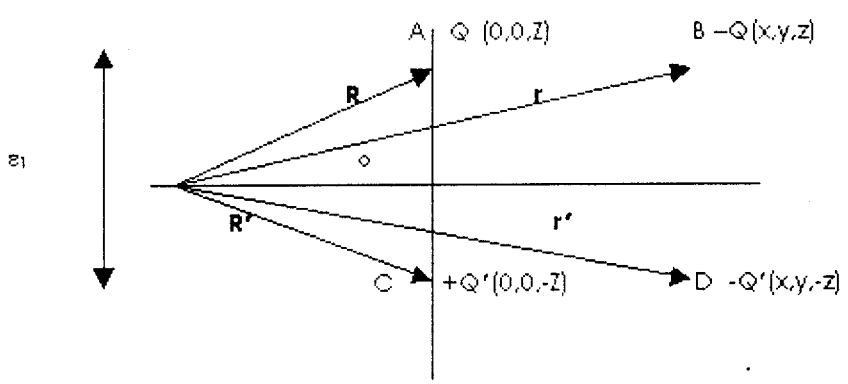

Fig.2.3.1. The different forces acting on the particle –Q when it is at z > 0.

The force **F** on the particle at B is

[Since Q' = aQ]

$$m\ddot{r} = \frac{1}{4\pi\varepsilon_1}\left[-\frac{Q^2(r-R)}{|r-R|^3} - \frac{Q^2 a(r-R')}{|r-R'|^3} + \frac{Q^2 a(r-r')}{|r-r'|^3}\right]$$

$$m\ddot{r} = \frac{Q^2}{4\pi\varepsilon_1}\left[-\frac{(x,y,z-Z)}{\left[x^2+y^2+(z-Z)^2\right]^{3/2}} - \frac{a(x,y,z+Z)}{\left[x^2+y^2+(z+Z)^2\right]^{3/2}} + \frac{a(0,0,2z)}{8z^3}\right] \quad (2.3.1)$$

$$m\ddot{r} = \frac{Q^2}{4\pi\varepsilon_1}\left[-\frac{(x,y,z-Z)}{\left[x^2+y^2+(z-Z)^2\right]^{3/2}} - \frac{a(x,y,z+Z)}{\left[x^2+y^2+(z+Z)^2\right]^{3/2}} + \frac{a(0,0,1)}{4z^2}\right] \quad (2.3.2)$$

The situation when the particle is at z<0 is shown in fig.2.3.2.

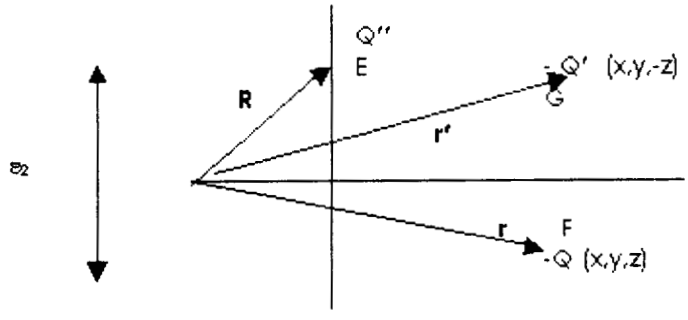

Fig.2.3.2. The different forces acting on –Q when it is at z < 0.

Q' = aQ , Q'' = bQ

The force on the particle at F is,

$$m\ddot{r} = \frac{1}{4\pi\varepsilon_2}\left[-\frac{bQ^2(r-R)}{|r-R|^3} + \frac{Q^2 a(r-r')}{|r-r'|^3}\right] \quad (2.3.3)$$

$$m\ddot{r} = \frac{Q^2}{4\pi\varepsilon_2}\left[-\frac{b(x,y,z-Z)}{\left[x^2+y^2+(z-Z)^2\right]^{3/2}} + \frac{a(0,0,1)}{4z^2}\right] \quad (2.3.4)$$

Equations (2.3.2) and (2.3.4) can also be written as,

$$\dot{p} = m\ddot{r} = \frac{Q^2}{4\pi\varepsilon_1}\left[-\frac{(x,y,z-Z)}{\left[x^2+y^2+(z-Z)^2\right]^{3/2}} - \frac{a(x,y,z+Z)}{\left[x^2+y^2+(z+Z)^2\right]^{3/2}}\right.$$

$$\left. + \frac{a(0,0,1)}{4z^2}\right] \quad \text{, for z>0} \qquad (2.3.5)$$

$$\dot{p} = m\ddot{r} = \delta\frac{Q^2}{4\pi\varepsilon_1}\left[-\frac{b(x,y,z-Z)}{\left[x^2+y^2+(z-Z)^2\right]^{3/2}} + \frac{a(0,0,1)}{4z^2}\right] \quad \text{, for z<0} \qquad (2.3.6)$$

where $\delta = \frac{\varepsilon_1}{\varepsilon_2}$

The corresponding Hamiltonian is obtained as

$$H = \frac{p^2}{2m} - \frac{Q^2}{4\pi\varepsilon_1}\left[\frac{1}{\left[x^2+y^2+(z-Z)^2\right]^{1/2}} + \frac{a}{\left[x^2+y^2+(z+Z)^2\right]^{1/2}}\right.$$

$$\left. - \frac{a}{4z}\right] \quad \text{, for z>0} \qquad (2.3.7)$$

and

$$H = \frac{p^2}{2m} - \delta\frac{Q^2}{4\pi\varepsilon_1}\left[\frac{b}{\left[x^2+y^2+(z-Z)^2\right]^{1/2}} - \frac{a}{4z}\right] \quad \text{, for z < 0} \qquad (2.3.8)$$

i.e., by knowing the Hamiltonian we can make use of Hamilton's equations $\dot{p} = -\frac{\partial H}{\partial q}$ and $\dot{q} = \frac{\partial H}{\partial p}$ for getting the equations of motion. In other words, equations (2.3.5) and (2.3.6) are obtained from (2.3.7) and (2.3.8) respectively.

The nature of the potential given by equation (2.3.7) is plotted in fig.2.3.3.

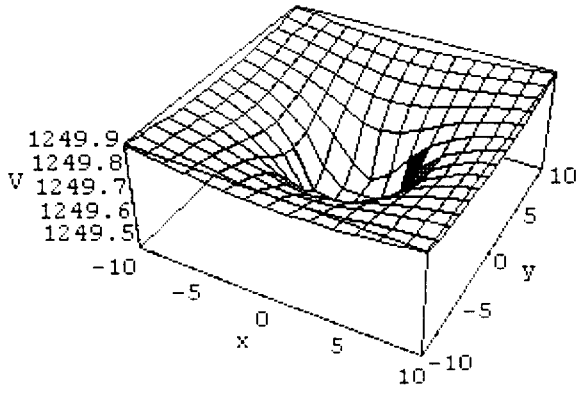

Fig. 2.3.3.The potential for the model dielectric very near to dielectric discontinuity (z=0) and for the positive charge 0.1 units above discontinuity.

Now we can eliminate Z by taking all distances in units of Z.

i.e., $x = Z\xi$, $\xi = x/Z$

$y = Z\eta$, $\eta = y/Z$

$z = Z\psi$, $\psi = z/Z$

Then equations (2.3.2) and (2.3.4) are modified as

$$mZ\frac{d^2}{dt^2}(\xi,\eta,\psi) = \frac{Q^2}{4\pi\varepsilon_1}\left[\frac{-Z(\xi,\eta,\psi-1)}{Z^3\left[\xi^2+\eta^2+(\psi-1)^2\right]^{3/2}}\right.$$

$$\left.-\frac{aZ(\xi,\eta,\psi+1)}{Z^3\left[\xi^2+\eta^2+(\psi+1)^2\right]^{3/2}}+\frac{a(0,0,1)}{Z^2 4\psi^2}\right], \psi>0 \qquad (2.3.9)$$

and

$$mZ\frac{d^2}{dt^2}(\xi,\eta,\psi) = \frac{Q^2}{4\pi\varepsilon_2}\left[\frac{-bZ(\xi,\eta,\psi-1)}{Z^3\left[\xi^2+\eta^2+(\psi-1)^2\right]^{3/2}}+\frac{a(0,0,1)}{Z^2 4\psi^2}\right], \psi<0 \qquad (2.3.10)$$

Putting

$$\tau = t\sqrt{\frac{Q^2}{4\pi\varepsilon_1 mZ^3}} \quad \text{or}$$

$$t = \tau\sqrt{\frac{4\pi\varepsilon_1 mZ^3}{Q^2}}$$

Then equations (2.3.9) and (2.3.10) can be re-written as,

$$\frac{d^2}{d\tau^2}(\xi,\eta,\psi) = \left[\frac{-(\xi,\eta,\psi-1)}{\left[\xi^2+\eta^2+(\psi-1)^2\right]^{3/2}}\right.$$

$$\left.-\frac{a(\xi,\eta,\psi+1)}{\left[\xi^2+\eta^2+(\psi+1)^2\right]^{3/2}}+\frac{a(0,0,1)}{4\psi^2}\right], \psi>0 \qquad (2.3.11)$$

$$\frac{d^2}{d\tau^2}(\xi,\eta,\psi) = \delta\left[\frac{-b(\xi,\eta,\psi-1)}{\left[\xi^2+\eta^2+(\psi-1)^2\right]^{3/2}}+\frac{a(0,0,1)}{4\psi^2}\right], \psi<0 \qquad (2.3.12)$$

The Hamiltonian of the corresponding equation of motion is,

$$H = \frac{p_1^2 + p_2^2 + p_3^2}{2} + \left[-\frac{1}{\left[\xi^2 + \eta^2 + (\psi - 1)^2\right]^{1/2}} - \frac{a}{\left[\xi^2 + \eta^2 + (\psi + 1)^2\right]^{1/2}} + \frac{a}{4\psi} \right], \quad \psi > 0 \quad (2.3.13)$$

$$H = \frac{p_1^2 + p_2^2 + p_3^2}{2} + \left[-\frac{b\delta}{\left[\xi^2 + \eta^2 + (\psi - 1)^2\right]^{1/2}} + \frac{a\delta}{4\psi} \right], \quad \psi < 0 \quad (2.3.14)$$

Now let us put $\xi = \rho Cos\theta$ and $\eta = \rho Sin\theta$

So that $\xi^2 + \eta^2 = \rho^2$,

We have $p_1 = \dot{\xi}, p_2 = \dot{\eta}, p_3 = \dot{\psi}$

But $\dot{\xi} = \dot{\rho} Cos\theta - \rho Sin\theta\dot{\theta}$

$$\dot{\eta} = \dot{\rho} Sin\theta + \rho Cos\theta\dot{\theta}$$

$$\dot{\xi}^2 + \dot{\eta}^2 = \dot{\rho}^2 + \rho^2\dot{\theta}^2$$

Then the Hamiltonian becomes

$$H = \frac{\dot{\rho}^2 + \rho^2\dot{\theta}^2}{2} + \frac{\dot{\psi}^2}{2} + \begin{cases} -\frac{1}{\sqrt{\rho^2 + (\psi - 1)^2}} - \frac{a}{\sqrt{\rho^2 + (\psi + 1)^2}} + \frac{a}{4\psi}, \psi > 0 \\ -\frac{b\delta}{\sqrt{\rho^2 + (\psi - 1)^2}} + \frac{a\delta}{4\psi}, \psi < 0 \end{cases}$$

and hence

$$p_\rho = \frac{\partial H}{\partial p_\rho} = \dot{\rho} \quad \text{or} \quad \dot{\rho} = p_\rho$$

$$p_\theta = \frac{\partial H}{\partial p_\theta} = \rho^2\dot{\theta} \quad \text{or} \quad \dot{\theta} = \frac{p_\theta}{\rho^2}$$

$$p_\psi = \frac{\partial H}{\partial p_\psi} = \dot{\psi} \quad \text{or} \quad \dot{\psi} = p_\psi$$

The Hamiltonian is re-written as

$$H = \frac{p_\rho^{\,2}}{2} + \frac{p_\theta^{\,2}}{2\rho^2} + \frac{p_\psi^{\,2}}{2} + \begin{cases} -\dfrac{1}{\sqrt{\rho^2+(\psi-1)^2}} - \dfrac{a}{\sqrt{\rho^2+(\psi+1)^2}} + \dfrac{a}{4\psi}, \psi > 0 \\ -\dfrac{b\delta}{\sqrt{\rho^2+(\psi-1)^2}} + \dfrac{a\delta}{4\psi}, \psi < 0 \end{cases} \tag{2.3.15}$$

From the Hamilton's equation of motion,

$$\left.\begin{aligned} \dot{\theta} &= \frac{\partial H}{\partial p_\theta} = \frac{p_\theta}{\rho^2} \quad \text{and} \\ \dot{p}_\theta &= -\frac{\partial H}{\partial \theta} = 0 \end{aligned}\right\} \tag{2.3.16}$$

i.e. $p_\theta = L$, a constant

and the modified Hamiltonian is

$$H = \frac{p_\rho^{\,2}}{2} + \frac{p_\psi^{\,2}}{2} + \begin{cases} \dfrac{L^2}{2\rho^2} - \dfrac{1}{\sqrt{\rho^2+(\psi-1)^2}} - \dfrac{a}{\sqrt{\rho^2+(\psi+1)^2}} + \dfrac{a}{4\psi}, \psi > 0 \\ \dfrac{L^2}{2\rho^2} - \dfrac{b\delta}{\sqrt{\rho^2+(\psi-1)^2}} + \dfrac{a\delta}{4\psi}, \psi < 0 \end{cases} \tag{2.3.17}$$

The potential in equation 2.3.17 in terms of ρ and ψ, very near to the discontinuity, is plotted in fig.2.3.4.

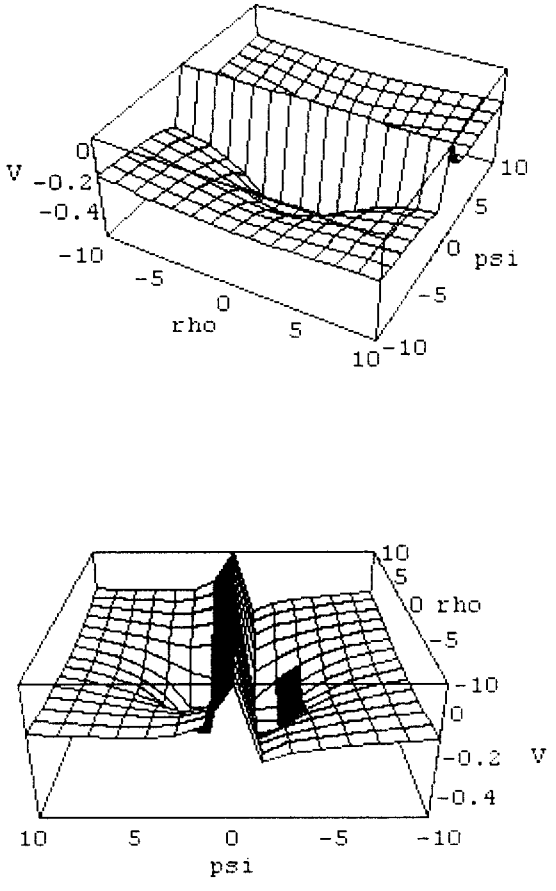

Fig. 2.3.4. The 3 D plot of the potential of the model dielectric viewed from different angles.

From equation (2.3.17) the Hamilton's equations of motion can be written as

$$\dot{\rho} = \frac{\partial H}{\partial p_\rho} = p_\rho$$

$$\dot{\psi} = \frac{\partial H}{\partial p_\psi} = p_\psi$$

$$\dot{p}_\rho = -\frac{\partial H}{\partial \rho} = -\begin{cases} -\dfrac{L^2}{\rho^3} + \dfrac{\rho}{\left[\rho^2 + (\psi-1)^2\right]^{3/2}} + \dfrac{a\rho}{\left[\rho^2 + (\psi+1)^2\right]^{3/2}}, \psi > 0 \\ -\dfrac{L^2}{\rho^3} + \dfrac{b\rho\delta}{\left[\rho^2 + (\psi-1)^2\right]^{3/2}}, \psi < 0 \end{cases}$$

$$\dot{p}_\psi = -\frac{\partial H}{\partial \psi} = -\begin{cases} \dfrac{(\psi-1)}{\left[\rho^2 + (\psi-1)^2\right]^{3/2}} + \dfrac{a(\psi+1)}{\left[\rho^2 + (\psi+1)^2\right]^{3/2}} - \dfrac{a}{4\psi^2}, \psi > 0 \\ \dfrac{b\delta(\psi-1)}{\left[\rho^2 + (\psi-1)^2\right]^{3/2}} - \dfrac{a\delta}{4\psi^2}, \psi < 0 \end{cases} \qquad (2.3.18)$$

The set of equations (2.3.18) can be numerically solved for different values of δ, L, ρ, ψ, p_ρ and p_ψ.

2.4. Stability Analysis for the model.

The Hamiltonian of the model is given by (from equation (2.3.17)),

$$H = \frac{p_\rho^2 + p_z^2}{2} + \frac{L^2}{2\rho^2} - \frac{1}{\sqrt{\rho^2 + (z-1)^2}} - \frac{a}{\sqrt{\rho^2 + (z+1)^2}} + \frac{a}{4z}, z > 0$$

$$H = \frac{p_\rho^2 + p_z^2}{2} + \frac{L^2}{2\rho^2} - \frac{b\delta}{\sqrt{\rho^2 + (z-1)^2}} + \frac{a\delta}{4z}, z < 0 \qquad (2.4.1)$$

Here we use z = ψ ≡ z/Z (i.e., we have replaced ψ by z, then the fixed charge is at (0,0,1)).

[The symbol ψ we preserve for quantum mechanical wave function considered in the next chapter]

Also we have $\delta = \frac{\varepsilon_1}{\varepsilon_2}, a = \frac{\delta - 1}{\delta + 1}, b = \frac{2}{1+\delta}$

If $\delta > 1$ then $a > 0$ and $a/4z > 0$ for $z > 0$ and for Lim. $(z \to 0+)$ $a/4z = +\infty$ then the wall $z=0$ is impenetrable for a particle placed in the region $z > 0$. If $\delta < 1$ then $a < 0$ and $a/4z > 0$ for $z<0$ and hence for Lim. $(z \to 0-)$ $a/4z = +\infty$. The wall is impenetrable for a particle placed in the region $z < 0$. The stability analysis is carried out for both $z < 0$ and $z > 0$ cases.

I. For $0 < \delta < 1$ and the particle placed in the region $z < 0$.

We use the second equation of (2.4.1)

The Hamilton's equations are

$$\left.\begin{aligned} \dot{\rho} &= \frac{\partial H}{\partial p_\rho} = p_\rho \\ \dot{z} &= \frac{\partial H}{\partial p_z} = p_z \\ \dot{p}_\rho &= -\frac{\partial H}{\partial \rho} = \frac{L^2}{\rho^3} - \frac{b\rho\delta}{\left[\rho^2 + (z-1)^2\right]^{3/2}} \\ \dot{p}_z &= -\frac{\partial H}{\partial z} = -\frac{b\delta(z-1)}{\left[\rho^2 + (z-1)^2\right]^{3/2}} + \frac{a\delta}{4z^2} \end{aligned}\right\} \qquad (2.4.2)$$

Now consider the steady state ρ^* and z^* such that

$$p_\rho^* = 0, p_z^* = 0 \quad \dot{p}_\rho^* = 0, \dot{p}_z^* = 0$$

Let us put $z^* = -\xi$ (where $\xi > 0$) then from last two of (2.4.2) we get

$$\frac{b\delta\rho^{*4}}{\left[\rho_*^2 + (1+\xi)^2\right]^{3/2}} = L^2 \qquad (2.4.3a)$$

$$\frac{b(1+\xi)}{\left[\rho_*^2 + (1+\xi)^2\right]^{3/2}} = \frac{\alpha}{4\xi^2} \qquad (2.4.3b)$$

where $\alpha = -a$.

Dividing (2.4.3a) by (2.4.3b) and rearranging we get

$$\rho^{*4} = \frac{4L^2\xi^2(1+\xi)}{\alpha\delta} \qquad (2.4.4)$$

Substituting for ρ^{*4} and ρ^{*2} from (2.4.4) in (2.4.3a) we get

$$\frac{4h\xi^2(1+\xi)}{\alpha} = \left[\frac{2L\xi\sqrt{(1+\xi)}}{\sqrt{\alpha\delta}} + (1+\xi)^2\right]^{3/2} \qquad (2.4.5)$$

Equation (2.4.5) is of the form $f_1(\xi) = f_2(\xi)$ where f_1 and f_2 are monotonically increasing functions of ξ.

From (2.4.5), $f_1(0)=0$

$$f_1(\xi) \sim \frac{4h}{\alpha}\xi^3 \quad \text{, for large } \xi$$

$f_2(0)=1$

$$f_2(\xi) \sim \xi^3 \quad \text{, for large } \xi$$

Since $h = \frac{2}{1+\delta}, \alpha = -a = \frac{1-\delta}{1+\delta}$

$$\frac{4h}{\alpha} = \frac{8}{1-\delta} > 0$$

Further $f_1(\xi) = f_2(\xi)$ for some $\xi > 0$.

That is, there exists one and only one ξ satisfying (2.4.5).Therefore there exists one and only one fixed point (ρ^*, z^*) with $z^* < 0$.

Linearising (2.4.2) near the fixed point (ρ^*, z^*) (i.e., by putting $\rho = \rho^*+\delta\rho$, and $z = z^*+\delta z$ in eq.2.4.2) we get the stability matrix as

$$\frac{d}{dt}\begin{bmatrix}\delta\rho\\ \delta z\\ \delta p_\rho\\ \delta p_z\end{bmatrix} = \begin{bmatrix}0 & 0 & 1 & 0\\ 0 & 0 & 0 & 1\\ -A & -C & 0 & 0\\ -C & -B & 0 & 0\end{bmatrix}\begin{bmatrix}\delta\rho\\ \delta z\\ \delta p_\rho\\ \delta p_z\end{bmatrix} \qquad (2.4.6)$$

Where

$$\left.\begin{aligned} A &= \frac{\partial^2 H}{\partial \rho^2} = \frac{3L^2}{\rho^4} + \frac{b\delta}{\left[\rho^2+(z-1)^2\right]^{3/2}} - \frac{3b\delta\rho^2}{\left[\rho^2+(z-1)^2\right]^{5/2}} \\ B &= \frac{\partial^2 H}{\partial z^2} = \frac{b\delta}{\left[\rho^2+(z-1)^2\right]^{3/2}} - \frac{3b\delta(z-1)^2}{\left[\rho^2+(z-1)^2\right]^{5/2}} + \frac{a\delta}{2z^3} \\ C &= \frac{\partial^2 H}{\partial \rho \partial z} = -\frac{3b\rho\delta(z-1)}{\left[\rho^2+(z-1)^2\right]^{5/2}} \end{aligned}\right|_{(\rho^*,z^*)} \qquad (2.4.7)$$

The eigenvalue equation for the stability matrix in (2.4.6) is given by

$\lambda^4 + (A+B)\lambda^2 + AB - C^2 = 0$, the solution of which is

$$\lambda^2 = \frac{-(A+B) \pm \sqrt{(A+B)^2 - 4(AB-C^2)}}{2} \qquad (2.4.8)$$

The system is unstable if $\mathrm{Re}(\lambda^2) > 0$. The possibilities are

(i) $A+B < 0$ irrespective of the sense of $AB - C^2$

(ii) $A+B > 0$ and $AB - C^2 < 0$.

II. For $\delta > 1$ and the particle placed in the region $z > 0$.

From first equation of (2.4.1) we get

$$\left.\begin{aligned} \dot{\rho} &= \frac{\partial H}{\partial p_\rho} = p_\rho \\ \dot{z} &= \frac{\partial H}{\partial p_z} = p_z \\ \dot{p}_\rho &= -\frac{\partial H}{\partial \rho} = \frac{L^2}{\rho^3} - \frac{\rho}{\left[\rho^2+(z-1)^2\right]^{3/2}} - \frac{a\rho}{\left[\rho^2+(z+1)^2\right]^{3/2}} \\ \dot{p}_z &= -\frac{\partial H}{\partial z} = -\frac{(z-1)}{\left[\rho^2+(z-1)^2\right]^{3/2}} - \frac{a(z+1)}{\left[\rho^2+(z+1)^2\right]^{3/2}} + \frac{a}{4z^2} \end{aligned}\right\} \qquad (2.4.9)$$

Now consider the steady state ρ^* and z^* such that

$p_\rho^* = 0, p_z^* = 0$, also we have $\dot{p}_\rho^* = 0, \dot{p}_z^* = 0$

From third equation of (2.4.9), L=0 and $\dot{p}_\rho^* = 0$ implies

$\rho^* = 0$ (2.4.10)

Then from fourth equation of (2.4.9)

$$\frac{(1-z^*)}{|1-z^*|^3} - \frac{a(1+z^*)}{|1+z^*|^3} + \frac{a}{4z^{*2}} = 0 \qquad (2.4.11)$$

We will get different stability conditions for $0 < z^* < 1$ and for $z^* > 1$.

Possibility 1, $0 < z^* < 1$,

Then $1-z^* > 0$ or $|1-z^*| = 1-z^*$.

Now (2.4.11) can be written as

$$\frac{1}{(1-z^*)^2} - \frac{a}{(1+z^*)^2} + \frac{a}{4z^{*2}} = 0$$

Taking common denominator and rearranging we get

$$f_1(z^*) = (1-\frac{3}{4}a)z^{*4} + 2(1+a)z^{*3} + (1-\frac{3}{2}a)z^{*2} + \frac{a}{4} = 0 \qquad (2.4.12)$$

$$1-\frac{3}{4}a = 1-\frac{3}{4}\frac{(\delta-1)}{(\delta+1)} = \frac{7+\delta}{4(\delta+1)} > 0$$

$$1-\frac{3}{2}a = 1-\frac{3}{2}\frac{(\delta-1)}{(\delta+1)} = \frac{5-\delta}{2(\delta+1)}$$ is > 0 for $\delta < 5$ and < 0 for $\delta > 5$.

That is for $1 < \delta < 5$, there is no fixed point with $0 < z^* < 1$.

For $\delta > 5$, from (2.4.12) we get

$$f_1(0) = \frac{a}{4} > 0$$

$$f_1(1) = 1-\frac{3}{4}a + 2(1+a) + (1-\frac{3}{2}a) + \frac{a}{4} = 4 > 0$$

i.e., for $\delta > 5$ also there is no root (hence no fixed point) in [0,1].

To summerise, there is no nontrivial fixed point for L=0 and for $a > 0$ in the region $0 < z < 1$.

Possibility 2, $z^* > 1$

Then $1-z^* = -(z^*-1)$ and $|1-z^*| = (z^*-1)$

Then from (2.4.11) we can write

$$-\frac{1}{(z^*-1)^2}-\frac{a}{(z^*+1)^2}+\frac{a}{4z^{*2}}=0$$

Rearranging we get

$$(-1-\frac{3}{4}a)z^{*4}-2(1-a)z^{*3}-(1+\frac{3}{2}a)z^{*2}+\frac{a}{4}=0 \quad \text{or}$$

$$f_2(z^*)=(1+\frac{3}{4}a)z^{*4}+2(1-a)z^{*3}+(1+\frac{3}{2}a)z^{*2}-\frac{a}{4}=0 \qquad (2.4.13)$$

From (2.4.13) we get

$$f_2(0)=-\frac{a}{4}<0$$

$$f_2(1)=1+\frac{3}{4}a+2(1-a)+(1+\frac{3}{2}a)-\frac{a}{4}=4>0$$

That is there is no value of z > 1 that satisfy the steady state condition for L=0* (from the above equation 0 < z* < 1 is a possible solution which can not be accepted, since as per *possibility 2, we have z* > 1*).

L ≠ 0 and for z > 0

From (2.4.9) by putting the steady state conditions $p_\rho^* = 0, p_z^* = 0$, we get,

$$\left.\begin{aligned}\frac{\rho^{*4}}{\left[\rho^{*2}+(z^*-1)^2\right]^{3/2}}+\frac{a\rho^{*4}}{\left[\rho^{*2}+(z^*+1)^2\right]^{3/2}}&=L^2\\ \frac{(z^*-1)}{\left[\rho^{*2}+(z^*-1)^2\right]^{3/2}}+\frac{a(z^*+1)}{\left[\rho^{*2}+(z^*+1)^2\right]^{3/2}}&=\frac{a}{4z^{*2}}\end{aligned}\right\} \qquad (2.4.14)$$

From equation (2.4.9) linearising we get the stability equation as

$$\frac{d}{dt}\begin{bmatrix}\delta\rho\\ \delta z\\ \delta p_\rho\\ \delta p_z\end{bmatrix}=\begin{bmatrix}0 & 0 & 1 & 0\\ 0 & 0 & 0 & 1\\ -A & -C & 0 & 0\\ -C & -B & 0 & 0\end{bmatrix}\begin{bmatrix}\delta\rho\\ \delta z\\ \delta p_\rho\\ \delta p_z\end{bmatrix}, \text{ where}$$

$$A = \frac{\partial^2 H}{\partial \rho^2} = \frac{3L^2}{\rho^4} + \frac{1}{\left[\rho^2 + (z-1)^2\right]^{3/2}} + \frac{a}{\left[\rho^2 + (z+1)^2\right]^{3/2}} - \frac{3\rho^2}{\left[\rho^2 + (z-1)^2\right]^{5/2}}$$

$$- \frac{3a\rho^2}{\left[\rho^2 + (z+1)^2\right]^{5/2}}$$

$$B = \frac{\partial^2 H}{\partial z^2} = \frac{1}{\left[\rho^2 + (z-1)^2\right]^{3/2}} + \frac{a}{\left[\rho^2 + (z+1)^2\right]^{3/2}} - \frac{3(z-1)^2}{\left[\rho^2 + (z-1)^2\right]^{5/2}}$$

$$- \frac{3a(z+1)^2}{\left[\rho^2 + (z+1)^2\right]^{5/2}} + \frac{a}{2z^3}$$

$$C = \frac{\partial^2 H}{\partial \rho \partial z} = -\frac{3\rho(z-1)}{\left[\rho^2 + (z-1)^2\right]^{5/2}} - \frac{3a\rho(z+1)}{\left[\rho^2 + (z+1)^2\right]^{5/2}}$$

$|_{(\rho^*, z^*)}$

The eigenvalue equation of the above matrix is

$\lambda^4 + (A+B)\lambda^2 + AB - C^2 = 0$, whose solution is given by (2.4.15)

$$\lambda^2 = \frac{-(A+B) \pm \sqrt{(A+B)^2 - 4(AB - C^2)}}{2} \quad (2.4.16)$$

The numerical calculation of the eigenvalue of the stability matrix (equation 2.4.16) shows that for z > 0, the system (2.4.1) is stable (λ^2 and hence λ have only negative values) for all values of δ (here we tested for $0 < \delta < 10$) and for angular momentum L < 1 (scaled) , near the fixed points. That is the steady state we obtained is $\rho^* = 0.09$, $z^* = 1.0$. In these cases the trajectory is neutrally stable and we may expect other fixed points far away from these, which are unstable (as in Henon-heils system). Here we study the system numerically with initial conditions away from steady state and indeed found some initial conditions lead to chaos.

2.5.Numerical studies of the model

We have studied the model derived in sec.2.2.numerically and some of the interesting results are reported here. The Hamiltonian of the system is given by (2.4.1)

We have studied the dynamics of this model for various values of the parameters δ and L (the angular momentum). However, the results are being presented here only for δ=3 and L=0.3. We have solved the Hamilton's equations (2.4.2) and (2.4.9) for various

initial values of (ρ, z, p_ρ , p_z). In general, initial conditions with sufficiently small values of ρ and z lead to irregular trajectories.

2.5.1.Time series and Lyapunov exponents.

We have calculated the Lyapunov Characteristic Exponents (LCE) for the model for different initial conditions and different parameter values δ and L. the LCE is calculated using the well known Wolf's algorithm [33] and also using the recently developed QR algorithm [34] (see appendix). The LCE calculated for different initial conditions are plotted in figures 2.5.1 and 2.5.2.

In fig.2.5.1, we have plotted the four LCEs for the initial condition (i) 0.23,0.18,0.1,0.1 and for δ = 3 ,L=0.3. Out of the four, one approaches positive value and the other negative. Other two LCEs approaches zero asymptotically. Since the system have a positive LCE, we expect chaos for this value of initial conditions. We also calculated the LCE for the initial condition (ii) (2.5,12.0, 0.3842077627766117, 0.0) for the same value of δ and L. The results are plotted in fig.2.5.2. Here also we get a positive, a negative and two zero LCEs. But the positive Lyapunov exponent obtained here is negligibly small compared to the positive LCE in fig.2.5.1. A comparison of these two positive LCEs is given in fig.2.5.3. From these calculations of LCEs we conclude that for δ =3, L=0.3 and initial condition (2.5,12.0, 0.3842077627766117, 0.0) the system behaves regularly.

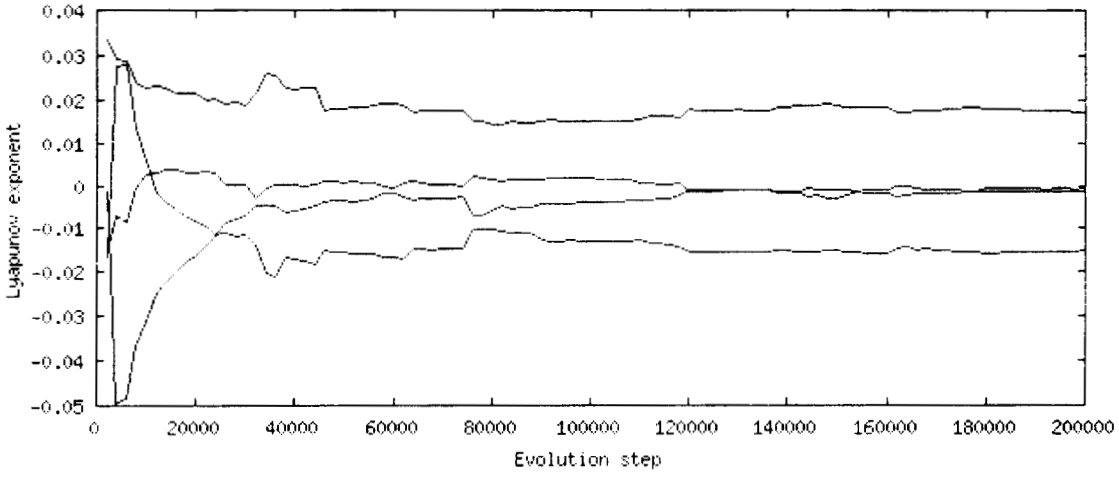

Fig.2.5.1. The Four Lyapunov exponents calculated for the model using QR algorithm for the initial conditions (0.23, 0.18, 0.1, 0.1) and for δ=3 and L=0.3.

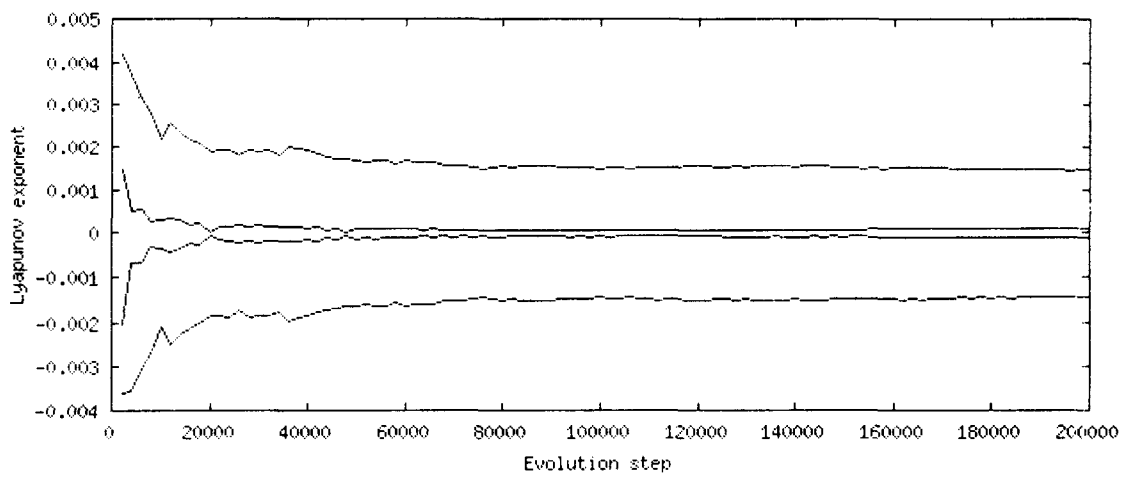

Fig.2.5.2. The Four Lyapunov exponents calculated for the model using QR algorithm for the initial conditions (2.5,12.0, 0.3842077627766117, 0.0) and for δ=3 and L=0.3.

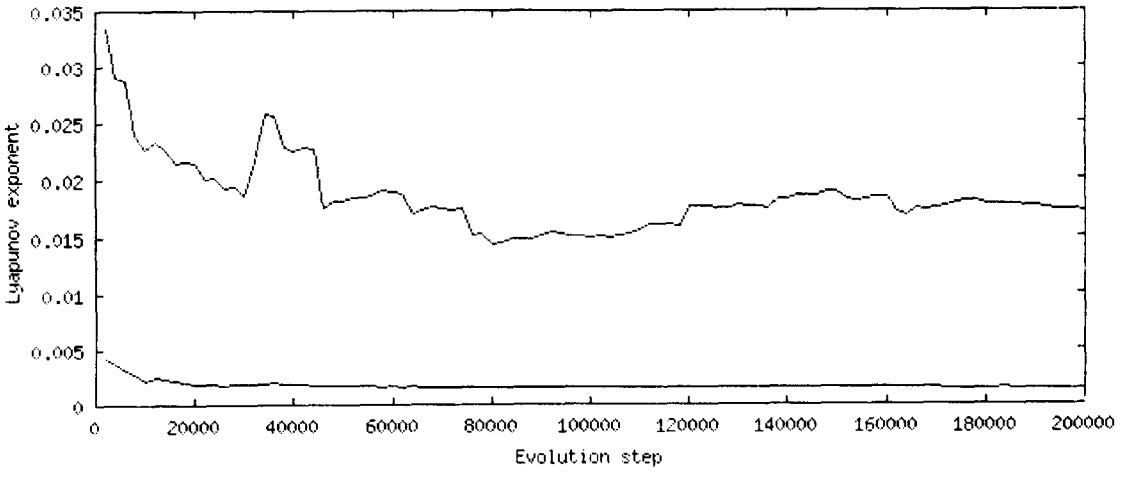

Fig.2.5.3. The positive LCEs from fig.2.5.1 (top) and from fig.2.5.2 (bottom).

The evolution of the system is studied by numerically solving equation 2.4.9 (for z > 0). The numerical calculations are done using the adaptive Runge-Kutta algorithm (with an accuracy of 1 part in 10^{10} per time step of integration). For getting an idea of how two nearby trajectories evolve, we start with two arbitrarily close initial conditions (with an initial separation of 10^{-6} units) and the trajectory is calculated. For the initial condition (i) (used in fig.2.5.1), the time series (for the variable ρ) for two arbitrarily close initial conditions is given in fig.2.5.4. Here we could see that, initially the two follow the same path, but after a few cycles they are widely separated. For this initial condition since one of the Lyapunov exponent is positive and also the time series separates widely (sensitively dependent on initial conditions), we can confirm chaos in the system. The relative distance between the two trajectories also suggest exponential divergence (fig.2.5.5) which confirms chaotic behaviour.

To compare this result with that of the regular case, we have done the same analysis for the initial condition (ii) (used in fig.2.5.2). Here the time series for the variable ρ for two nearby initial conditions exactly superimpose (see fig.2.5.6). The relative distance between trajectories does not increase exponentially (fig.2.5.7). This can be interpreted as a regular behaviour, which also is expected from the values of Lyapunov exponents (see fig.2.5.2. , here all Lyapunov exponents asymptotically tend to zero). The trajectory in this case may reside on an invariant torus in phase space.

The ρ vs. z plot for the two initial conditions (i) and (ii) are given in figure (2.5.8a and b). The sensitive dependence on initial condition is clearly seen in figure 2.5.8a which corresponds to the initial condition (i) giving chaos (Solid line and dotted line are for two arbitrarily close initial conditions).

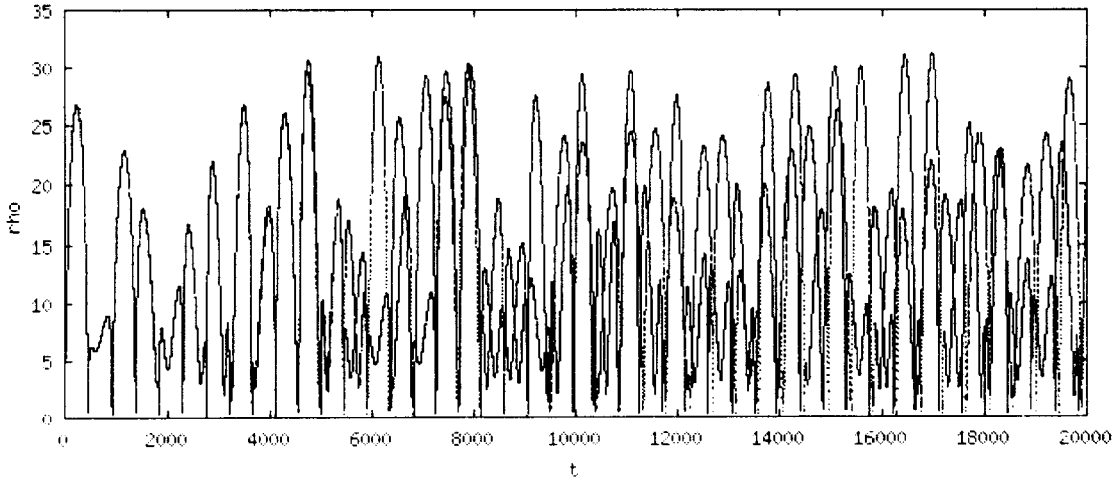

Fig.2.5.4. ρ as a function of time for the model with δ =3 and L=0.3, with initial condition ρ=0.23, z=0.18, p_ρ=0.1, p_z=0.1 (solid line) and another initial condition at a distance of 10^{-6} (dotted)

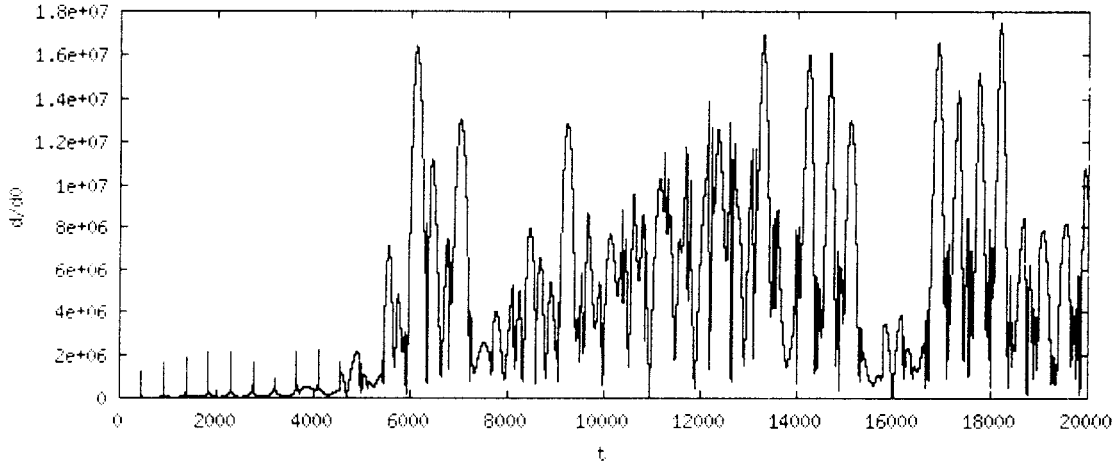

Fig.2.5.5. Relative distance d_t/d_0 between two trajectories shown in Fig.2.5.4

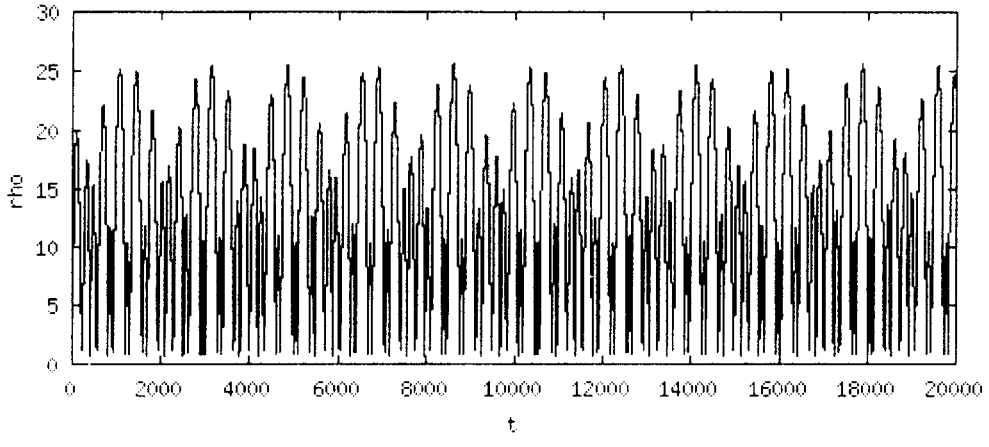

Fig.2.5.6. ρ as a function of time for the model with δ =3 and L=0.3, with initial condition ρ=2.5, z=12.0, p_+=, 0.3842077627766117, p_-=0.0

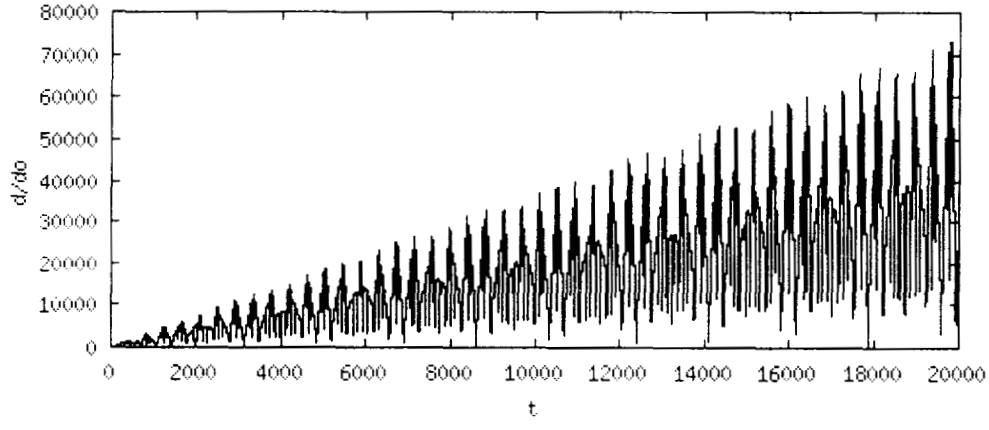

Fig.2.5.7. Relative distance d_1/d_0 between two trajectories shown in Fig.2.5.6

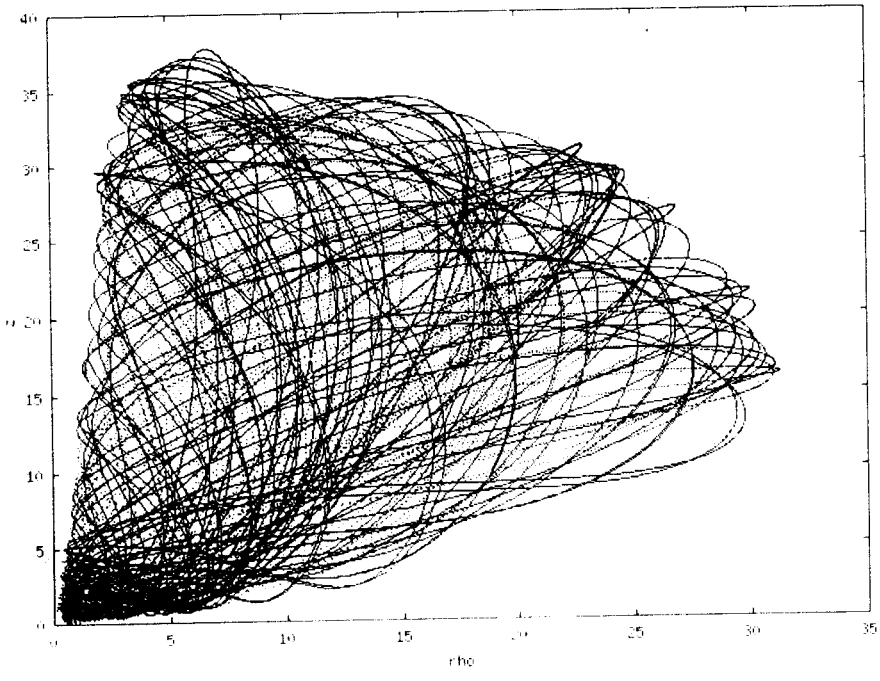

Fig.2.5.8a The ρ vs. z plot for the initial condition (i) (corresponds to chaos)

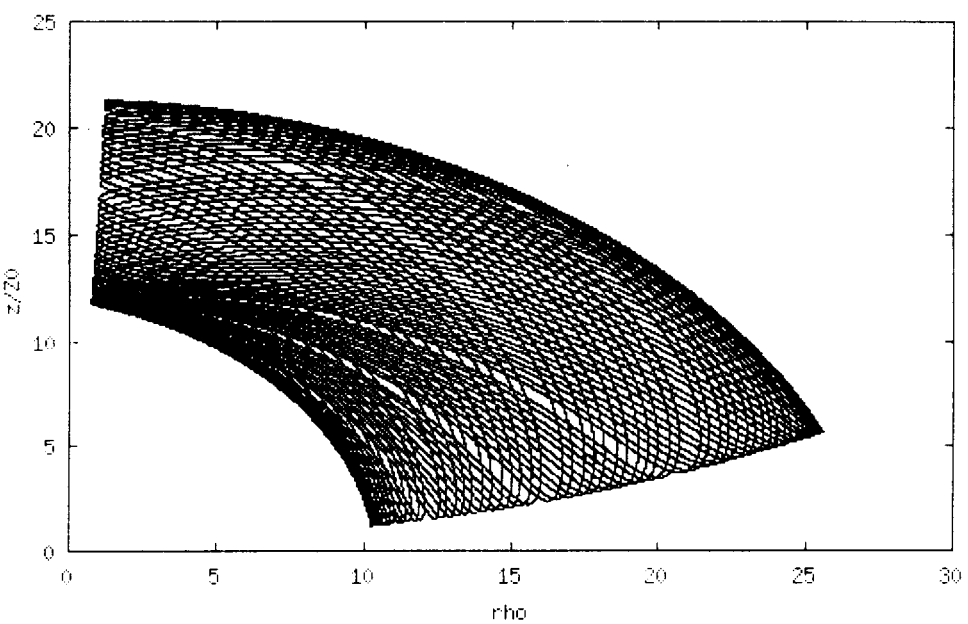

Fig.2.5.8b. The ρ vs. z plot for the initial condition (ii) (corresponds to regular solution)

2.5.2. Poincare Surface of section.

In order to get a clear picture of the manner in which regular and irregular trajectories are organized in phase space, we study the poincare surface of sections. We have used the parameter values $\delta = 3$ and $L = 0.3$ in the model. The poincare section for different surfaces were tried and we finally fixed a surface which cut the orbits at $\rho = 2.5$, which appears to be in a better shape. The surface of sections is plotted for the same parameter values and for different initial conditions but for the same energy. For some initial conditions we obtained closed curves, which are cross sections of invariant tori depicting regular motion. For some other initial condition scattered points are obtained which represents a destroyed torus and corresponding to chaotic motion. The initial conditions (a) (0.23, 0.18, 0.1,0.1) gives chaotic motion and (b) (2.5, 8.0, 0.5103819756739857, 0.0), (c) (2.5, 10.0, 0.4397460977022776, 0.0) and (d) (2.5, 12.0, 0.3842077627766117, 0.0) give regular motion. The poincare sections for all these initial conditions are plotted in fig.2.5.9. Here we choose the $z - p_z$ plane to cut the trajectory at $\rho = 2.5$.

Here also we could see that initial conditions corresponding to (a) give chaotic solution and that corresponding to (d) an invariant torus, which represent regular motion. This agrees with our earlier observations in time series and Lyapunov exponents.

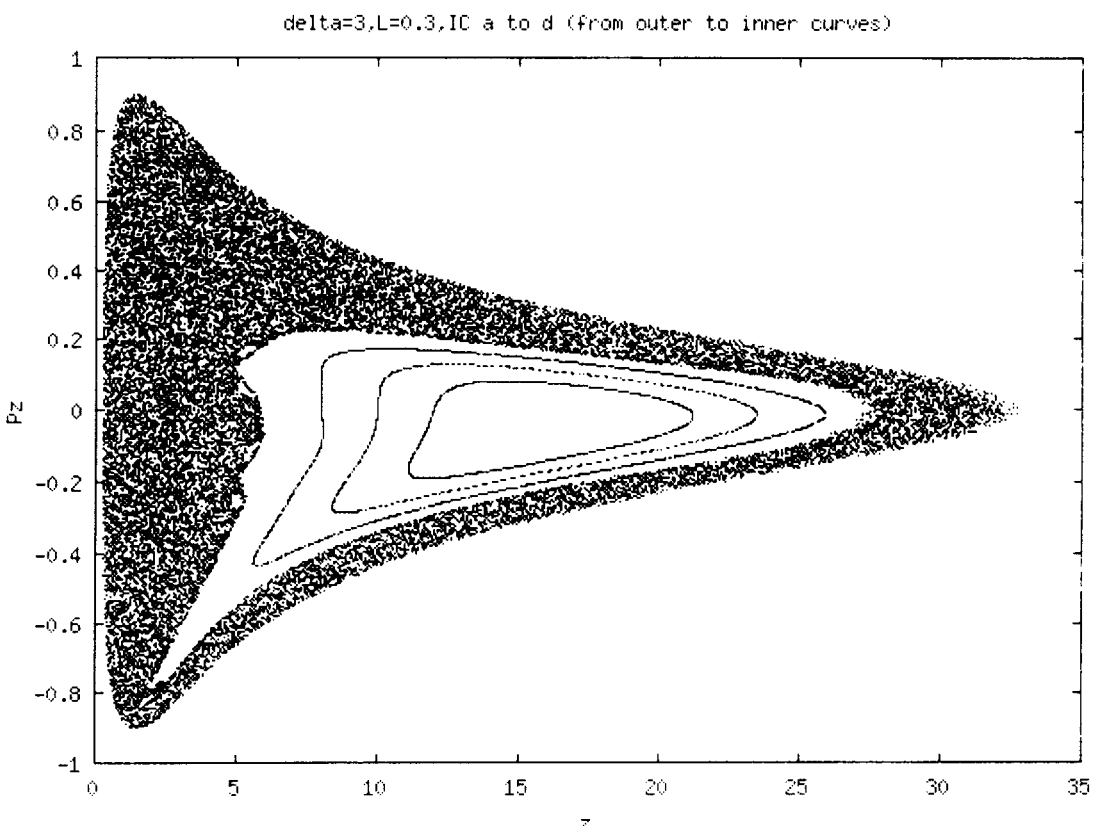

Fig.2.5.9. Poincare sections corresponding to the initial conditions (a) 0.23, 0.18, 0.1, 0.1 (outer scattered points), (b) 2.5, 8.0, 0.5103819756739857, 0.0 (second closed curve), (c) 2.5, 10.0, 0.4397460977022776, 0(third closed curve) and (d) 2.5, 12.0, 0.3842077627766117, 0.0 (inner most closed curve).

2.5.3. Poincare Return time.

The histogram of the time between successive intersections with the Poincare section is shown in Fig. 2.5.10. for the initial conditions (a) and (d) in the upper and lower panels, respectively. We see that a range of values are possible for the return times, with a distribution having two broad peaks for the chaotic situations, whereas two extremely sharp peaks are seen for the regular motion which appears to be quasiperiodic.

The return time histogram studied for Henon-Heils is found to be basically different from that of our model. In Henon-Heils the distribution is not bimodal, but looks almost like a Guassian distribution, with peak observed at the average value of return time. For the chaotic case (E=1/6) the distribution is broadened compared to the quasiperiodic case (E=1/12), with peaks observing almost at the same value for both cases. Earlier studies [Gilmore, 1998][35] in this area suggest that the return time distribution for stochastic data (which is almost uniformly distributed) is different from that of chaotic data (which shows a number of peaks in it).

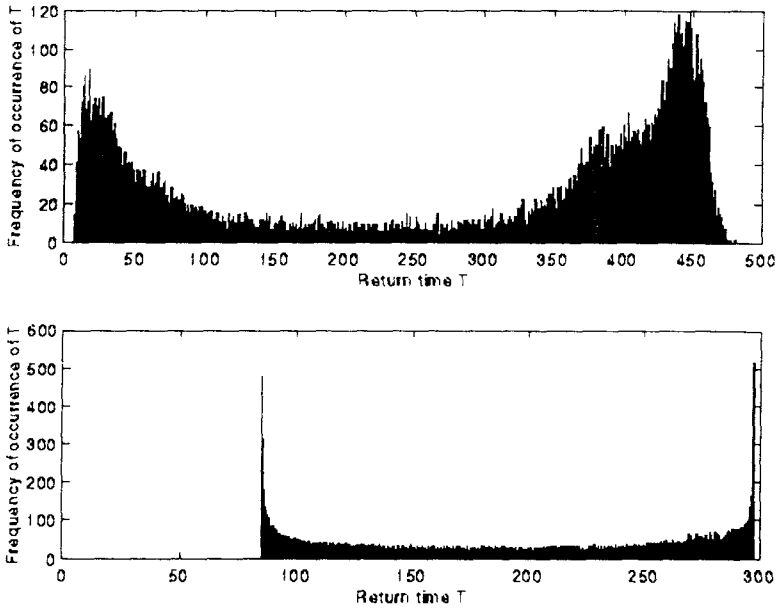

Fig. 2.5.10. Histogram of the time between successive intersections of the Poincare section for the initial conditions (a) and (d) shown upper and lower panels, respectively.

2.5.4. Power spectra of the time series.

The power spectra of the time series for ρ are shown in Fig.2.5.11a. for the initial conditions (a) and Fig.2.5.11b. for the initial condition (d). The time series consists of 1048576 points at a time step of 0.1. The dark plot corresponds to one single time series and the lighter one corresponds to the power spectrum averaged over 100 such series obtained by continuing the integration of the equation of motion. Clearly the initial condition (a) gives a broadband spectrum signaling chaos, in contrast to the sharp peaks for the initial condition (d) corresponding to quasiperiodic motion. There are, however, difference in the nature of power spectrum for a Hamiltonian system and dissipative systems. In contrast to the exponential decay [P(f)~exp(-constant x f)], for small frequencies, seen in dissipative systems, the decay of power spectrum seen here is much slower.

There seems to be a difference in the decay of power spectrum for our model and that for the well known Henon-Heils model discussed in chapter 1 (fig.1.6.8.). The fall of power spectrum in the small frequency range is faster in Henon-Heils (for example, when E=1/6, corresponding to chaos) than in our model. But the shape of the curve in the high frequency range is almost the same in both cases. Probably, the power spectrum for different Hamiltonian systems may behave differently.

We have also tested the power spectrum for its dependence on the number of data generated numerically (N) and on the interval of each data points (△t). As observed by Valsakumar et al. [36] the power spectrum of our model also is found to depend on N and △t, which suggests that the data in the time series is Bandwidth limited and there is aliasing (i.e., the power spectrum depends on Nyquist frequency or sampling time △t) observed (figs. 2.5.12 and 2.5.13).

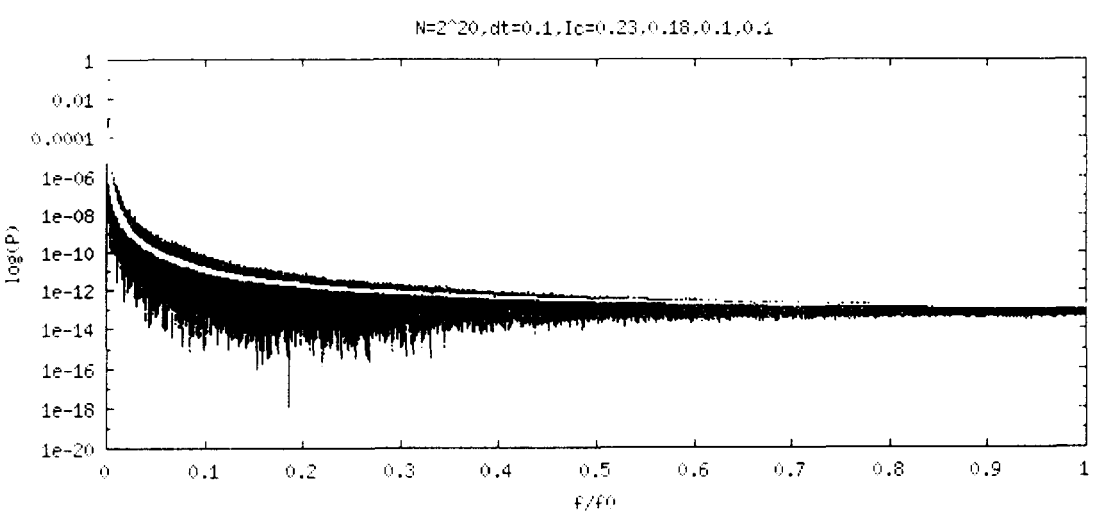

Fig. 2.5.11a. Power spectra of the time series for ρ, for the initial conditions (a) given in fig.2.5.9. The inner lighter plot gives the averaged power spectrum.

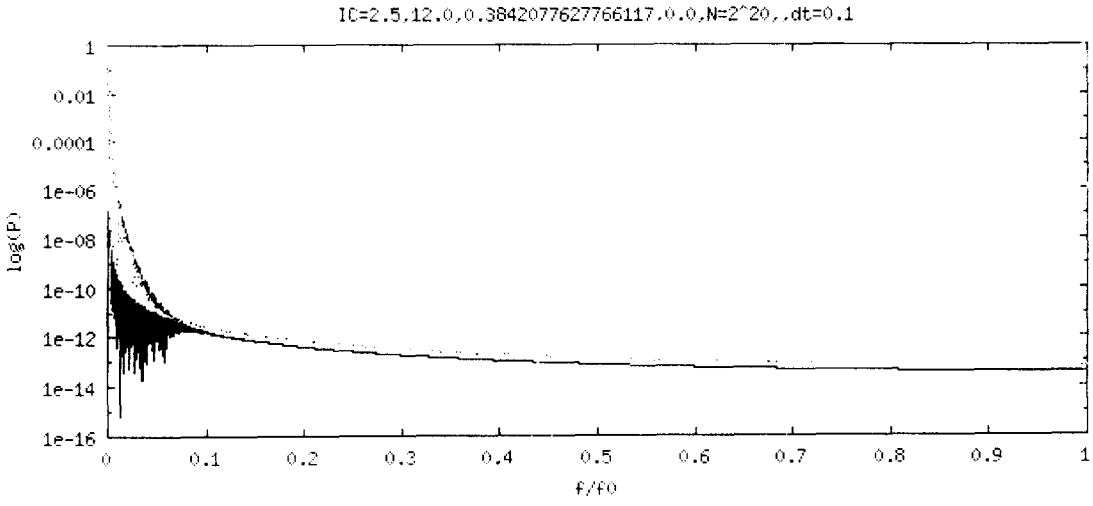

Fig. 2.5.11b. Power spectra of the time series for ρ, for the initial conditions (d) given in fig.2.5.9. The inner lighter plot gives the averaged power spectrum.

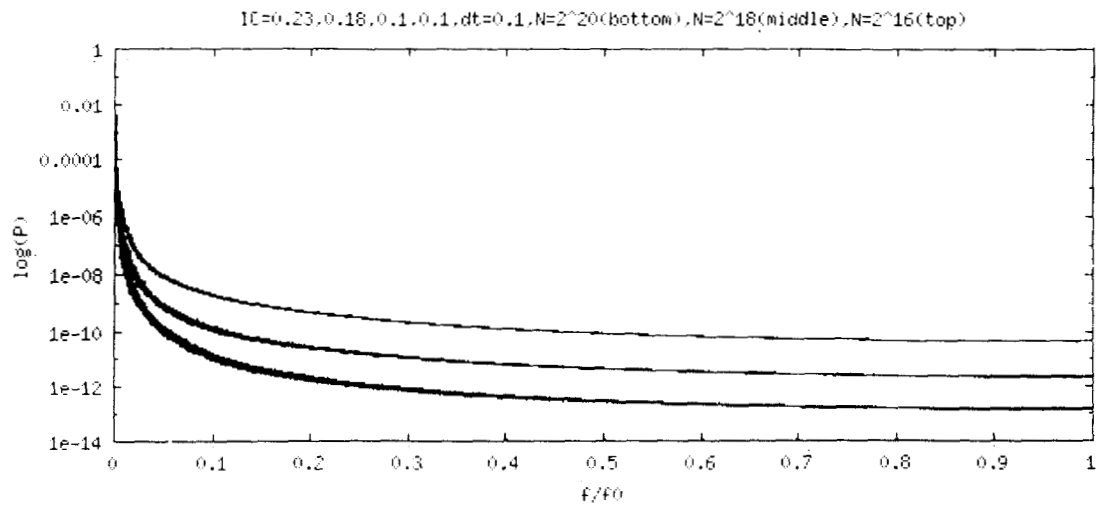

Fig.2.5.12. The variation of power spectra with number of data (N) in the time series.

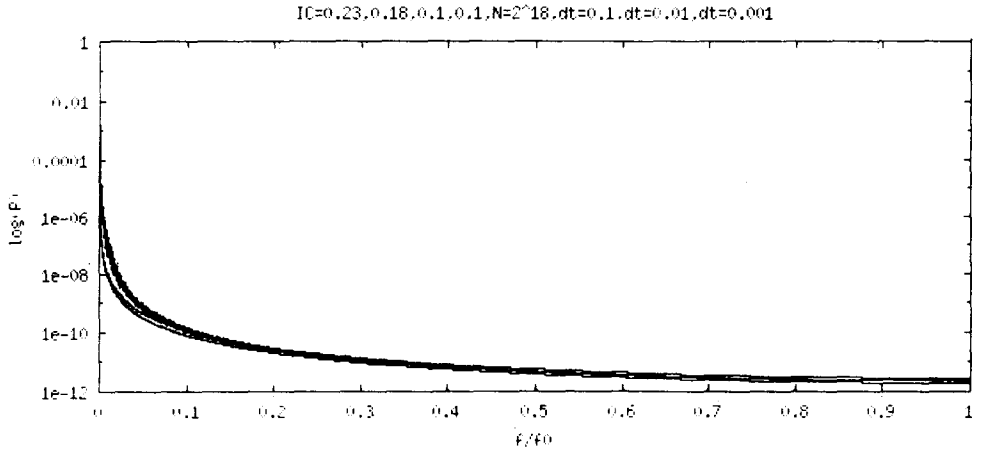

Fig.2.5.13. The variation of power spectra with sampling interval (Δ t).

When the number of data in the time series tends to infinity ($N \rightarrow \infty$), the power spectrum of the system goes to zero suggesting that in numerical processes there is always a *finite size effect* will be there (Fig.2.5.12.). In other words, the calculated power spectrum represents the true power spectrum only when the number of data is infinity. Fig.2.5.13 shows that the power spectrum depends on Nyquist frequency ($f_c=1/(2\Delta t)$) or sampling time Δt also. This effect can be minimized if the sampling interval is made infinitesimally small ($\Delta t \rightarrow 0$). Since during a numerical computation or a measurement, we can not make the sampling time zero, the power spectrum calculated from the data will be different from the true power spectrum. The effect due to frequency greater than Nyquist frequency will be reflected (or folded back) in the calculated power spectrum (this is called *aliasing*)[36]

In the next chapter we study the quantum mechanical signature of the model when it shows regular as well as chaotic behaviour.

CHAPTER 3

QUANTUM MECHANICAL CALCULATIONS OF THE MODEL.

3.1.Introduction.

The description of physical systems via classical mechanics as embodied in Hamiltons equations may be viewed as an approximation to the exact description of quantum mechanics. Depending on the relevant time, length and energy scales appropriate to a given situation, one of these descriptions may be most efficacious. If the typical wavelength in the quantum problem is very small compared to all length scales of the system, then classical description will be good. The field of study, which addresses problems related to quantum nature of classically chaotic system is called **quantum chaos**. Quantum chaos questions are of great practical importance because of the many physical systems that exist in sub atomic region [22,28].

There are several major differences between classical and quantum mechanics.

In contrast to classical mechanics (where a classical description is only necessary if the system becomes chaotic in time) quantum mechanics allows only statistical predictions. Although Schrodinger equation is linear in ψ and can be solved exactly (say) for a harmonic oscillator with the result that ψ depends regularly on time (i.e., no chaos), this does not mean that the motion is completely deterministic, since $|\psi(x, t)|^2 dx$ is only the probability to find an electron in a region Δx around x.

Because of Heisenberg's uncertainty principle $\Delta p. \Delta q > h/2$ there are no trajectories in quantum mechanics (if one measures q with precision Δq, one disturbs the momentum by Δp). Therefore the *characterization of chaos based on the exponentially fast separation of nearby trajectories* becomes useless for quantum systems.

The uncertainty principle implies also that points in 2N- dimensional phase-space within a volume h^N can not be distinguished i.e., the phase-space becomes coarse grained. This means that regions in phase-space in which the motion is classically chaotic

but which have volumes smaller than h^N are not seen in quantum mechanics, and for the corresponding quantum system we expect a regular behaviour in time. Thus a finite value of Planck's constant tends to suppress chaos. On the other hand, the limit $h \rightarrow 0$ becomes difficult (for quantum systems which have a classical counterpart which displays chaos) because if h becomes smaller, more and more irregular structures will appear.

We can assign deterministic diffusion as an indicator of chaos. Even though classical system shows deterministic diffusion, its quantum version does not. Instead, one finds quantum resonance or almost periodicity [37]. This almost periodicity is similar to the quasiperiodic motion in classical systems. In short no quantum system seems to exist which exhibits deterministic chaos. But there is of course a difference in the behaviour of quantum systems with a chaotic classical counterpart and those (quantum systems) with a regular classical limit.

McDonald and Kaufmann[38] calculated numerically the wave functions and eigenvalue spectra of a free particle in a stadium and in a circular disc by solving the Schrodinger equation for a free particle in 2-D

$$\nabla^2\psi = E\,\psi$$

with boundary condition $\psi(x, y) = 0$ at the walls, which clearly shows the difference between quantum behaviour of a classically chaotic system and an integrable system. The distribution of eigenvalue level spacing is maximum for $\Delta E = 0$ for the integrable system and for chaotic system the maximum occurs at $\Delta E \neq 0$, which is an indication of level repulsion in classically chaotic system [39]. The level repulsion seems to be a characteristic feature of quantum system whose classical limit shows chaos [40,41]. It is related to the fact that no symmetries exist in these systems i.e., there are no degeneracies (and no selection rules which prevent mutual interaction of levels) such that $\text{Lim.}(\Delta E)\rightarrow 0 \;\; N(\Delta E) = 0$. Several theoretical explanations for the phenomena have

been offered, and an interesting connection to Random Matrix Theory (which is used to explain level repulsion in Nuclear spectra) has been suggested [40,41,42]. Also the distribution of Level spacing is related to the eigenvalue spectrum of the quantum version of the Liouville operator **L** because

$\hat{L}|n\rangle\langle m| \propto \left[\hat{H},|n\rangle\langle m|\right] = (E_n - E_m)|n\rangle\langle m|$, where H is the Hamiltonian operator and $|n>, |m>$ are its eigen vectors..

In addition to the conventional description of chaotic motion of quantum systems in terms of level repulsion in the nearest neighbour spacing of energy spectrum and Random Matrix Theory, we also have another description in terms of *Bohmian Mechanics*. In the *Quantum Theory of Motion* (Q.T.M.) described by David Bohm[43,44,45,46] we can even define a trajectory of a particle, whose center can be taken as the center of the wave function. So the sensitive dependence on initial conditions can also be seen in this framework. Hence the quantum mechanical study of classically chaotic systems is possible in Q.T.M. without calculating the energy spectrum etc.

In the next section we give this theory (QTM) and its applications to classically chaotic systems. We use this theory to calculate the evolved wave function, the relative separation of two trajectories started from two arbitrarily close points etc. for the well known model-the Henon-Heils model. The results obtained agree with that reported in literature [52]. The QTM is also used to characterize the model described in this thesis-charged particle motion near a dielectric discontinuity- which is classically chaotic for certain values of initial conditions and parameters.

3.2 Quantum theory of motion and signature of chaos.

The correspondence between the classical and quantum world has been an important research subject since the advent of quantum mechanics. This study becomes more intriguing when the classical motion is chaotic. A causal interpretation of quantum

mechanics in terms of the Quantum Theory of Motion (QTM) [43,44] in the sense of de Broglie and Bohm and quantum fluid dynamics of Madelung has been shown to be useful in analyzing the quantum domain behaviour of a classically chaotic system.

3.2.1.Basic Postulates of Bohm.

The essence of Bohmian Mechanics is given in the postulates listed below[45,46].

i) An individual physical system comprises of a wave propagating in space and time together with a point particle, which moves continuously under guidance of the wave.

ii) The wave is mathematically described by $\psi(\mathbf{r}, t)$, a solution of Schrodinger equation.

iii) The particle motion is obtained as the solution **r** (t) to the given equation

$$\dot{r} = \left.\frac{\nabla S(r,t)}{m}\right|_{r=r(t)} \tag{3.2.1}$$

where S is the phase of ψ. Or ψ is given by

$$\psi(r,t) = R(r,t)\exp\left[\frac{iS(r,t)}{\hbar}\right]$$

To solve this equation we have to specify the initial conditions **r** (0)=$\mathbf{r}_0$. This specification constitute the only extra information introduced by the theory that is not contained in $\psi(\mathbf{r}, t)$ (the initial velocity is fixed once we know S). An ensemble of possible motions associated with the same wave is generated by varying r_0.

iv) The probability that a particle in the ensemble lies in the volume element $d^3\mathbf{r}$ around **r** at time t is given by $R^2(\mathbf{r}, t)\, d^3\mathbf{r}$ where $R^2 = |\psi|^2$

Postulates **i** to **iii** on their own, constitute a consistent theory of motion. In order to ensure the comparability of the motions of the ensembles of particles with the results of quantum mechanics, the fourth postulate is made. The fourth helps us selecting from all the possible motions implied by the law **iii** those that are compatible with an initial distribution $R^2(r, t=0) = R_0^2(r)$. It is thus a consistent subsidiary condition imposed on a causal theory of motion and has no more fundamental status than that. Notice that postulate **iv** is in terms of the probability that a particle actually is at a precise location at

time 't'. The usual interpretation of $|\psi|^2$ is that it determines the probability density of finding a particle at r at time t if a suitable *measurement* is carried out. In fact, our notion is applicable to all states of the particle and in particular to those interactions which are characterized by the term *measurement* (if the theory is consistently extended to include such interactions); i.e., the *probability of finding* is a special case of the *probability of being*.

This theory applies to all matter, regardless of scale, although the wave aspect is generally apparent only in phenomena involving microscopic particles.

In general, we can say that an individual material system comprises the following two components.

a) A wave having an amplitude and phase at each space-time point. Its law of motion is

$$i\hbar\frac{\partial\psi}{\partial t} = (-\frac{\hbar^2}{2m}\nabla^2 + V)\psi \qquad (3.2.2)$$

b) A mass point pursuing a space-time trajectory, the law of motion is

$$\dot{r} = \frac{\nabla S(r,t)}{m}\bigg|_{r=r(t)} \quad \text{or} \qquad (3.2.3)$$

$$\frac{d(m\dot{r})}{dt} = -\nabla(V + V_q)\big|_{r=r(t)} \qquad (V_q \text{ is the quantum potential}) \qquad (3.2.4)$$

The most striking feature of the QTM is the simultaneous existence of wave and particle in the complete description of a physical system rather than the conventional *wave or particle* picture. The wave motion is characterized by the solution of the time dependent Schrodinger equation (TDSE)

$$\left[-\frac{\hbar^2}{2m}\nabla^2 + V(r)\right]\psi(r,t) = i\hbar\frac{\partial\psi(r,t)}{\partial t} \qquad (3.2.5)$$

while that of a point particle (for a given initial position) guided by this wave is governed by the velocity (3.2.3)

$$\dot{r} = \frac{\nabla S(r,t)}{m}\bigg|_{r=r(t)}$$

where S is the phase of ψ appearing in the following polar form

$$\psi(r,t) = R(r,t)\exp\left[\frac{iS(r,t)}{\hbar}\right] \tag{3.2.6}$$

since $$\frac{\partial \psi}{\partial t} = e^{\frac{iS}{\hbar}}\left[\frac{\partial R}{\partial t} + \frac{iR}{\hbar}\frac{\partial S}{\partial t}\right]$$ and

$$\nabla^2\psi = \nabla\cdot\nabla\psi = \nabla\cdot\left(e^{\frac{iS}{\hbar}}\left[\nabla R + i\frac{R}{\hbar}\nabla S\right]\right)$$

$$= e^{\frac{iS}{\hbar}}\left[\nabla^2 R + \frac{i}{\hbar}\nabla S\cdot\nabla R + \frac{i}{\hbar}\nabla\cdot(R\nabla S) - \frac{R}{\hbar^2}(\nabla S)^2\right],$$

the TDSE (3.2.5) becomes

$$-\frac{\hbar^2}{2m}\left[\nabla^2 R + \frac{i}{\hbar}\nabla S\cdot\nabla R + \frac{i}{\hbar}\nabla\cdot(R\nabla S) - \frac{R}{\hbar^2}(\nabla S)^2\right]e^{\frac{iS}{\hbar}} + V\,\mathrm{Re}^{\frac{iS}{\hbar}}$$

$$= i\hbar e^{\frac{iS}{\hbar}}\left[\frac{\partial R}{\partial t} + \frac{iR}{\hbar}\frac{\partial S}{\partial t}\right] \tag{3.2.7}$$

or

$$-\frac{\hbar^2}{2m}\left[\nabla^2 R - \frac{R}{\hbar^2}(\nabla S)^2\right] + VR - \frac{\hbar^2}{2m}\left[\frac{i}{\hbar}\nabla S\cdot\nabla R + \frac{i}{\hbar}\nabla\cdot(R\nabla S)\right]$$

$$= i\hbar\frac{\partial R}{\partial t} - R\frac{\partial S}{\partial t} \tag{3.2.8}$$

Separating real and imaginary parts, we get

$$-\frac{\hbar^2}{2m}\left[\frac{1}{\hbar}\nabla S\cdot\nabla R + \frac{1}{\hbar}\nabla\cdot(R\nabla S)\right] = \hbar\frac{\partial R}{\partial t} \tag{3.2.9}$$

and

$$-\frac{\hbar^2}{2m}\left[\nabla^2 R - \frac{R}{\hbar^2}(\nabla S)^2\right] + VR = -R\frac{\partial S}{\partial t} \tag{3.2.10}$$

Equation (3.2.9) becomes

$$\frac{\partial R}{\partial t} = -\frac{1}{2m}\left[\nabla\cdot(R\nabla S) + \nabla S\cdot\nabla R\right]$$

multiplying through out by 2R, we get

$$2R\frac{\partial R}{\partial t} = -\frac{1}{2m}\left[2R\nabla\cdot(R\nabla S) + 2R\nabla S\cdot\nabla R\right]$$

$$\frac{\partial R^2}{\partial t} = -\frac{1}{2m}\left[\nabla S\cdot\nabla R^2 + (\nabla R^2)\cdot\nabla S + 2R^2\cdot\nabla^2 S\right]$$

$$\frac{\partial R^2}{\partial t} = -\frac{1}{m}\left[\nabla R^2\cdot\nabla S + R^2\cdot\nabla^2 S\right]$$

or

$$\frac{\partial R^2}{\partial t} = -\nabla\cdot\left(\frac{R^2\nabla S}{m}\right) \qquad (3.2.11)$$

We identify $R^2 = \rho$ and $\frac{\nabla S}{m} = v$, we get

$$\frac{\partial \rho}{\partial t} + \nabla\cdot\rho v = 0 \qquad (3.2.12)$$

which is the continuity equation in fluid dynamics.

Similarly (3.2.10) can be written as

$$\frac{\partial S}{\partial t} - \frac{\hbar^2}{2m}\frac{\nabla^2 R}{R} + \frac{(\nabla S)^2}{2m} + V = 0$$

$$\frac{\partial S}{\partial t} + \frac{(\nabla S)^2}{2m} + \left[V - \frac{\hbar^2}{2m}\frac{\nabla^2 R}{R}\right] = 0 \qquad (3.2.13)$$

which is similar to Hamilton-Jacobi equation

$$\frac{\partial S}{\partial t} + H = 0 \qquad (3.2.14)$$

Equation (3.2.12) and (3.2.13) are a pair of coupled Partial Differential Equation in which the fields R and S codetermine one another. If ψ is normalized, this uniquely fixes R but S is

defined only up to an additive constant. The extra term $-\frac{\hbar^2}{2m}\frac{\nabla^2 R}{R}$ in (3.2.13) apart from Hamilton- Jacobi equation is called *Quantum Potential* (V_q) [44].

$$\text{i.e., } \frac{\partial S}{\partial t}+\frac{(\nabla S)^2}{2m}+\left[V+V_q\right]=0 \tag{3.2.15}$$

Let us apply the operator ∇ on (3.2.15), then

$$\frac{\partial(\nabla S)}{\partial t}+\frac{2(\nabla S)\nabla\cdot\nabla S}{2m}+\left[\nabla V+\nabla V_q\right]=0$$

$$\left[\frac{\partial}{\partial t}+\frac{\nabla S\cdot\nabla}{m}\right]\nabla S=-\nabla(V+V_q) \tag{3.2.16}$$

If we identify $\frac{\nabla S}{m}=\dot{r}=v$ then (3.2.16) becomes

$$\frac{d(m\dot{r})}{dt}=-\nabla(V+V_q) \tag{3.2.17}$$

where $\frac{d}{dt}\equiv\frac{\partial}{\partial t}+\dot{r}\cdot\nabla$

(3.2.17) is having the form of Newton's law where the particle is subject to a *Quantum Force* $-\nabla V_q$ in addition to the classical force $-\nabla V$. The effective potential acting on the particle is $V+V_q$. Here we solve either the equation $\dot{r}=\frac{\nabla S}{m}$ or $\frac{d(m\dot{r})}{dt}=-\nabla(V+V_q)$ for calculating the trajectory of the particle in the quantum field and the evolution of the trajectory for two nearby initial conditions can be calculated and possible chaotic or regular behaviour can be characterized. We can see that solving $\dot{r}=\frac{\nabla S}{m}$ is much easier than solving the equation $\frac{d(m\dot{r})}{dt}=-\nabla(V+V_q)$.

$\dot{r}=\frac{\nabla S}{m}$ in terms of the wave function is

$$\dot{r} = \frac{\nabla S}{m} = \frac{\hbar}{m}\mathrm{Im}\left[\frac{\nabla\psi}{\psi}\right]_{r=r(t)} \tag{3.2.18}$$

which can easily obtained by using $\psi = \mathrm{Re}^{\frac{iS}{\hbar}}$

Then $\nabla\psi = \left(\nabla R + \frac{iR}{\hbar}\nabla S\right)e^{\frac{iS}{\hbar}}$

$$\frac{\nabla\psi}{\psi} = \frac{\nabla R}{R} + \frac{i}{\hbar}\nabla S$$

$$\nabla S = \hbar\,\mathrm{Im}\left[\frac{\nabla\psi}{\psi}\right]$$

There fore

$$\dot{r} = \frac{\nabla S}{m} = \frac{\hbar}{m}\mathrm{Im}\left[\frac{\nabla\psi}{\psi}\right]_{r=r(t)}$$

Some of the systems in which the QTM is applied can be found in references [47-51].

3.3. Algorithm for the time evolution of the wave function and trajectory.

We have used a new and efficient algorithm to evolve the wave function and calculate the trajectory of motion in Bohmian mechanics which is superior to that used in the earlier work reported in the literature [52]. Here the method used by us [53] strictly maintains the unitary property of the evolution operator and hence the norm of the wave function is conserved exactly.

The time dependent Schrodinger equation (in X-Y co-ordinates) is given by

$$i\hbar\frac{\partial\psi(x,y,t)}{\partial t} = \hat{H}\psi(x,y,t) \tag{3.3.1}$$

The formal solution of the above equation can be written as

$$\psi(x,y,t) = \hat{T}(t-t_0)\psi(x,y,t_0) \quad or$$
$$\psi(x,y,t+\delta t) = \hat{T}(\delta t)\psi(x,y,t) \tag{3.3.2}$$

where $\hat{T}(\tau) = \exp(-\frac{i\tau\hat{H}}{\hbar})$ (is the time evolution operator). (3.3.3.)

Since $\hat{H} = \left[-\frac{\hbar^2}{2m}\left(\frac{\partial^2}{\partial x^2}+\frac{\partial^2}{\partial y^2}\right)+V\right]$

$$\hat{T}(\tau) = \exp\left(\frac{i\tau\hbar}{2m}\frac{\partial^2}{\partial x^2}+\frac{i\tau\hbar}{2m}\frac{\partial^2}{\partial y^2}-\frac{i\tau}{\hbar}V(x,y)\right) \quad (3.3.4a)$$

This is of the form $\hat{T}(\tau) = \exp(\hat{A}+\hat{B}+\hat{C})$ (3.3.4b)

Here [A,B] = 0, [A,C] ≠ 0 ,[B,C] ≠ 0

By using *Trotters* formula (3.3.4b) can be approximated for sufficiently small τ, as

$$\exp(A+B+C) \cong (\exp C/2)(\exp A)(\exp B)(\exp(C/2) \quad (3.3.5)$$

Now using (3.3.5) in (3.3.4a) and then in (3.3.2) we get

$$\psi(x,y,t+\tau) = \exp\left[-\frac{i\tau V(x,y)}{2\hbar}\right]\exp\left[\frac{i\tau\hbar}{2m}\frac{\partial^2}{\partial x^2}\right]\exp\left[\frac{i\tau\hbar}{2m}\frac{\partial^2}{\partial y^2}\right]\exp\left[-\frac{i\tau V(x,y)}{2\hbar}\right]\psi(x,y,t)$$

$$= \exp\left(-\frac{i\tau V(x,y)}{2\hbar}\right)\hat{O}_x\hat{O}_y\phi(x,y,t) \quad (3.3.6)$$

where $\hat{O}_x = \exp\left(\frac{i\tau\hbar}{2m}\frac{\partial^2}{\partial x^2}\right), \hat{O}_y = \exp\left(\frac{i\tau\hbar}{2m}\frac{\partial^2}{\partial y^2}\right), \varphi(x,y,t) = \exp\left(-\frac{i\tau V(x,y)}{2\hbar}\right)\psi(x,y,t)$

Now

$$\hat{O}_y\varphi(x,y,t) = \exp\left(\frac{i\tau\hbar}{2m}\frac{\partial^2}{\partial y^2}\right)\varphi(x,y,t) = \left[1+\frac{i\tau\hbar}{2m}\frac{\partial^2}{\partial y^2}+\frac{1}{2!}\left(\frac{i\tau\hbar}{2m}\frac{\partial^2}{\partial y^2}\right)^2+\ldots\right]\varphi(x,y,t)$$

But we can write

$$\left(\frac{i\tau\hbar}{2m}\frac{\partial^2}{\partial y^2}\right)\varphi(x,y,t) \approx \frac{i\tau\hbar}{2m}\frac{\varphi(x,y+\delta y,t)-2\varphi(x,y,t)+\varphi(x,y-\delta y,t)}{(\delta y)^2}$$

Let us define $\varphi'_{j,k} = \varphi(x = j\delta x+\alpha, y = k\delta y+\beta, t)$

Where α and β are x and y directional shift from the (j,k)th grid point.

Then $$\frac{\partial^2}{\partial y'^2}\varphi_{j,k} = \frac{\varphi_{j,k+1} - 2\varphi_{j,k} + \varphi_{j,k-1}}{(\delta y')^2}$$

For a fixed j the action of $\frac{\partial^2}{\partial y'^2}$ on $\varphi_{j,k}$ for all k is given as

$$\left(\frac{i\tau\hbar}{2m}\frac{\partial^2}{\partial y'^2}\right)\begin{pmatrix}\varphi_{j,1}\\ \varphi_{j,2}\\ .\\ \varphi_{j,N_Y}\end{pmatrix} = \frac{i\tau\hbar}{2m(\delta y')^2}\begin{pmatrix}-2 & 1 & 0 & .\\ 1 & -2 & 1 & .\\ 0 & 1 & -2 & .\\ . & . & . & .\end{pmatrix}\begin{pmatrix}\varphi_{j,1}\\ \varphi_{j,2}\\ .\\ \varphi_{j,N_Y}\end{pmatrix}$$

which can be written as

$$\left(\frac{i\tau\hbar}{2m}\frac{\partial^2}{\partial y'^2}\right)\varphi_j = M\varphi_j$$

Then $$\exp\left(\frac{i\tau\hbar}{2m}\frac{\partial^2}{\partial y'^2}\right)\varphi_j = \exp(M\varphi_j)$$

Where $\varphi_j = (\varphi_{j,1}, \varphi_{j,2}, ...\varphi_{j,N_Y})^T$, is a column vector

Let us put

$$M_y = \frac{-i\tau\hbar}{2m(\delta y')^2}\begin{pmatrix}2 & -1 & 0 & .\\ -1 & 2 & -1 & .\\ 0 & -1 & 2 & .\\ . & . & . & .\end{pmatrix} = \alpha_y\begin{pmatrix}2 & -1 & 0 & .\\ -1 & 2 & -1 & .\\ 0 & -1 & 2 & .\\ . & . & . & .\end{pmatrix} = \alpha_y M'$$

Let us transform the matrix M′ to get it diagonalized.

ie., $S^T M' S = D$, the diagonal eigenvalue matrix of M′

or $M' = S D S^T$

Where the elements of matrix S is given by $S_{ij} = \sqrt{\frac{2}{N_y+1}} Sin\left(\frac{ij\pi}{N_y+1}\right)$ and that of D is given by $d_j = 2\left(1 - Cos\left(\frac{\pi j}{N_y+1}\right)\right)$

We have $\exp(\alpha_y M') = 1 + \alpha_y M' + 1/2!\ \alpha^2_y M'^2 + \ldots$

Or $\exp(\alpha_y M') = S\,(1 + \alpha_y D + 1/2!\ \alpha^2_y D^2 + \ldots)\, S^T$

$= S \exp(\alpha_y D)\, S^T$

$$= S \begin{bmatrix} \exp(\alpha_y d_1) & . & . & . \\ . & \exp(\alpha_y d_2) & . & . \\ . & . & . & . \\ . & . & . & \exp(\alpha_y d_{N_y}) \end{bmatrix} S^T$$

where d_1, d_2, etc are eigenvalues of the matrix M'

$\hat{O}_y \varphi(x,y,t)$ thus obtained is again operated by $\hat{O}_x$ which also can be evaluated by the same procedure.

Then the wave function after ($\delta t = \tau$) is obtained by multiplying this with $\exp\left(-\frac{i\tau V(x,y)}{2\hbar}\right)$ [ref. equation (3.3.6)]

From (3.2.18) the velocity is $\dot{r} = \frac{\nabla S}{m} = \frac{\hbar}{m} \mathrm{Im}\left[\frac{\nabla \psi}{\psi}\right]_{r=r(t)}$. During the evolution of the wave function ψ, the velocity is calculated from the initial value and in each case **r** is calculated. The trajectory of the evolution is thus computed during the time evolution. For this calculation we have used Runge-Kutta method for numerical integration. Here we have to calculate ψ at two time steps to get **r** at one time step.

Let us start with r(t) and $\psi(x,y,t)$. Obtain $\psi' = \psi(x(t),y(t),t)$ by interpolation of $\psi(x,y,t)$ [ref. Sec.3.3.1]at the points (x=x(t),y=y(t)).

Using this we can calculate the velocities v'_x, v'_y

TH
531.163 RAJ/C
NB4536

$$v_x^I = \frac{\hbar}{m}\mathrm{Im}\left[\frac{\partial\psi^I}{\partial x}\Big/\psi^I\right]_{x(t),y(t)} \qquad v_y^I = \frac{\hbar}{m}\mathrm{Im}\left[\frac{\partial\psi^I}{\partial y}\Big/\psi^I\right]_{x(t),y(t)}$$

Now define $k_{x1} = v^I_x\ \delta t$,$k_{y1} = v^I_y\ \delta t$.

Calculate $\psi(x,y,t+\delta t/2)$ by the time evolution.

Obtain $\psi^{II} = \psi(x(t)+ k_{x1}/2\ ,y(t)+ k_{y1}/2\ ,t+\delta t/2)$ by interpolation.

From this calculate v^{II}_x and v^{II}_y.

$$v_x^{II} = \frac{\hbar}{m}\mathrm{Im}\left[\frac{\partial\psi^{II}}{\partial x}\Big/\psi^{II}\right]_{x(t),y(t)} \qquad v_y^{II} = \frac{\hbar}{m}\mathrm{Im}\left[\frac{\partial\psi^{II}}{\partial y}\Big/\psi^{II}\right]_{x(t),y(t)}$$

Define $k_{x2} = v^{II}_x\ \delta t$,$k_{y2} = v^{II}_y\ \delta t$.

Using same $\psi(x,y,t+\delta t/2)$ calculate

$\psi^{III} = \psi(x(t)+ k_{x2}/2\ ,y(t)+ k_{y2}/2\ ,t+\delta t/2)$ and obtain v^{III}_x and v^{III}_y.

$$v_x^{III} = \frac{\hbar}{m}\mathrm{Im}\left[\frac{\partial\psi^{III}}{\partial x}\Big/\psi^{III}\right]_{x(t),y(t)} \qquad v_y^{III} = \frac{\hbar}{m}\mathrm{Im}\left[\frac{\partial\psi^{III}}{\partial y}\Big/\psi^{III}\right]_{x(t),y(t)}$$

Define $k_{x3} = v^{III}_x\ \delta t$,$k_{y3} = v^{III}_y\ \delta t$.

Now calculate $\psi(x,y,t+\delta t)$

Using this get

$\psi^{IV} = \psi(x(t)+ k_{x3}\ ,y(t)+ k_{y3}\ ,t+\delta t)$ and obtain v^{IV}_x and v^{IV}_y.

$$v_x^{IV} = \frac{\hbar}{m}\mathrm{Im}\left[\frac{\partial\psi^{IV}}{\partial x}\Big/\psi^{IV}\right]_{x(t),y(t)} \qquad v_y^{IV} = \frac{\hbar}{m}\mathrm{Im}\left[\frac{\partial\psi^{IV}}{\partial y}\Big/\psi^{IV}\right]_{x(t),y(t)}$$

Define $k_{x4} = v^{IV}_x\ \delta t$,$k_{y4} = v^{IV}_y\ \delta t$.

Now calculate

$$r(t+\delta t) = r(t) + 1/6\ [k_{x1} + 2k_{x2} + 2k_{x3} + k_{x4}\ ,\ k_{y1} + 2k_{y2} + 2k_{y3} + k_{y4}\ ].$$

3.3.1. Interpolation of ψ

To interpolate ψ at the point r (t), first identify the rectangle to which r (t) belongs.

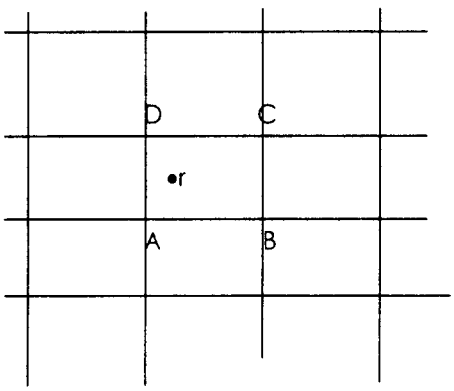

Let $r(t) = (x_I + \alpha\ ,\ y_J + \beta)$

We must first interpolate ψ to r(t) using the value of ψ at the four corners A,B,C and D.

Let $\psi_A = \psi(x_I\ ,\ y_J)$ $\psi_B = \psi(x_I + \delta x,\ y_J) = \psi(x_{I+1},\ y_I)$

$\psi_C = \psi(x_I + \delta x,\ y_J + \delta y)$ $\psi_D = \psi(x_I\ ,\ y_J + \delta y)$

Then

$$\psi(x_I + \alpha, y_J + \beta) = (1 - \frac{\alpha}{\delta x})(1 - \frac{\beta}{\delta y})\psi_A + \frac{\alpha}{\delta x}(1 - \frac{\beta}{\delta y})\psi_B + \frac{\alpha}{\delta x}\frac{\beta}{\delta y}\psi_C + (1 - \frac{\alpha}{\delta x})\frac{\beta}{\delta y}\psi_D$$

and

$$(\nabla\psi)_{r(t)} = \left(\frac{1}{\delta x}\left[(\psi_B - \psi_A)(1 - \frac{\beta}{\delta x}) + (\psi_C - \psi_D)\frac{\beta}{\delta y}\right], \frac{1}{\delta y}\left[(\psi_C - \psi_B)\frac{\alpha}{\delta x} + (\psi_D - \psi_A)(1 - \frac{\alpha}{\delta x})\right]\right)$$

Thus the interpolation of ψ and the calculation of its gradient at the point r(t) is done. The calculation done for Henon-Heils model in the next section (3.4) is based on this algorithm.

In section (3.5) we have used a modified algorithm to calculate trajectory etc. of our model. The details of this algorithm will be reported later [53].

3.4. Henon-Heils model.

The Henon-Heils model with a potential as in (3.4.1) is studied in detail using the QTM by Sengupta and Chattaraj[52].

$$V(x,y)=0.5(x^2+y^2)+\lambda x(y^2-x^2/3) \qquad (3.4.1)$$

Their results are reproduced using a better algorithm here. In [52] they used an initial wave function

$$\psi(x,y,t=0)=\frac{1}{\sqrt{\pi}}\exp\left[-\frac{1}{2}\left\{(x-x_0)^2+(y-y_0)^2\right\}\right] \qquad (3.4.2)$$

with boundary conditions

$$\psi(\pm\infty,y,t)=0.\forall y,t$$

$$\psi(x,\pm\infty,t)=0.\forall x,t$$

in the modified program we used an initial wave function

$$\psi(x,y,0)=\frac{1}{\sqrt{\pi S_x S_y}}\exp\left[-\frac{(x-x_0)^2}{2S_x^2}-\frac{(y-y_0)^2}{2S_y^2}+i(P_{x_0}x+P_{y_0}y)\right] \qquad (3.4.3)$$

The evolved wave function and the trajectory for two nearby initial conditions(separated by 10^{-5}) and the relative distance between the two trajectories for three different cases are calculated. We have chosen the evolution up to 10000 with a time step 0.02 and x and y ranges from –6 to +6 with 48 grid points. We put $S_x = S_y = 1$ and $P_x = P_y = 0$ to be consistant with that of ref.52.

The three cases considered are,

1) for $\lambda = 0$ (linear isotropic harmonic oscillator) and the Gaussian wave packet initially carried at $x_0 = 1.36719$, $y_0 = 1.36719$.

2) for $\lambda = 0.1118034$ (non-linear non integrable oscillator) and the Gaussian wave packet initially carried at $x_0 = 1.36719$, $y_0 = 1.36719$.

3) for $\lambda = 0.1118034$ (non-linear non integrable oscillator) and the Gaussian wave packet initially carried at $x_0 = 2.929688$, $y_0 = 1.953425$.

The evolved wave function, the trajectories and relative distances in the three cases are plotted in figures 3.4.1 through 3.4.7. In Fig.3.4.8.the total energy during evolution for the regular and chaotic cases are plotted. In chaotic case the fluctuations in energy is considerably large, which may be attributed to the error caused in the numerical computation for chaotic case where the function fluctuates rapidly even locally, which is not the case for regular case.

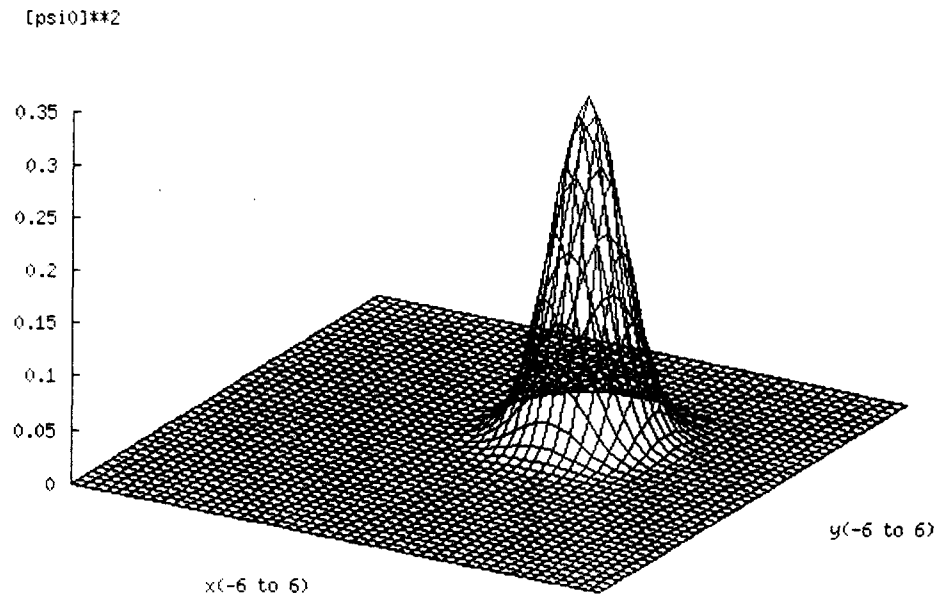

Fig.3.4.1. The initial wave function used for evolution in the henon-heils problem with initial conditions x_0=1.36719, y_0=1.36719, $p_{x0}=p_{y0}=0, s_x=s_y=1$

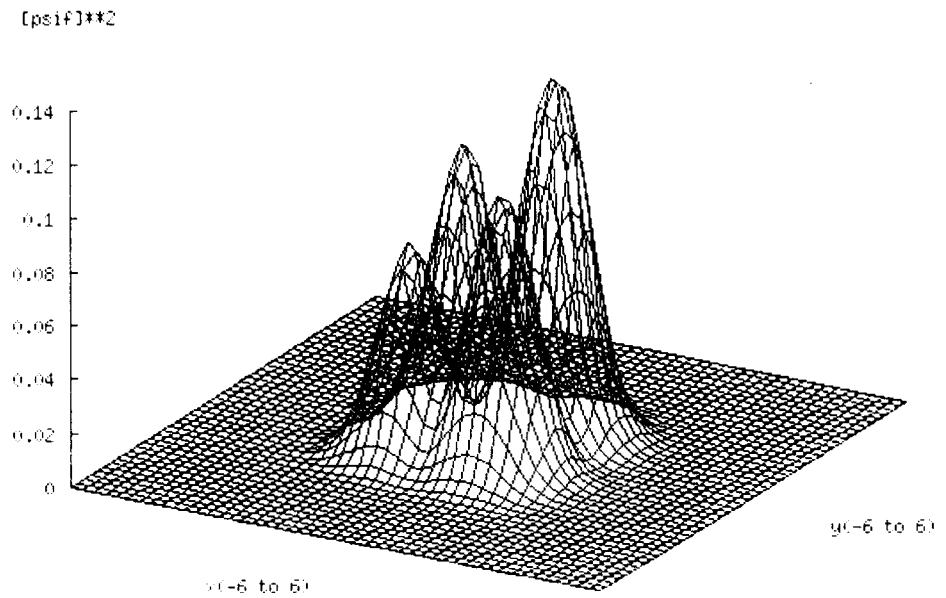

Fig.3.4.2. The final wave function after evolution in the Henon-Heils problem with initial conditions x_0=1.36719, y_0=1.36719, p_{x0}=p_{y0}=0,s_x=s_y=1 (λ=0)

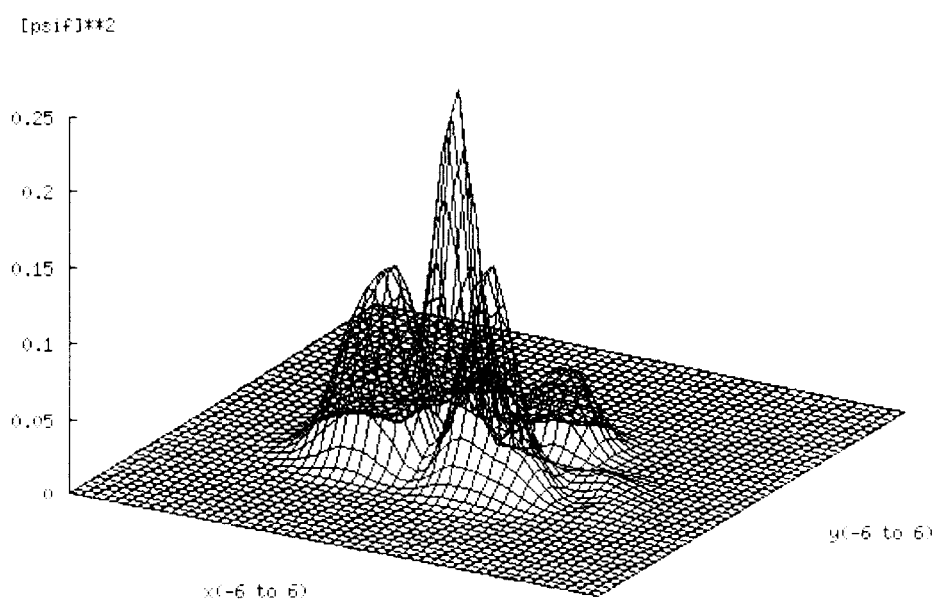

Fig.3.4.3. The final wave function after evolution in the Henon-Heils problem with initial conditions x_0=1.36719, y_0=1.36719, p_{x0}=p_{y0}=0,s_x=s_y=1 (λ=0.1118034)

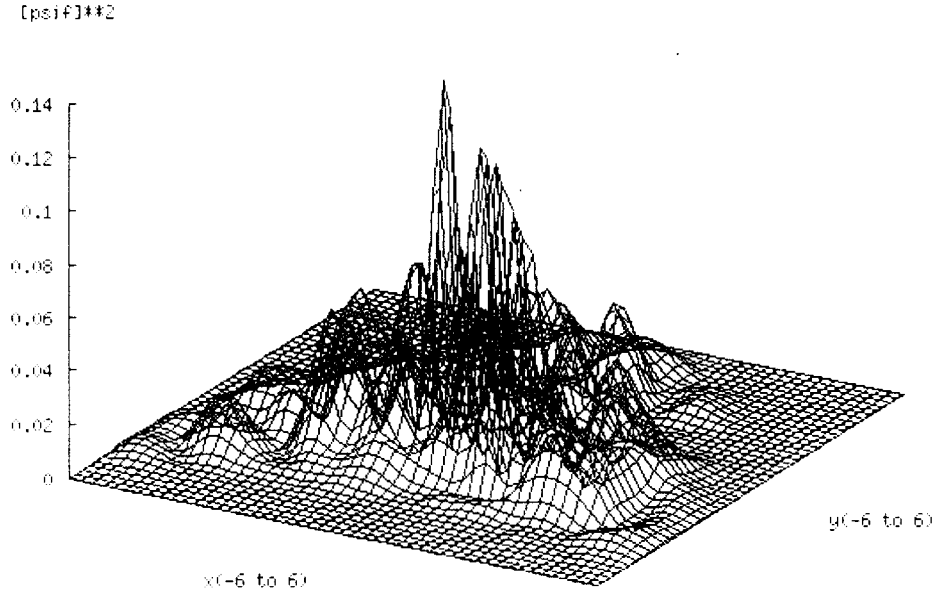

Fig.3.4.4. The final wave function after evolution in the henon-heils problem with initial conditions x_0= 2.929688, y_0= 1.953125, $p_{x0}=p_{y0}=0, s_x=s_y=1$ (λ=0.1118034)

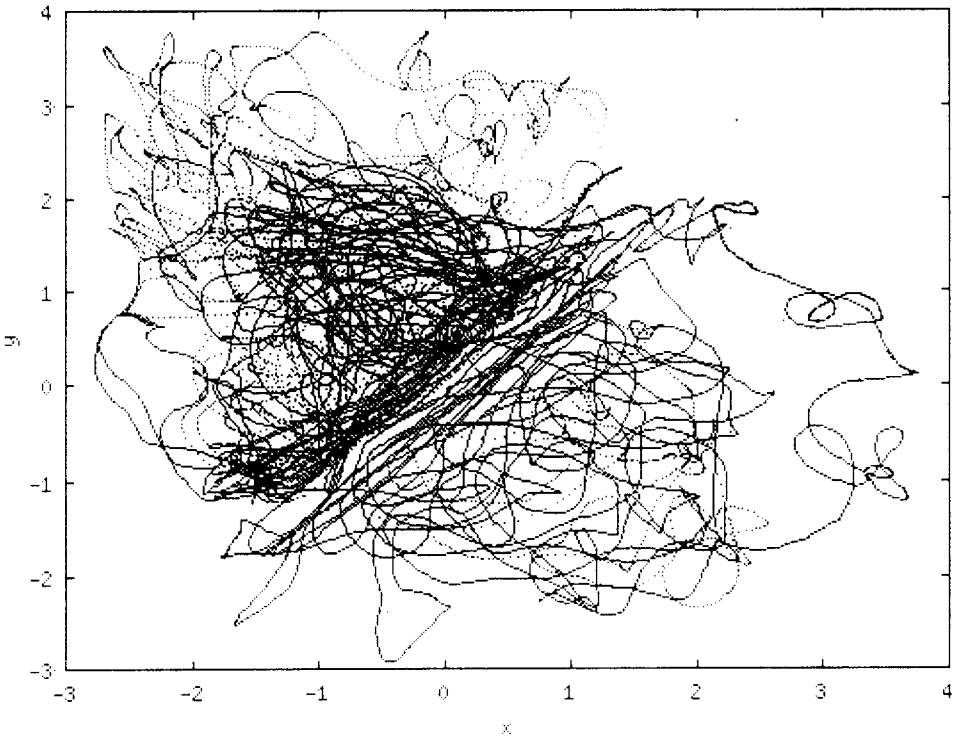

Fig.3.4.5. The trajectory for two nearby initial conditions (thick and dotted lines) for Henon-Heils model with λ=0.1118034 and initial conditions x_0=1.36719, y =1.36719, $p_{x0}=p_{y0}=0, s_x=s_y=1$

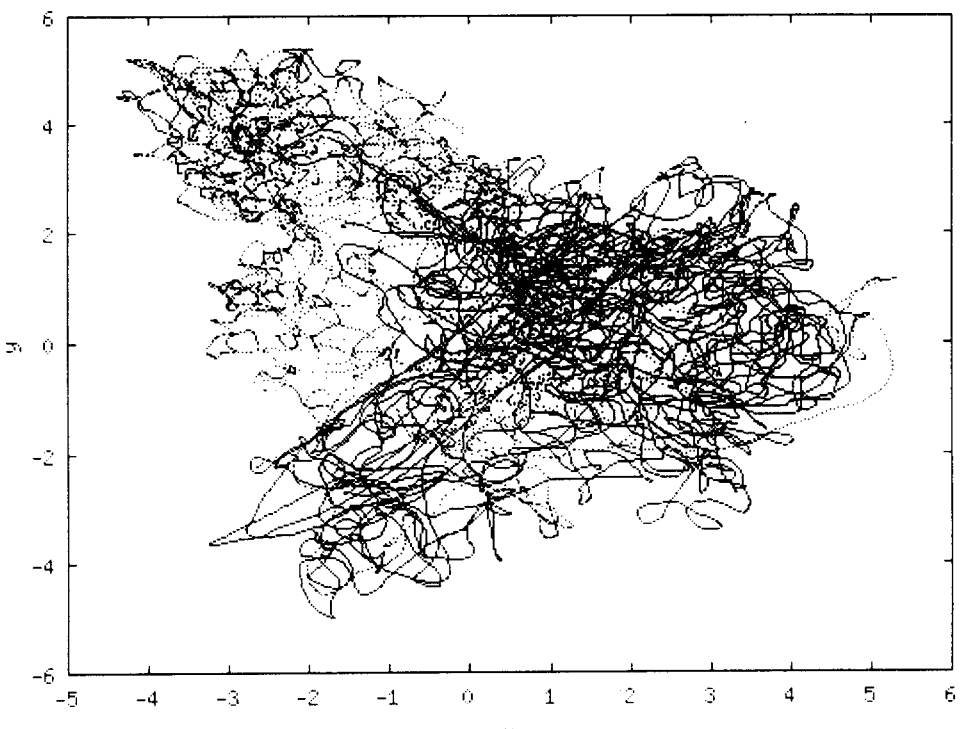

Fig.3.4.6. The trajectory for two nearby initial conditions for henon-heiis model with λ=0.1118034 and initial conditions x_0= 2.929688, y_0= 1.953125, $p_{x0}=p_{y0}=0, s_x=s_y=1$

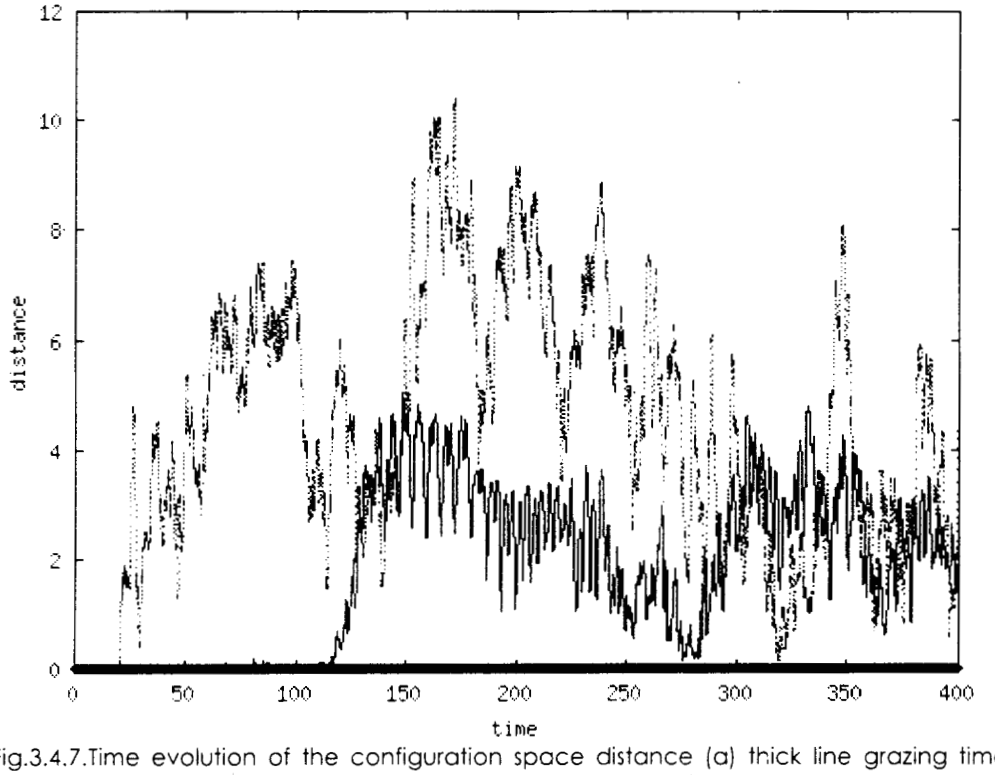

Fig.3.4.7.Time evolution of the configuration space distance (a) thick line grazing time axis with x_0=1.36719, y_0 =1.36719, p_{x0}= p_{y0}=0, s_x=s_y=1 (λ=0) (b) solid line for x_0 =1.36719, y_0=1.36719, p_{x0}=p_{y0} =0, s_x=s_y=1 (λ=0.1118034) (c) dotted line for x_0=2.929688, y_0=1.953125, p_{x0}= p_{y0} =0, s_x=s_y=1 (λ=0.1118034).

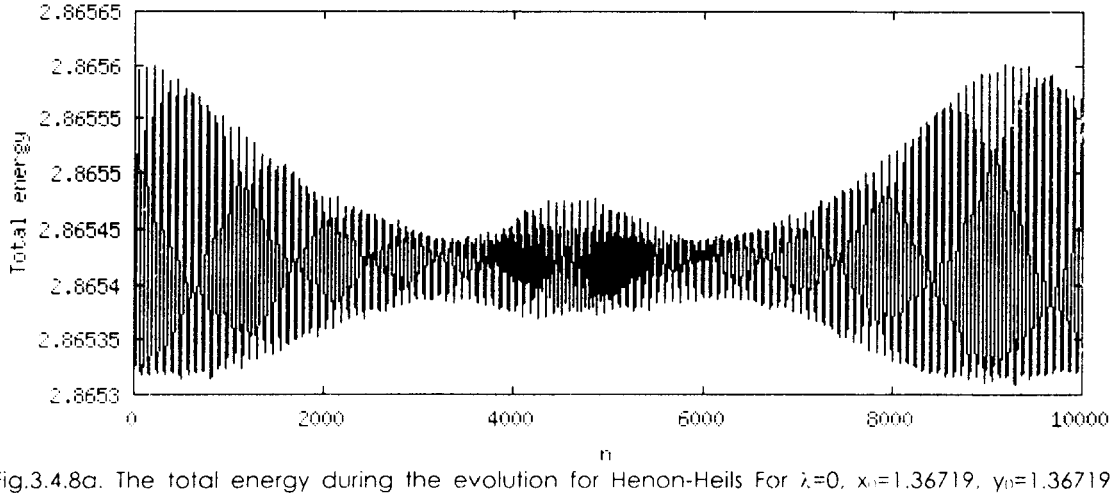

Fig.3.4.8a. The total energy during the evolution for Henon-Heils For λ=0, x_0=1.36719, y_0=1.36719, p_{x0}=p_{y0}=0,s_x=s_y=1 (regular)

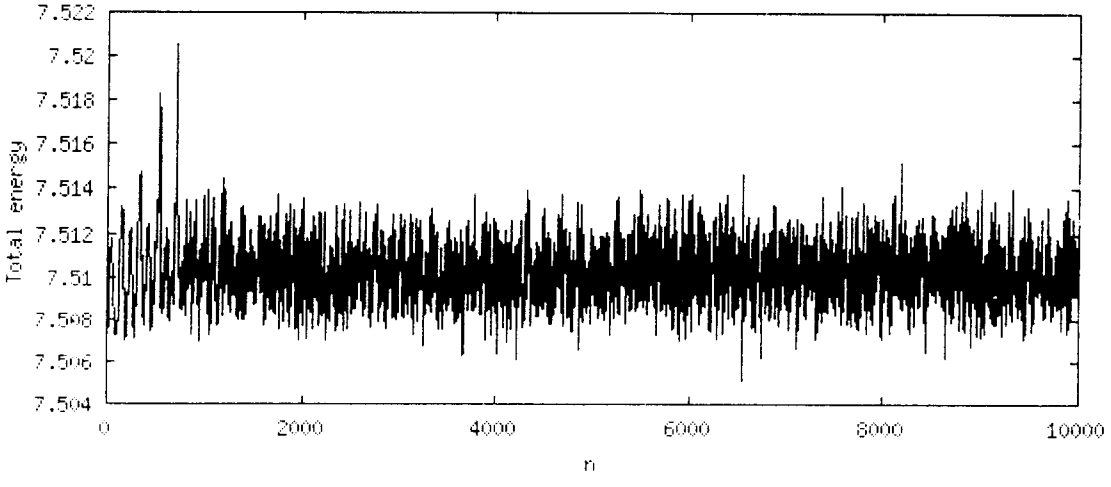

Fig.3.4.8b. The total energy during the evolution for Henon-Heils For λ=0.1118034, x_0=2.929688, y_0=1.953125, $p_{x0}=p_{y0}=0, s_x=s_y=1$ (chaotic).

From figure 3.4.1 to 3.4.4. , it is seen that the evolved wave function becomes more and more fluctuating, when the system is more and more chaotic, classically. The trajectories plotted in figs.3.4.5. and 3.4.6. show exponential divergence for two arbitrarily close initial conditions. The total energy for the chaotic case (fig.3.4.8b) shows more rapid fluctuations than that for regular case (fig.3.4.8a). Even though the system is Hamiltonian (with constant energy) the fluctuations in energy for the chaotic case can be attributed to the rapid fluctuations in the wave function, which is reflected in the numerical integration for the calculation of energy.

Note that in all cases $\langle x \rangle = x_0$ and $\langle y \rangle = y_0$ and as we go from case (1) through (3) the system becomes more and more *chaotic*, since its *classical* energy increases.

The two nearby initial conditions can be taken as the centers of two Gaussian wave packets with (x_0,y_0) and $(x_0+\Delta,y_0+\Delta)$ as centers. In our calculation we take two points (x_0,y_0) and $(x_0+\Delta,y_0+\Delta)$ in the same wave packet, which also is equivalent to two separate wave packets centered at two points.

In the next section we apply the Quantum theory of motion to the model developed in chapter 2.

3.5.Quantum theory of motion applied to the model.

In chapter 2 we have explained a model with Hamiltonian given by (2.4.1) which shows chaos classically for some initial conditions and parameter values. Now we use the QTM. to characterize the classically chaotic and regular motion of the model for different initial conditions. Here we use the potential (From. Eqn.2.4.1)

$$V = \frac{L^2}{2\rho^2} - \frac{1}{\sqrt{\rho^2+(z-1)^2}} - \frac{a}{\sqrt{\rho^2+(z+1)^2}} + \frac{a}{4z}, z > 0$$

$$V = \frac{L^2}{2\rho^2} - \frac{b\delta}{\sqrt{\rho^2+(z-1)^2}} + \frac{a\delta}{4z}, z < 0$$

where $\delta = \frac{\varepsilon_1}{\varepsilon_2}, a = \frac{\delta-1}{\delta+1}, b = \frac{2}{1+\delta}$ and $\rho = \sqrt{\xi^2+\eta^2}$

$$\xi = \frac{x}{Z}, \eta = \frac{y}{Z}, z = \frac{z}{Z}$$

3.5.1. Bohmian mechanics in the ρ , z co-ordinate system.

In the (ρ , **z)** co-ordinate system we can write the Schrodinger equation as

$$i\hbar\frac{\partial\psi}{\partial t} = \hat{H}\psi \tag{3.5.1}$$

where the Hamiltonian is

$$\hat{H} = -\frac{\hbar^2}{2m}\left[\frac{1}{\rho}\frac{\partial}{\partial\rho}\rho\frac{\partial}{\partial\rho} - \frac{L^2}{\rho^2} + \frac{\partial^2}{\partial z^2}\right] + V(\rho, z) \tag{3.5.2}$$

or
$$\frac{\partial\psi}{\partial t} = \frac{i\hbar}{2m}\left[\frac{1}{\rho}\frac{\partial}{\partial\rho}\rho\frac{\partial}{\partial\rho} - \frac{L^2}{\rho^2} + \frac{\partial^2}{\partial z^2}\right]\psi - \frac{i}{\hbar}V(\rho, z)\psi \tag{3.5.3}$$

Let us put $\psi = R \exp\left(\frac{iS}{\hbar}\right)$

Then $$\rho\frac{\partial\psi}{\partial t} = \rho\exp\left(\frac{iS}{\hbar}\right)\left[\frac{\partial R}{\partial\rho} + \frac{i}{\hbar}R\frac{\partial S}{\partial\rho}\right]$$

and

$$\frac{\partial}{\partial\rho}\rho\frac{\partial\psi}{\partial\rho} = \exp\left(\frac{iS}{\hbar}\right)\left\{\rho\frac{\partial^2 R}{\partial\rho^2} + \frac{\partial R}{\partial\rho} - \frac{\rho}{\hbar^2}R\left(\frac{\partial S}{\partial\rho}\right)^2 + \frac{i}{\hbar}\left(\rho R\frac{\partial^2 S}{\partial\rho^2} + \rho\frac{\partial R}{\partial\rho}\frac{\partial S}{\partial\rho} + R\frac{\partial S}{\partial\rho} + \rho\frac{\partial R}{\partial\rho}\frac{\partial S}{\partial\rho}\right)\right\} \tag{3.5.4}$$

also

$$\frac{\partial\psi}{\partial z} = \exp\left(\frac{iS}{\hbar}\right)\left[\frac{\partial R}{\partial z} + \frac{i}{\hbar}R\frac{\partial S}{\partial z}\right]$$

and

$$\frac{\partial^2\psi}{\partial z^2} = \exp\left(\frac{iS}{\hbar}\right)\left[\frac{\partial^2 R}{\partial z^2} - \frac{1}{\hbar^2}R\left(\frac{\partial S}{\partial z}\right)^2 + \frac{i}{\hbar}\left(R\frac{\partial^2 S}{\partial z^2} + 2\frac{\partial R}{\partial z}\frac{\partial S}{\partial z}\right)\right] \tag{3.5.5}$$

Putting (3.5.4) and (3.5.5) in (3.5.3) we get

$$\frac{\partial R}{\partial t}+\frac{i}{\hbar}R\frac{\partial S}{\partial t}=\frac{i\hbar}{2m}\left\{\frac{\partial^2 R}{\partial\rho^2}+\frac{1}{\rho}\frac{\partial R}{\partial\rho}-\frac{1}{\hbar^2}R\left(\frac{\partial S}{\partial\rho}\right)^2+\right.$$
$$\frac{i}{\hbar}\left(R\frac{\partial^2 S}{\partial\rho^2}+2\frac{\partial R}{\partial\rho}\frac{\partial S}{\partial\rho}+\frac{R}{\rho}\frac{\partial S}{\partial\rho}\right)+$$
$$\left.\left[\frac{\partial^2 R}{\partial z^2}-\frac{1}{\hbar^2}R\left(\frac{\partial S}{\partial z}\right)^2+\frac{i}{\hbar}\left(R\frac{\partial^2 S}{\partial z^2}+2\frac{\partial R}{\partial z}\frac{\partial S}{\partial z}\right)\right]-\frac{L^2R}{\rho^2}\right\}-\frac{i}{\hbar}VR$$

Separating real and imaginary parts,

$$\frac{\partial R}{\partial t}=-\frac{1}{2m}\left[R\frac{\partial^2 S}{\partial\rho^2}+2\frac{\partial R}{\partial\rho}\frac{\partial S}{\partial\rho}+\frac{R}{\rho}\frac{\partial S}{\partial\rho}+R\frac{\partial^2 S}{\partial z^2}+2\frac{\partial R}{\partial z}\frac{\partial S}{\partial z}\right] \tag{3.5.6}$$

$$\frac{\partial S}{\partial t}=-V+\frac{\hbar^2}{2mR}\left[\frac{\partial^2 R}{\partial\rho^2}+\frac{1}{\rho}\frac{\partial R}{\partial\rho}-\frac{R}{\hbar^2}\left(\frac{\partial S}{\partial\rho}\right)^2+\frac{\partial^2 R}{\partial z^2}-\frac{R}{\hbar^2}\left(\frac{\partial S}{\partial z}\right)^2-\frac{L^2R}{\rho^2}\right]$$

$$=-\left(V+\frac{\hbar^2}{2m}\frac{L^2}{\rho^2}\right)+\frac{\hbar^2}{2m}\left[\frac{\nabla^2 R}{R}\right]-\frac{1}{2m}\left[\left(\frac{\partial S}{\partial\rho}\right)^2+\left(\frac{\partial S}{\partial z}\right)^2\right]$$

that is,

$$\frac{\partial S}{\partial t}+\frac{1}{2m}\left[\left(\frac{\partial S}{\partial\rho}\right)^2+\left(\frac{\partial S}{\partial z}\right)^2\right]+\left(V+\frac{\hbar^2}{2m}\frac{L^2}{\rho^2}\right)-\frac{\hbar^2}{2m}\left[\frac{\nabla^2 R}{R}\right]=0 \tag{3.5.7}$$

Comparing (3.5.7) with (3.2.13) we see that

$-\frac{\hbar^2}{2m}\left[\frac{\nabla^2 R}{R}\right]$ is the Quantum potential and $\left(V+\frac{\hbar^2}{2m}\frac{L^2}{\rho^2}\right)-\frac{\hbar^2}{2m}\left[\frac{\nabla^2 R}{R}\right]$ is the effective potential. The particle will move in this effective potential.

We have $\frac{\partial R^2}{\partial t}=2R\frac{\partial R}{\partial t}$,so from (3.5.6)

$$\frac{\partial R^2}{\partial t}=-\frac{1}{m}\left[R^2\frac{\partial^2 S}{\partial\rho^2}+\frac{\partial R^2}{\partial\rho}\frac{\partial S}{\partial\rho}+\frac{R^2}{\rho}\frac{\partial S}{\partial\rho}+R^2\frac{\partial^2 S}{\partial z^2}+\frac{\partial R^2}{\partial z}\frac{\partial S}{\partial z}\right] \tag{3.5.8}$$

The above equation can be written as

$\frac{\partial R^2}{\partial t} = -\nabla(R^2\vec{v})$ which is same as (3.2.11).

Here $\vec{v} = (v_\rho, v_z) = \frac{\nabla S}{m}$ with $v_\rho = \frac{1}{m}\frac{\partial S}{\partial \rho}$ and $v_z = \frac{1}{m}\frac{\partial S}{\partial z}$.

Also $\vec{v} = \dot{r} = (v_\rho, v_z) = \frac{\nabla S}{m} = \frac{\hbar}{m}\mathrm{Im}\left[\frac{\nabla \psi}{\psi}\right]$ which is calculated after interpolation of ψ to find the gradient at point where r is to be calculated and find $\mathrm{Im}\left[\frac{\nabla \psi}{\psi}\right]_{r(t)}$, then r(t+Δt) is calculated using Runge-Kutta algorithm as described in sec. 3.3.

3.5.2. Numerical results for the model.

We observe that the trajectories of evolution diverge for the initial condition (I.C.) (i) given in section 2.5. {δ=3, L=0.3, ρ=0.23, z=0.18, P_ρ=0.1, P_z=0.1} which is classically chaotic, for a small displacement (here 10^{-5}) of the I.C.(see fig.3.5.2) which is clear from the distance plotted between two trajectories.(fig.3.5.5). The trajectories and distance between two trajectories started from arbitrarily close I.Cs. for the case (ii) of sec.2.5. {δ=3, L=0.3, ρ=2.5, z=12.0, P_ρ=0.3842077627766117, P_z=0}, which is classically non-chaotic, are expected to behave as regular. We get the two trajectories evolved from two nearby initial conditions almost superimpose, a sign of regular motion (fig.3.5.4). But some authors have observed [47] that even the classically non-chaotic case sometimes shows chaotic trajectories in QTM.

The variation in total energy plotted using QTM for the classically regular case is smaller. At the same time the energy plotted shows large variation for the chaotic case (fig.3.5.6). The fluctuations in the energy for chaotic case can perhaps be attributed to inaccuracy of numerical integration. This happens because evolved wave function varies rapidly and the integration procedure (Simpson's rule) would fail at this high gradient region. Nevertheless these fluctuation in energy calculated numerically can be taken as the signature of chaotic systems, even though the classically regular systems

remain on constant energy surface in phase space. So we find that the energy calculated in QTM can be used to characterize chaotic or regular behaviour of a system [54].

The trajectories are evolved using a wave function centered at the I.C. (i) and (ii) with ρ and z ranges from 0 to 20 with a 200 step grid at an interval Δt=0.01 and N=10000. Another set of trajectories is also evolved from a nearby point separated by 10^{-5} from the first initial condition.

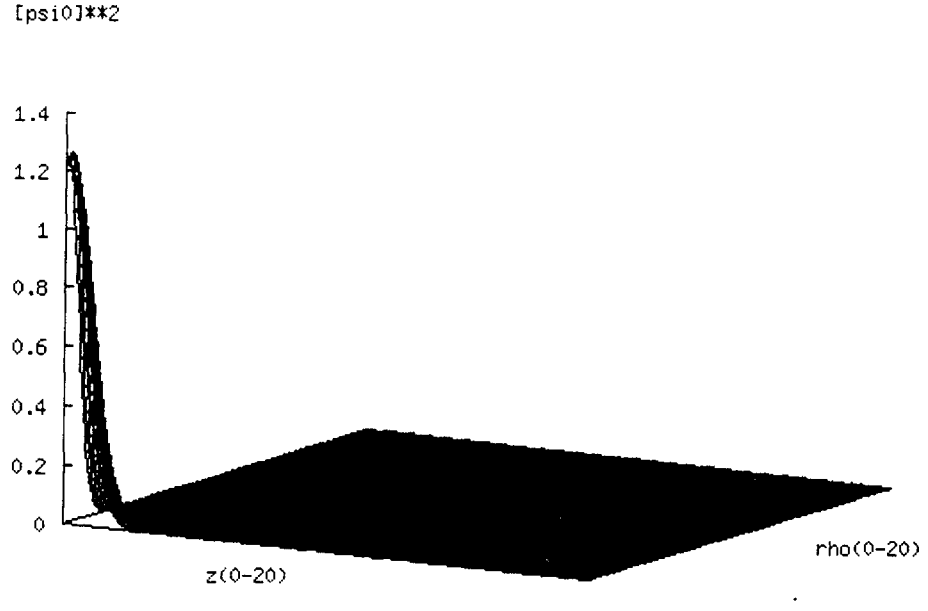

Fig.3.5.1a. The initial wave function for δ=3, L=0.3 ρ=0.23, z=0.18, P_ρ=0.1, P_z=0 (corresponds to chaos).

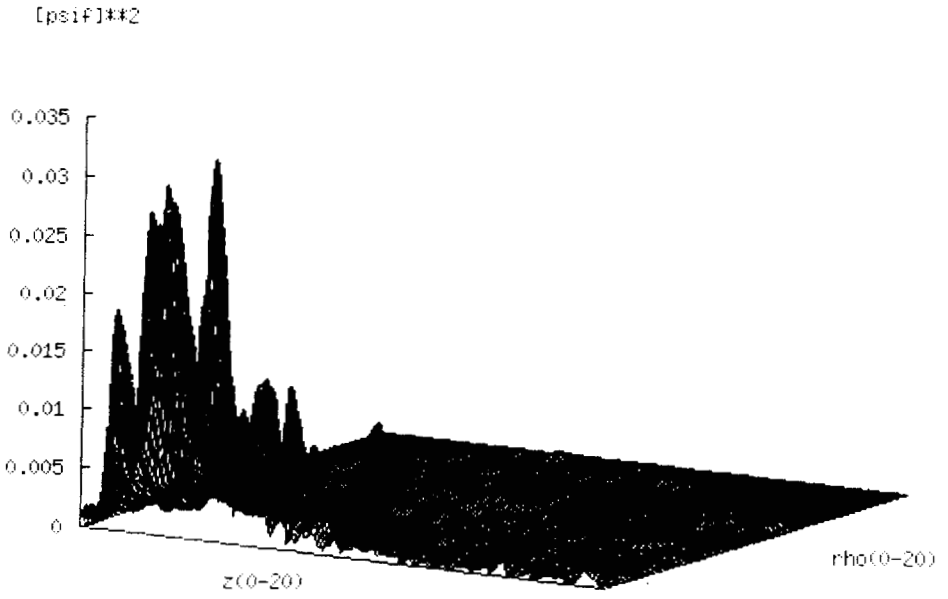

Fig.3.5.1b. The evolved wave function for δ=3, L=0.3 ρ=0.23, z=0.18, P_ρ=0.1, P_z=0 (corresponds to chaos).

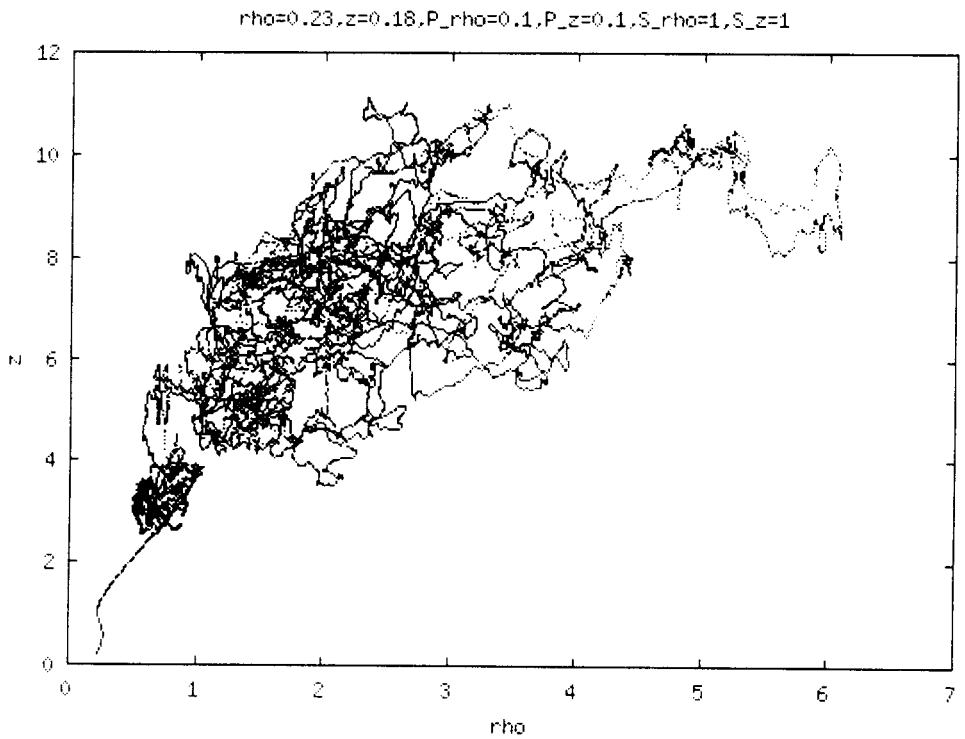

Fig.3.5.2. The trajectories of the particle started from two nearby points for the IC and parameters given in fig.3.5.1.

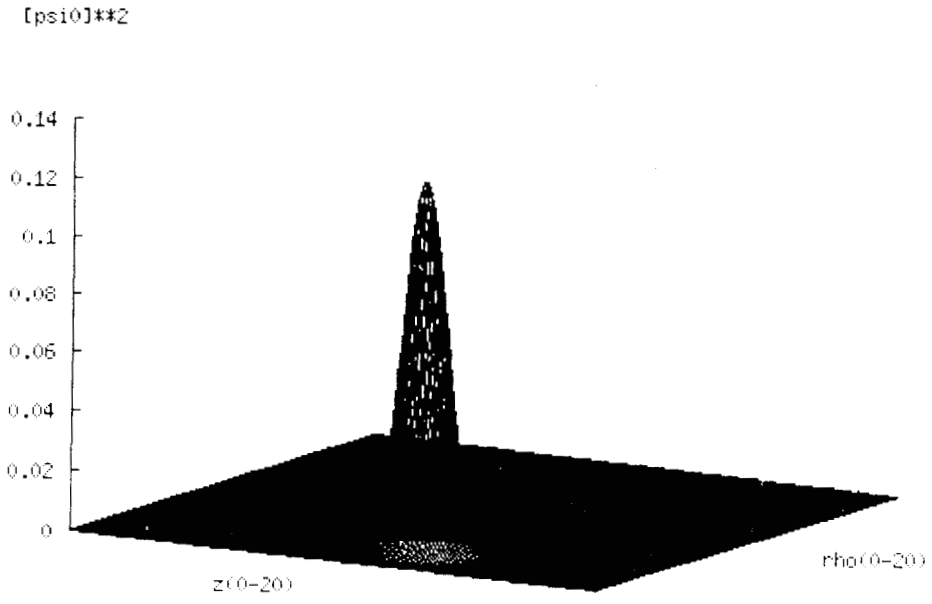

Fig.3.5.3a. The initial wave function for δ=3, L=0.3, ρ=2.5, z=12.0, P_ρ=0.3842077627766117, P_z=0 (corresponds to regular motion)

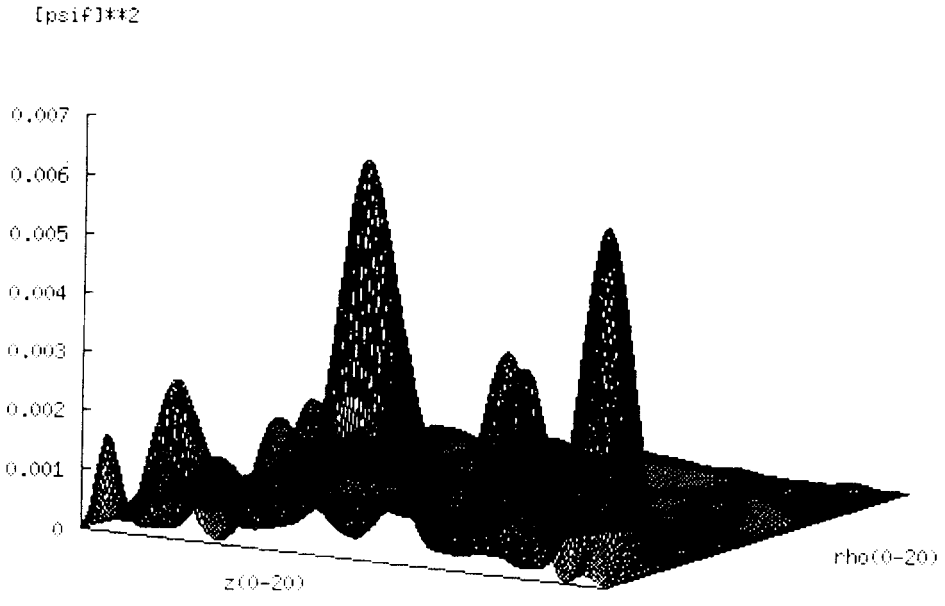

Fig.3.5.3b. The evolved wave function for δ=3, L=0.3, ρ=2.5, z=12.0, P_ρ=0.3842077627766117, P_z=0 (corresponds to regular motion)

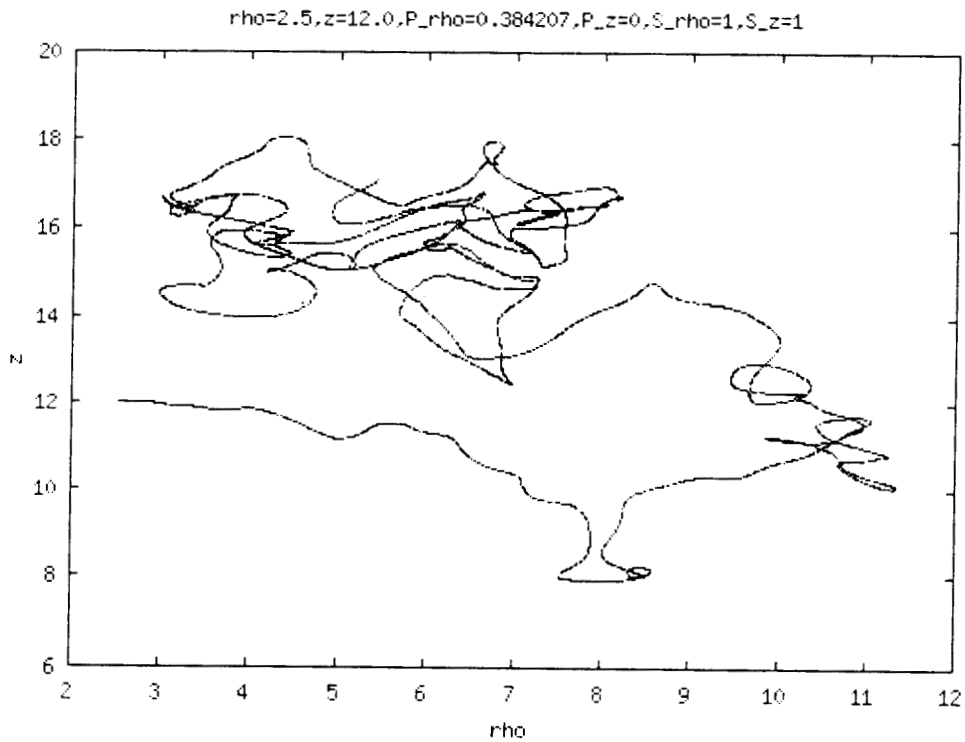

Fig.3.5.4. The trajectories of the particle started from two nearby points for the IC and parameters given in fig.3.5.3. (They exactly superimpose)

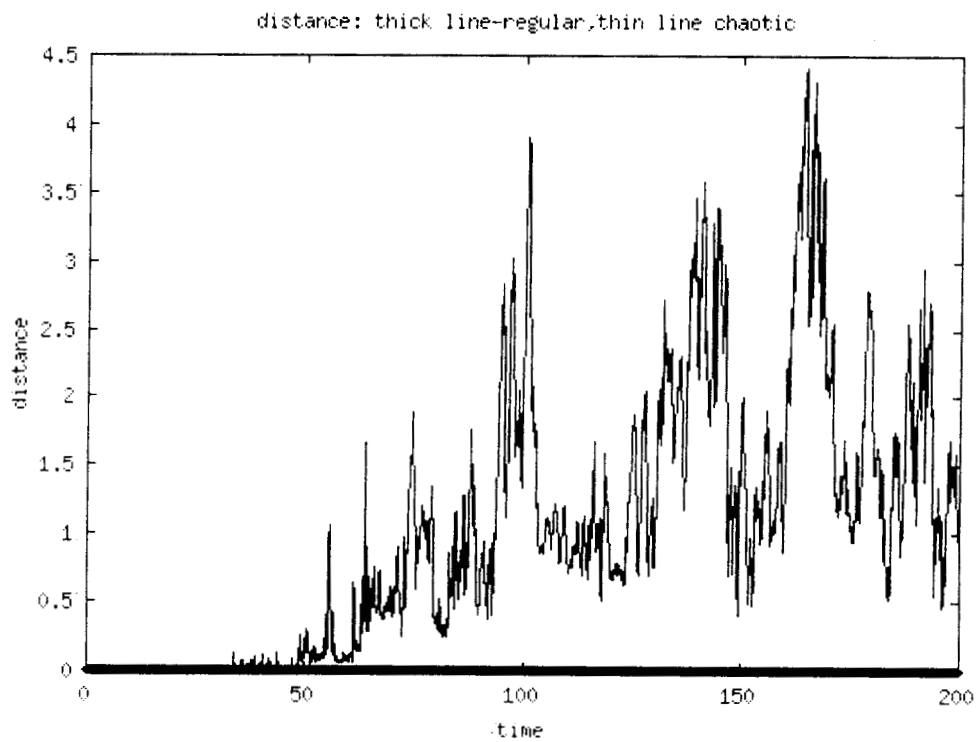

Fig.3.5.5.The distance between two trajectories (i) Solid line for δ=3, L=0.3 ρ=0.23, z=0.18, P_ρ=0.1, P_z= 0.1(chaotic) and (ii) thick line grazing time axis for δ=3, L=0.3, ρ=2.5, z=12.0, P_ρ=0.3842077627766117, P_z=0 (regular).

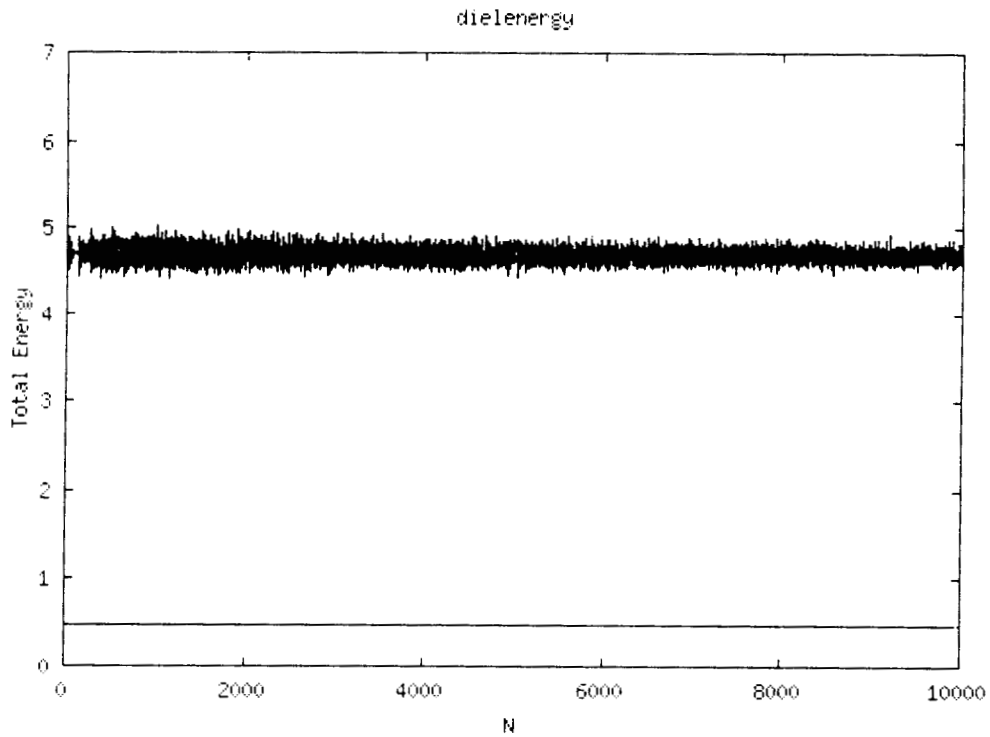

fig.3.5.6. The total energy during evolution for the case (i) top and (ii) bottom (as in fig.3.5.5).

From fig.3.5.1. it is seen that when the classical motion is chaotic the wave function evolved is distorted more compared to the evolved wave function for regular motion, which is less distorted as in fig.3.5.3. (See also figures 3.4.1. to 3.4.4. in sec.3.4). So the distortion of evolved wave function may be taken as a signature of chaos in QTM. Also we have seen that just as in classical case, in QTM we can define a trajectory and the divergence of these trajectories for nearby initial conditions is a good signature of chaos (see figures 3.5.2 and 3.5.4). The distance between two trajectories, which is closely related to Lyapunov exponent, also indicate the difference between the dynamics of the system for regular and chaotic initial conditions.(fig.3.5.5.). Even though the Hamiltonian system preserves energy (the evolution is unitary) for a given initial condition, the total energy calculated for the chaotic case shows large variations compared to regular case. This is attributed to the numerical inaccuracy of the calculation of the wave function during the evolution. In the case of chaotic evolution the function changes sharply for small regions, which makes the integration inaccurate. Further work in this area is to be conducted for the confirmation of this hypothesis.

CHAPTER 4

CONNECTION BETWEEN CHAOTIC MAPS AND DIFFERENTIAL EQUATIONS.

Introduction

To model a physical system we use either a differential equation or a difference equation. When the system considered evolves continuous in time, we use differential equations as the model. But when the evolution of the system is discrete in time, such as population dynamics of insects, growth of deposit in a bank etc. we use difference equations to model them. In this chapter we try to study connection between discrete maps (difference equations) and ordinary differential equations. Here we take a Taylor series expansion of a map (function) and equate that to the function itself. The infinite series Taylor expansion is truncated for different orders and equated to the function. The behaviour of this series is expected to approach the original function when the order of the series approaches infinity. But it is found that when the function taken is a chaotic map, the series need not represent the original function, as the number of terms in the series increases. If the series is truncated to first or second order, the system does not show any chaotic dynamics, as the minimum requirement of three degrees of freedom is not satisfied. Also when the order of truncation is five or greater, it can be shown using Routh - Hurwitz theorem, that the system becomes unstable, irrespective of the map chosen. But for an order of truncation three or four, it is rather difficult to do the analysis for general maps. Hence we study the behaviour of the system for an order of truncation three and four, for a specific map (say logistic map). Here we see interesting behaviours like period doubling bifurcation leading to chaos, reverse bifurcations, instability in some regions etc. These type of behaviours are entirely different from that of the map used. In addition we see the system show *riddled parameter space* (suddenly switch from regular to chaos or to unstable by slight variation in parameter), which is an indication of *structural instability* [55-66]. Recently several authors reported necessary conditions like

total number of terms and number of non-linear terms needed for observing chaos in ordinary differential equations [67-70].

4.1. Ordinary differential equations corresponding to discrete maps.

Consider the 1-D map

$$X_{n+1} = f(x_n) \tag{4.1.1}$$

We can embed this as a continuous time problem with

$$x(t+1)=f(x(t)) \tag{4.1.2}$$

i.e., given $x(t_0)$, we can calculate $x(t_0 + n)$, n=1,2,3...

Let us put $x_n = x(t_0 + n)$ and from (4.1.2) we get,

$$x_{n+1} = f(x_n) \tag{4.1.3}$$

which is same as (4.1.1).

We can expand x (t+1) (L.H.S. of (4.1.2)) as a formal series

$$x(t+1) = x(t) + \frac{dx}{dt} + \frac{1}{2!}\frac{d^2x}{dt^2} + \ldots$$

or (4.1.2) can be written as

$$\sum_{j=0}^{\infty} \frac{1}{j!}\frac{d^j x(t)}{dt^j} = f(x(t)) \tag{4.1.4}$$

which is an infinite order differential equation. We consider truncating the above series to finite order N as,

$$\sum_{j=0}^{N} \frac{1}{j!}\frac{d^j x}{dt^j} = f(x) \tag{4.1.5}$$

If x(t) is a real analytic function, one could equate the solution of (4.1.5) to that of (4.1.4) as N increases.

4.1.1.Stability analysis.

We can show that (4.1.5) leads to unstable solution for almost any initial condition using Routh-Hurwitz theorem for N≥5. We prove this for N > 5 formally and then for N=5. Equation (4.1.5) can be written as

$$\sum_{j=1}^{N} \frac{1}{j!} \frac{d^j x}{dt^j} + g(x) = 0 \ , \qquad \text{where } g(x)=x(t)-f(x)$$

Consider stability of this around an arbitrary reference point x* (not necessarily a fixed point). Writing x (t)=x*+δ x(t), one gets

$$\sum_{j=1}^{N} \frac{1}{j!} \frac{d^j \delta x(t)}{dt^j} + \alpha \delta x(t) = 0 \quad \text{where } \alpha = g'(x^*) \qquad (4.1.6)$$

Since this equation is linear, we can write

$$\delta x(t) \approx c e^{\mu t}$$

Substituting this in (4.1.6), we get

$$\sum_{j=1}^{N} \frac{1}{j!} \mu^j + \alpha = 0 \qquad (4.1.7a)$$

We now show that there will exist at least one μ with positive real part irrespective of the value of α, if N ≥ 5.

This would imply that the solution of the equation (4.1.5) is unstable for any finite N ≥ 5 for almost any initial condition. Now equation (4.1.7a) is of the form

$$a_0 \mu^N + a_1 \mu^{N-1} + \ldots + a_{N-1} \mu + a_N = 0 \qquad (4.1.7b)$$

With $a_j = \frac{1}{(N-j)!}$ for $0 \le j \le N-1$ and $a_N = \alpha$.

Nature of zeros of (4.1.7b) can be examined by Routh-Hurwitz theorem

Define $T_0 = a_0$

$$T_1 = a_1$$

$$T_2 = \begin{bmatrix} a_1 & a_0 \\ a_3 & a_2 \end{bmatrix}$$

$$T_3 = \begin{bmatrix} a_1 & a_0 & 0 \\ a_3 & a_2 & a_1 \\ a_5 & a_4 & a_3 \end{bmatrix}$$

$$T_4 = \begin{bmatrix} a_1 & a_0 & 0 & 0 \\ a_3 & a_2 & a_1 & a_0 \\ a_5 & a_4 & a_3 & a_2 \\ a_7 & a_6 & a_5 & a_4 \end{bmatrix}$$

etc.,

$$a_j = \frac{1}{(N-j)!}, \quad 0 \le j \le N-1 \quad \text{and } a_N = \alpha.$$

The number of roots with positive real parts equals the number of sign changes in the sequence of T_n. If at least one sign change occurs in the sequence of T's then the series (4.1.7b) has at least one root with positive real part and the solution of (4.1.5) is unstable in the neighbourhood of the reference point x*. If this happen for almost any x*, then the solution is unstable for any initial condition, globally.

Let us now calculate the T_i s.

$$T_2 = \begin{vmatrix} a_1 & a_0 \\ a_3 & a_2 \end{vmatrix} = \begin{vmatrix} \frac{1}{(N-1)!} & \frac{1}{N!} \\ \frac{1}{(N-3)!} & \frac{1}{(N-2)!} \end{vmatrix} = \frac{1}{N!}\frac{1}{(N-2)!}\begin{vmatrix} j & 1 \\ N-2 & 1 \end{vmatrix} = \frac{2}{N!(N-2)!} > 0$$

$$T_3 = \begin{vmatrix} a_1 & a_0 & 0 \\ a_3 & a_2 & a_1 \\ a_5 & a_4 & a_3 \end{vmatrix} = \begin{vmatrix} \frac{1}{(N-1)!} & \frac{1}{N!} & 0 \\ \frac{1}{(N-3)!} & \frac{1}{(N-2)!} & \frac{1}{(N-1)!} \\ \frac{1}{(N-5)!} & \frac{1}{(N-4)!} & \frac{1}{(N-3)!} \end{vmatrix}$$

$$= \frac{1}{N!}\frac{1}{(N-1)!}\frac{1}{(N-3)!}\begin{vmatrix} j & 1 & 0 \\ (N-1)(N-2) & (N-1) & 1 \\ (N-3)(N-4) & (N-3) & 1 \end{vmatrix} = \frac{-2(N-5)}{N!(N-1)!(N-3)!}$$

$\frac{-2(N-5)}{N!(N-1)!(N-3)!} < 0$, for N > 5 irrespective of the value of α.

That is for N > 5 the equation (4.1.5) gives unstable solution irrespective of the form of f(x).

We can explicitly show that for N = 5 also, both the fixed points of (4.1.7b) are unstable.

For N=5, $T_0 = a_0 = \frac{1}{N!} > 0.$ $T_1 = a_1 = \frac{1}{(N-1)!} > 0$

$$T_2 = \begin{vmatrix} a_1 & a_0 \\ a_3 & a_2 \end{vmatrix} = \begin{vmatrix} \frac{1}{(N-1)!} & \frac{1}{N!} \\ \frac{1}{(N-3)!} & \frac{1}{(N-2)!} \end{vmatrix} = \frac{1}{N!}\frac{1}{(N-2)!}\begin{vmatrix} N & 1 \\ N-2 & 1 \end{vmatrix} = \frac{2}{N!(N-2)!} > 0$$

$$T_3 = \begin{vmatrix} a_1 & a_0 & 0 \\ a_3 & a_2 & a_1 \\ a_5 & a_4 & a_3 \end{vmatrix} = \begin{vmatrix} \frac{1}{4!} & \frac{1}{5!} & 0 \\ \frac{1}{2!} & \frac{1}{3!} & \frac{1}{4!} \\ \alpha & 1 & \frac{1}{2!} \end{vmatrix}$$

$$= \frac{1}{5!}\frac{1}{4!}\frac{1}{2!}\begin{vmatrix} 5 & 1 & 0 \\ 12 & 4 & 1 \\ 2\alpha & 2 & 1 \end{vmatrix} = \frac{1}{5!}\frac{1}{4!}(\alpha - 1)$$

We get $T_3 < 0$ when $\alpha < 1$ (which is conditional). But if we take T_4

$$T_4 = \begin{bmatrix} a_1 & a_0 & 0 & 0 \\ a_3 & a_2 & a_1 & a_0 \\ a_5 & a_4 & a_3 & a_2 \\ 0 & 0 & a_5 & a_4 \end{bmatrix} = \begin{vmatrix} \frac{1}{4!} & \frac{1}{5!} & 0 & 0 \\ \frac{1}{2!} & \frac{1}{3!} & \frac{1}{4!} & \frac{1}{5!} \\ \alpha & \frac{1}{1!} & \frac{1}{2!} & \frac{1}{3!} \\ 0 & 0 & \alpha & \frac{1}{1!} \end{vmatrix} = \frac{1}{5!}\frac{1}{5!}\frac{1}{3!}\begin{vmatrix} 5 & 1 & 0 & 0 \\ 60 & 20 & 5 & 1 \\ 6\alpha & 6 & 3 & 1 \\ 0 & 0 & \alpha & 1 \end{vmatrix}$$

Subtracting last row from second and third,

$$T_4 = \frac{1}{5!}\frac{1}{5!}\frac{1}{3!}\begin{vmatrix} 5 & 1 & 0 & 0 \\ 60 & 20 & 5-\alpha & 0 \\ 6\alpha & 6 & 3-\alpha & 0 \\ 0 & 0 & \alpha & 1 \end{vmatrix} = \frac{1}{5!}\frac{1}{5!}\frac{1}{3!}\begin{vmatrix} 5 & 1 & 0 \\ 60 & 20 & 5-\alpha \\ 6\alpha & 6 & 3-\alpha \end{vmatrix} = -6\left[\alpha^2 - \frac{10}{3}\alpha + 5\right]$$

$$= -6\left[\left(\alpha - \frac{5}{3}\right)^2 + \frac{20}{3}\right]$$

which is less than zero for all α. i.e., T_1, T_2 are positive. If T_3 is positive, then a sign change occurs at T_4. This means that any reference point is unstable for N = 5 also.

Since the minimum dimensionality required for chaos is 3, we cannot expect any chaotic behaviour for the order of truncation 1 and 2 (N=1 and 2). We are, however not in a position to make any general statement about N=3 and 4. In what follows, we consider the special case of the logistic map, f(x) = p x (1-x).

4.2. Truncated for first order (i.e., when N=1).

Equation (4.1.5) becomes

$$\frac{dx}{dt} + x = f(x) \qquad \text{or}$$

$$\frac{dx}{dt} = f(x) - x \tag{4.2.1}$$

Let x* be the steady state solution of (4.2.1).

i.e., 0 = f (x*) - x*

or x* is same as the fixed points of the map (e.g. For Logistic map x* = 0,1- (1/p))

Linearising (4.2.1) by expanding the function around x* (i.e., x =x*+ δx) we get

$$\frac{d(\delta x)}{dt} = [f'(x^*) - 1]\delta x$$

Then $\delta x = \delta x_0 \, e^{t[f'(x^*)-1]}$ (4.2.2)

If f (x)=p x (1-x) (logistic map) then x*=0, 1- (1/p) and

$$(f'(x) - 1)\big|_{x^*=0} = p - 1 \text{ and } (f'(x) - 1)\big|_{x^*=1-1/p} = 1 - p$$

Then from (4.2.2), the system is stable when p < 1 and unstable when p > 1 for x*=0.

For x*=1- (1/p), the system is stable for p > 1. In short if p <1, x (t) will converge to zero for all initial conditions and for p > 1, x (t) will converge to 1-1/p. Or chaos cannot be expected in this case.

4.3. Truncated for second order (i.e., when N=2).

Equation (4.1.5) becomes

$$\frac{1}{2!}\frac{d^2x}{dt^2}+\frac{dx}{dt}=f(x)-x \qquad \text{or}$$

$$\frac{d^2x}{dt^2}+2\frac{dx}{dt}-2g(x)=0, \text{ where } g(x) = f(x) - x$$

which can be split into two autonomous first order differential equations as follows,

(putting $x=x_1$)

$$\begin{aligned}\dot{x}_1 &= x_2\\ \dot{x}_2 &= -2x_2+2g(x_1)\end{aligned} \tag{4.3.1}$$

The steady state can be obtained by putting $\dot{x}_1 = 0$ and $\dot{x}_2 = 0$

Again we get for $f(x) = p\,x\,(1-x)$, $x_1^*=0$ or $1-(1/p)$

Linearising (4.3.1) near the steady state, we get the stability matrix as

$$\frac{d}{dt}\begin{bmatrix}\delta x_1\\ \delta x_2\end{bmatrix}=\begin{bmatrix}0 & 1\\ 2g'(x_1^*) & -2\end{bmatrix}\begin{bmatrix}\delta x_1\\ \delta x_2\end{bmatrix}$$

eigenvalues of the stability matrix is given by

$$\lambda = -1\pm\sqrt{1+2g'(x_1^*)} \tag{4.3.2}$$

When $x_1^*= 0$, $g'(x_1^*) = p - 1$ then,

$$\lambda = -1\pm\sqrt{2p-1}$$

for $0 < p < \frac{1}{2}$, $\lambda = -1\pm i\sqrt{1-2p}$

Here we get $x_1^*= 0$ is stable spiral in the 2-dimensional phase space $(x,\dot{x})$, for $0 < p < \frac{1}{2}$.

For $\frac{1}{2} < p < 1$, $\lambda = -1\pm\sqrt{2p-1}$ and $\lambda_{1,2} < 0$. That is $x_1^*= 0$ is stable node in the 2-dimensional phase space.

In short for $0 < p < 1$, $x_1^* = 0$ is a stable fixed point.

When p > 1, (2p–1) > 1 and hence $\lambda_1 = -1+\sqrt{2p-1} > 0$ and $\lambda_2 = -1-\sqrt{2p-1} < 0$.

Then $x_1^* = 0$ is a saddle point (unstable) in the 2-dimensional phase space.

When $x_1^* = 1-(1/p)$, $g'(x_1^*) = 1- p$

From (4.3.2) $\lambda = -1 \pm \sqrt{1+2(1-p)} = -1 \pm \sqrt{3-2p}$

For 1 < p < 3/2, we get 0 < (3 – 2p) < 1 and hence $\lambda_{1,2} < 0$. $x_1^* = 1-(1/p)$ is a stable node.

Also for P > 3/2, $\lambda = -1 \pm i\sqrt{2p-3}$, then $x_1^* = 1-(1/p)$ is stable spiral. In short, $x_1^* = 0$ is stable for 0 < p < 1. This is unstable for p > 1. At the same time the fixed point $x_1^* = 1-(1/p)$ is unstable for p < 1 and stable for p > 1.

4.4. Truncated for third order (i.e., when N=3).

Equation (4.1.5) becomes

$$\frac{1}{3!}\frac{d^3x}{dt^3}+\frac{1}{2!}\frac{d^2x}{dt^2}+\frac{dx}{dt}+x = f(x) \qquad (4.4.1a)$$

$$\frac{d^3x}{dt^3}+3\frac{d^2x}{dt^2}+6\frac{dx}{dt} = 6(f(x)-x) \qquad (4.4.1b)$$

Equation (4.4.1) can be written as three coupled first order differential equations.

$$\left.\begin{aligned} \dot{x}_1 &= x_2 \\ \dot{x}_2 &= x_3 \\ \dot{x}_3 &= -3x_3 - 6x_2 + 6g(x_1) \end{aligned}\right\} \qquad (4.4.2)$$

If f(x) is the Logistic equation, the fixed points are $x_1^* = 0$ or $1-(1/p)$, $x_2^* = 0$ and $x_3^* = 0$.

i.e., the fixed points are (0,0,0) and (1-(1/p) ,0,0).

Linearising (4.4.2) near the fixed point we get

$$\frac{d}{dt}\begin{bmatrix}\delta x_1\\ \delta x_2\\ \delta x_3\end{bmatrix} = \begin{bmatrix}0 & 1 & 0\\ 0 & 0 & 1\\ 6g'(x_1^*) & -6 & -3\end{bmatrix}\begin{bmatrix}\delta x_1\\ \delta x_2\\ \delta x_3\end{bmatrix} \qquad (4.4.3)$$

Eigenvalues of the stability matrix are obtained by the relation,

$$\lambda^3 + 3\lambda^2 + 6\lambda - 6g'(x_1^*) = 0 \qquad (4.4.4)$$

For $x_{1*}=0$, the above equation becomes

$$\lambda^3 + 3\lambda^2 + 6\lambda - 6(p-1) = 0 \qquad (4.4.5a)$$

and for $x_{1*}=1-1/p$ it becomes

$$\lambda^3 + 3\lambda^2 + 6\lambda - 6(1-p) = 0 \qquad (4.4.5b)$$

We can solve the above cubic equation by using *Cardano's* method.

Let us put $\lambda=\mu-1$ then (4.4.4) becomes,

$$\mu^3 + 3\mu - (4+\alpha) = 0$$
$$\alpha = 6g'(x_{1*}) \qquad (4.4.6)$$

Since the roots of a cubic equation of the form $z^3 + rz + q = 0$ are given by

$$z_1 = A + B, z_{2,3} = -\frac{(A+B)}{2} \pm i\frac{\sqrt{3}}{2}(A-B) \qquad \text{where}$$

$$A = \left(-\frac{q}{2} + \sqrt{Q}\right)^{1/3}, B = \left(-\frac{q}{2} - \sqrt{Q}\right)^{1/3}, Q = \left(\frac{r}{3}\right)^3 + \left(\frac{q}{2}\right)^2$$

Here we get

$$A + B = \left[\left(2+\frac{\alpha}{2}\right) + \sqrt{1+\left(2+\frac{\alpha}{2}\right)^2}\right]^{1/3} + \left[\left(2+\frac{\alpha}{2}\right) - \sqrt{1+\left(2+\frac{\alpha}{2}\right)^2}\right]^{1/3}$$

$$\mu_1 = A + B, \mu_{2,3} = -\frac{A+B}{2} \pm i\frac{\sqrt{3}}{2}(A-B)$$

Therefore, $\lambda_1 = \mu_1 - 1, \lambda_{2,3} = \mu_{2,3} - 1$

We will get $\lambda_1,\lambda_2,\lambda_3$ all < 0 for p < 1 and

$\lambda_1 > 0$, $\lambda_{2,3} < 0$ for p > 1, near the fixed point (0,0,0). That is the system is stable near the fixed point (0,0,0) when p < 1 and unstable when p > 1. But for the fixed point (1-(1/p), 0,0), p < 1 gives unstable solution and p > 1 gives stable solution up to p= 4 (the maximum possible parameter value for Logistic map).[Since p < 1 does not satisfy the condition for the fixed point (1-(1/p),0,0), we can ignore that part. In other words if, we take the limit of

the parameter p as that of Logistic equation (i.e., $0 < p \leq 4$), we cannot expect any chaotic behaviour in the system of equations (4.4.2.). But the Poincare-Bendixon theorem says that autonomous first order Ordinary differential equations with continuous functions with at least three dimensions (three degree of freedom) may give bounded chaotic solutions. So, we search for possible chaotic solution for (4.4.2) for the parameter range $p > 4$. We observed a lot of interesting behaviour for this set of equations for this parameter range.

Equation (4.4.1b) can be rewritten as (by putting f (x) = p x (1-x)),

$$\frac{d^3x}{dt^3} + 3\frac{d^2x}{dt^2} + 6\frac{dx}{dt} - 6(p-1)x + 6px^2 = 0 \qquad (4.4.7)$$

which can be scaled by using the change of variables $x = \alpha X$ and $t = \beta\tau$

Then (4.4.7) becomes

$$\frac{\alpha}{\beta^3}\frac{d^3X}{d\tau^3} + 3\frac{\alpha}{\beta^2}\frac{d^2X}{d\tau^2} + 6\frac{\alpha}{\beta}\frac{dX}{d\tau} - 6(p-1)\alpha X + 6p\alpha^2X^2 = 0 \qquad \text{or}$$

$$\frac{d^3X}{d\tau^3} + 3\beta\frac{d^2X}{d\tau^2} + 6\beta^2\frac{dX}{d\tau} - 6\beta^3(p-1)X + 6p\beta^3\alpha X^2 = 0 \qquad (4.4.8)$$

Take $6p\beta^3\alpha = 1$, $3\beta = 1$

Then $\beta = 1/3$, $6\beta^2 = 6/9 = 2/3$

$6\beta^3(p-1) = (2/9)(p-1)$, $\alpha = 1/(6p\beta^3) = 9/(2p)$

Then (4.4.8) becomes

$$\frac{d^3X}{d\tau^3} + \frac{d^2X}{d\tau^2} + \frac{2}{3}\frac{dX}{d\tau} - \frac{2}{9}(p-1)X + X^2 = 0 \qquad (4.4.9)$$

(We will get original variables from the scaled one by putting $x = (9/2p)X$, and $t = \tau/3$)

Let us put $\nu = 2/3$ and $\lambda = 2(p-1)/9$

Then we get from (4.4.9)

$$\frac{d^3X}{d\tau^3} + \frac{d^2X}{d\tau^2} + \nu\frac{dX}{d\tau} - \lambda X + X^2 = 0 \qquad (4.4.10)$$

Writing (4.4.10) as three autonomous first order equations,

$$\left.\begin{aligned} \dot{X}_1 &= X_2 \\ \dot{X}_2 &= X_3 \\ \dot{X}_3 &= -X_3 - \nu X_2 + \lambda X_1 - X_1^2 \end{aligned}\right\} \qquad (4.4.11)$$

Equations similar to (4.4.11) were studied by Coulett et al,[71] and Arneodo et al [72] and they observed regular as well as chaotic behaviour for different parameter values.

In our system of equations (4.4.11) we observed regular, chaos and no solution regions in the parameter space (ν,λ) or (ν, p) [73].

In figure (4.4.1) we have the bifurcation diagram for ν =2/3 which shows reverse bifurcation as the parameter λ or p is varied. For ν =0.7 (fig.4.4.2) and 0.71 (fig.4.4.3) also reverse bifurcation is seen. But for ν=0.71 we could see region where no solution is obtained (for 6.5< p < 7.0). Around this value, our numerical algorithm fails to give bounded solution and we get an unstable region. In fig.4.4.4. we have a plot for ν = 0.8 which shows period doubling root to chaos. Unstable region is seen in this case also and after this region suddenly chaos occur and the reverse bifurcation is seen afterwards.

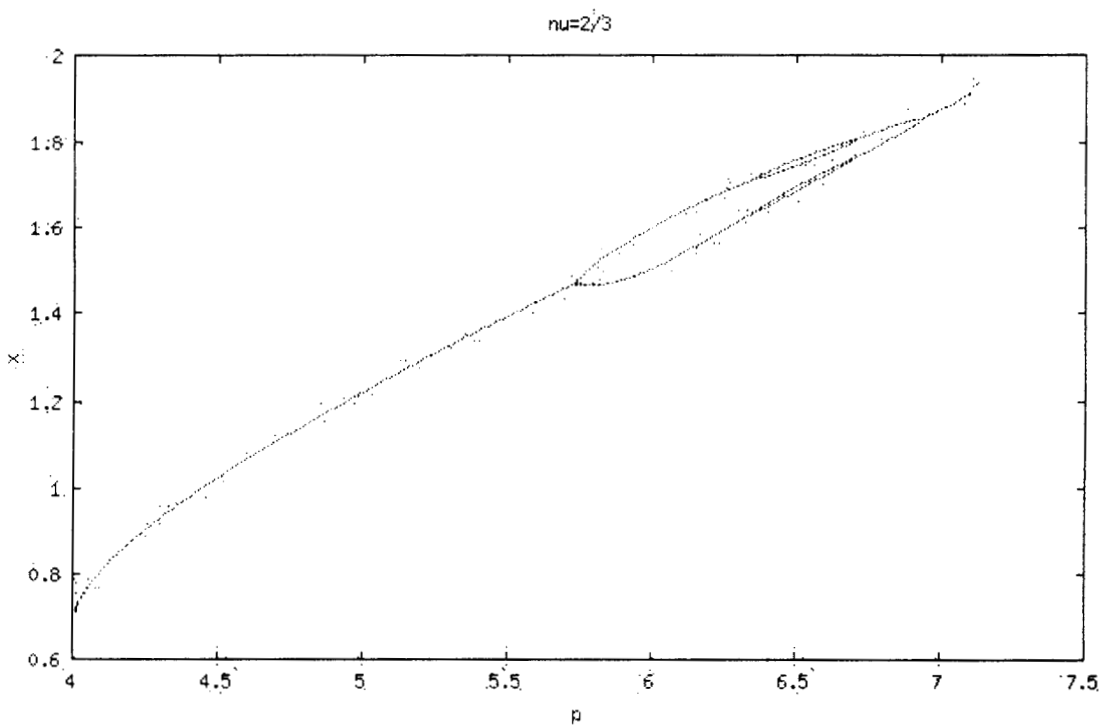

Fig.4.4.1. The bifurcation diagram for the equation (4.4.11) for different values of p or λ and for ν =2/3

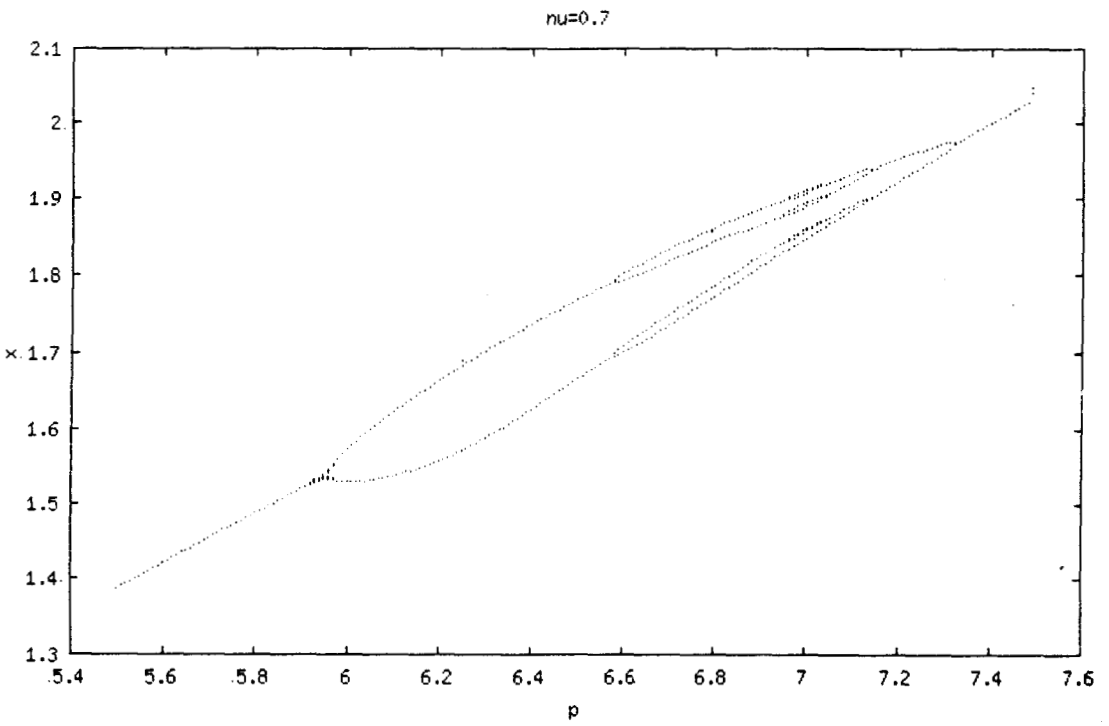

Fig.4.4.2. The bifurcation diagram for the equation (4.4.11) for different values of p or λ and for ν =0.7

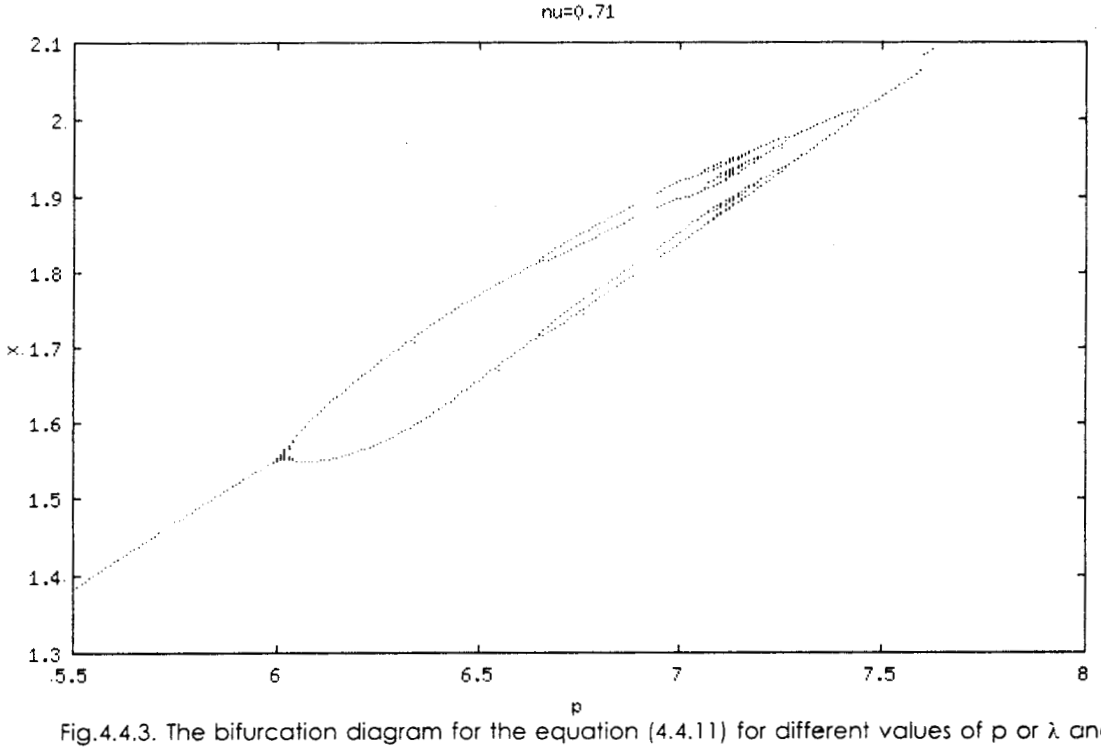

Fig.4.4.3. The bifurcation diagram for the equation (4.4.11) for different values of p or λ and for ν =0.71

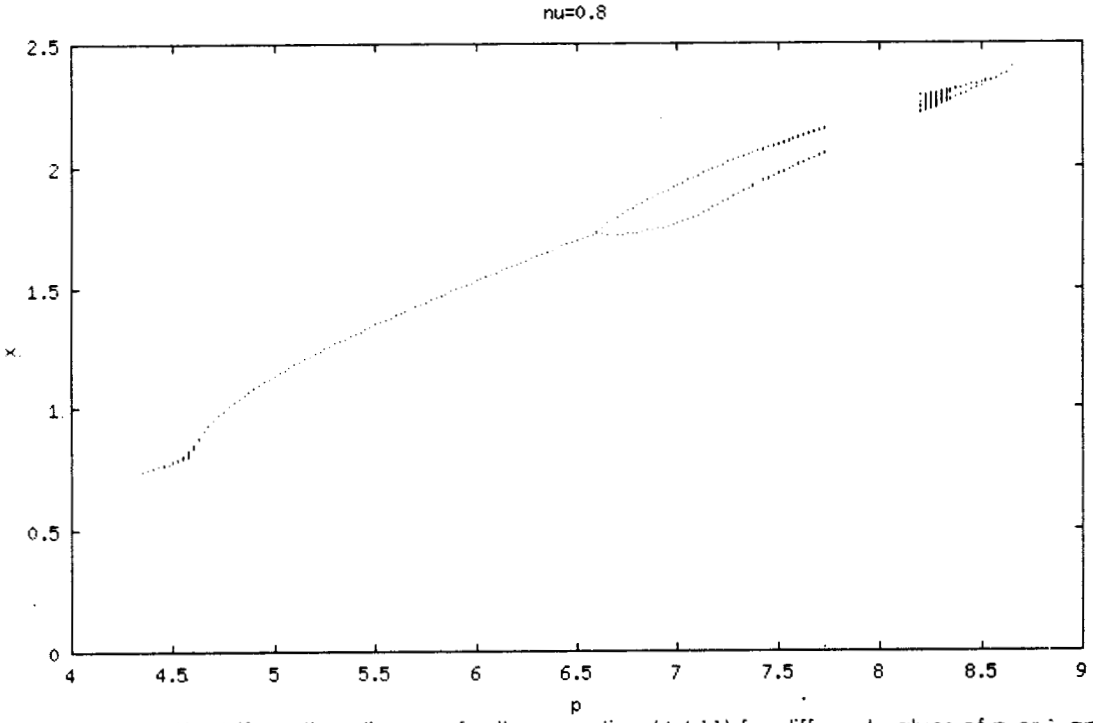

Fig.4.4.4a. The bifurcation diagram for the equation (4.4.11) for different values of p or λ and for ν =0.8

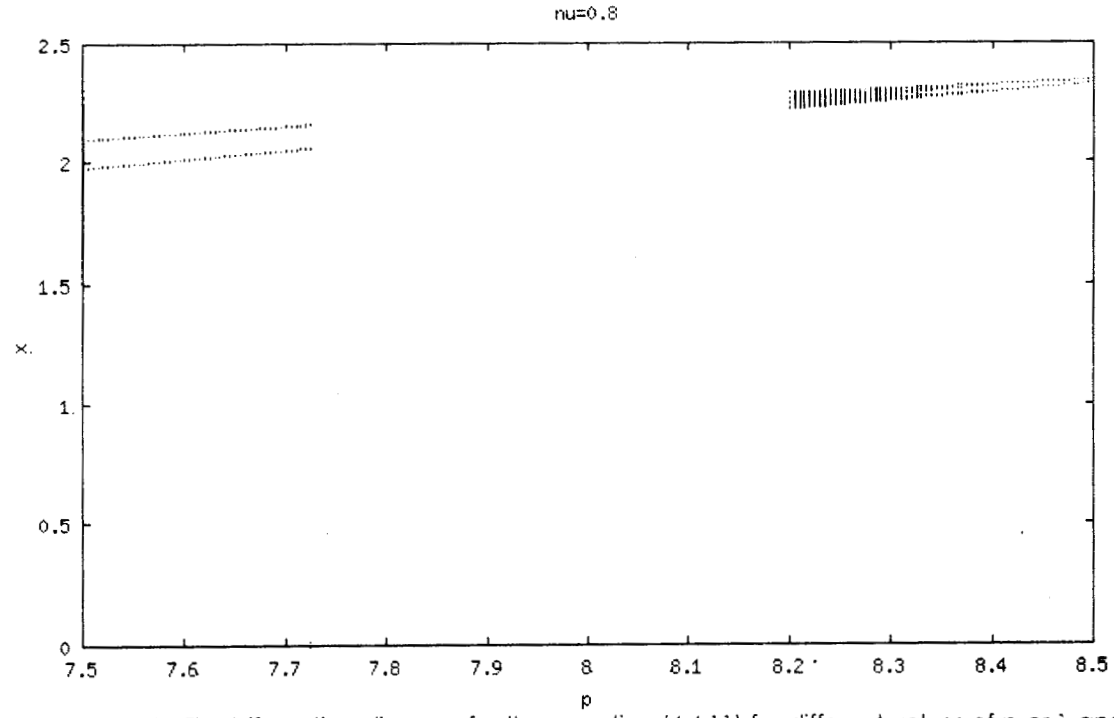

Fig.4.4.4b. The bifurcation diagram for the equation (4.4.11) for different values of p or λ and for ν =0.8 (expanded version of a part from fig.4.4.4a.)

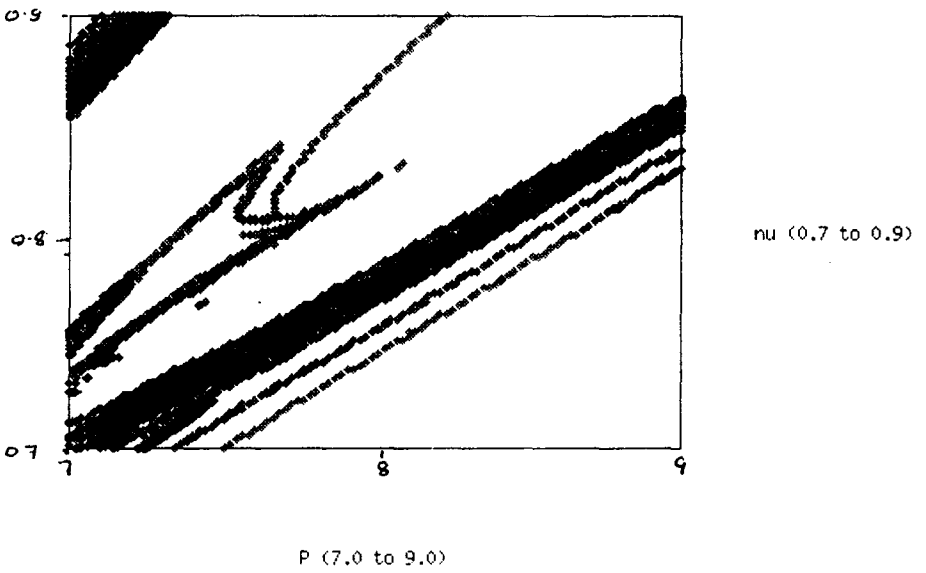

Fig.4.4.5. The plot of peaks in p-ν plane for equation (4.4.10). Along X-axis we have plotted p which range from 7 to 9 (or λ, 1.33333 to 1.77778) and along Y-axis ν, ranges from 0.7 to 0.9 .

The plot of number of peaks for different values of p (or λ) and ν shows that the parameter space is rich in different dynamical properties. The darker regions represent chaotic or periodic solutions and the light (white) region represent unstable or steady state solutions. The situation here is like cases reported earlier with riddled parameters [55].

4.5. Truncated for fourth order (i.e., when N=4).

Equation (4.1.5) becomes (for N=4),

$$\frac{1}{4!}\frac{d^4x}{dt^4}+\frac{1}{3!}\frac{d^3x}{dt^3}+\frac{1}{2!}\frac{d^2x}{dt^2}+\frac{dx}{dt}+x=f(x) \tag{4.5.1}$$

$$\frac{d^4x}{dt^4}+4\frac{d^3x}{dt^3}+12\frac{d^2x}{dt^2}+24\frac{dx}{dt}+24(x-f(x))=0 \tag{4.5.2}$$

If we put f(x)=px(1-x), the logistic equation, (4.5.2) becomes,

$$\frac{d^4x}{dt^4}+4\frac{d^3x}{dt^3}+12\frac{d^2x}{dt^2}+24\frac{dx}{dt}+24((1-p)x+px^2)=0 \tag{4.5.3}$$

Let us rescale (4.5.3) by putting x=X and t=bτ. Then we get,

$$\frac{d^4X}{d\tau^4}+4b\frac{d^3X}{d\tau^3}+12b^2\frac{d^2X}{d\tau^2}+24b^3\frac{dX}{d\tau}-24(p-1)b^4X+24pb^4X^2=0$$

We put b=1/4 and 24 pb^4 = 1, Then we get

$$\frac{d^4X}{d\tau^4}+\frac{d^3X}{d\tau^3}+\alpha\frac{d^2X}{d\tau^2}+\frac{3}{8}\frac{dX}{d\tau}-\beta X+X^2=0 \tag{4.5.4}$$

where $\beta=\frac{3}{32}(p-1)$ *or* $p=1+\frac{32}{3}\beta$, α = ¾.

To apply Routh-Hurwitz theorem, we put

$a_0=1, a_1=1, a_2=\alpha, a_3=3/8, a_4=b'$

Then $T_0=a_0=1>0. T_1=a_1=1>0. T_2=\begin{bmatrix} a_1 & a_0 \\ a_3 & a_2 \end{bmatrix}=\begin{vmatrix} 1 & 1 \\ \frac{3}{8} & \alpha \end{vmatrix}=\alpha-\frac{3}{8}$

If α <3/8 then T_2 < 0 (change of sign). Then the fixed points are unstable. For α > 3/8 we try more terms.

$$T_3=\begin{bmatrix} a_1 & a_0 & 0 \\ a_3 & a_2 & a_1 \\ a_5 & a_4 & a_3 \end{bmatrix}=\begin{vmatrix} 1 & 1 & 0 \\ \frac{3}{8} & \alpha & 1 \\ 0 & b' & \frac{3}{8} \end{vmatrix}=\frac{3}{8}\alpha-b'-\frac{9}{64}$$

Let b' =β. If $T_3 = \frac{3}{8}\alpha - \beta - \frac{9}{64} < 0$, then the system of equation is unstable. For stable solutions $\frac{3}{8}\alpha - \beta - \frac{9}{64} > 0 \quad or \quad \frac{3}{8}\alpha - \frac{9}{64} > \beta$

$$\frac{3}{8}\alpha - \frac{9}{64} > \frac{3}{32}(p-1) \quad .4\alpha - \frac{3}{2} > p-1 \quad or \quad p < 4\alpha - \frac{1}{2} .$$

That is the system of equations (4.5.4) have stable solution only for $\alpha > 3/8$ and $p < 4\alpha - 1/2$. The plot of β versus α shows that there are points with stable solutions (possibly with chaos also) along a line defined by $p < 4\alpha - \frac{1}{2}$. The dark points in the plot are either chaotic or periodic points. (fig. 4.5.1)

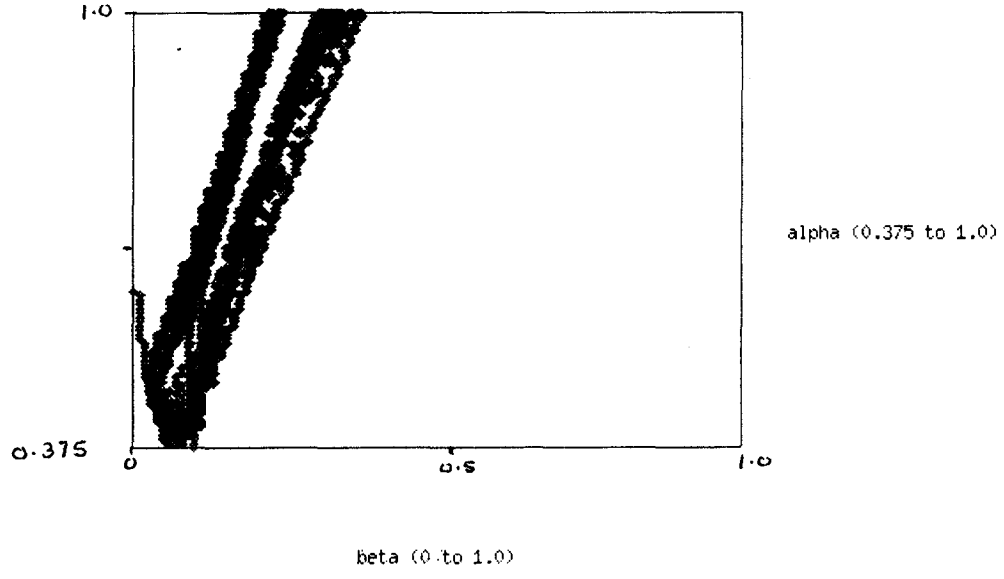

Fig.4.5.1. The plot of peaks in the β - α plane for equation (4.5.4). Along the X-axis we have plotted β which ranges from 0.0 to 1.0 and along y-axis, α which ranges from 0.375(3/8) to 1.0.

In the above plot the dark region represents either periodic or chaotic points and in between and on either side of these points we have regions which give unstable or

steady state solutions (white region). The situation here corresponds to riddled parameter space reported in [55].

Here we get entirely different bahaviour than the map itself, for the corresponding differential equation. Also the function x(t) is not real anlytic, since the truncated Taylor series does not approach the function as order of truncation increases.

CHAPTER 5

CONCLUSIONS

The principal and new findings of the thesis are briefly summarized below.

- We have proposed a new model describing the dynamics of a charged particle in a medium with dielectric discontinuity.
- Even without an external field, we get chaos in our model. The characterization of chaos has been done using time series analysis, Poincare section, power spectrum etc. The model, which is a Hamiltonian system, shows regular as well as chaotic behaviour for different parameter values and initial conditions. We observe that for the parameters δ = 3 and L=0.3 and for initial conditions 0.23,0.18,0.1,0.1, the system becomes chaotic and for initial conditions 2.5,12.0, 0.3842077627766117, 0.0 it shows regular behaviour. This type of behaviour is a common feature of Hamiltonian systems. The phase space dynamics of Hamiltonian systems show regular as well as chaotic behaviour for different initial conditions.
- We have used Bohmian mechanics formalism as a good tool for characterizing, classically chaotic Hamiltonian systems.
- We have developed a new and efficient algorithm to calculate the Bohmian trajectory, and the guiding quantum mechanical wave trajectory. In Bohmian frame work we can define a trajectory which is not possible in usual quantum mechanical calculations. The sensitive dependence on initial conditions, which is the characterizing feature of a chaotic system, can be realized in these calculations. The exponential divergence of the trajectories also is demonstrated in our calculation.
- We find that even for a Hamiltonian system with no explicit time dependence, the energy fluctuations are large, when the dynamics is chaotic. This is attributed

to the rapid spatial variations of wave function, which causes fluctuations in the energy calculated by numerical integration (using Simpson's rule).

- In chapter 4 we discuss the connection between a map and the differential equation. We find that Taylor series of a function show much difference from the function itself, for a finite order truncation. The series represent the original function only if the terms in the series are infinity. We have proved, in general, for an order of truncation greater than or equal to 5, the series corresponding to any function becomes unstable in the neighbour hood of the reference point. For an order of truncation 1 and 2 we cannot expect any chaos, because it does not satisfy the minimum dimensionality condition for getting chaos. For an order of truncation 3 and 4 we study for a special case of the series expansion of logistic map. The truncated series is found to behave differently from the original map considered. We observe no chaos in the system up to the parameter value p=4, which is the maximum value possible for a logistic map. Above this value, we get period doubling, chaos, reverse bifurcation etc. By a simple transformation of the equation we made the system a two parameter one. This transformed equation shows still interesting features such as riddled parameter space, which is an indication of structural instability.

The future work which can be done and not attempted by us in this thesis are,

- In the classical analysis, the Poincare return time for chaotic and regular motion seems to be different. Further study is needed to confirm this for a Hamiltonian system.
- The work can be extended to a charged particle moving in a dielectric medium sandwiched between two dielectrics.
- In the Bohmian mechanics, the fluctuation in energy seems to be a characteristic property of chaotic motion, even though in the physical situation,

the energy is conserved. This fluctuation is attributed to the spatial variations in the wave function, which causes an error in numerical integration. This has to be investigated further.

APPENDIX.

The QR algorithm for calculation of lyapunov Exponents.

The method of calculation of Lyapunov exponents using QR algorithm is given briefly below,

Consider an n-dimensional continuous time dynamical system

$$\frac{dZ}{dt} = F(Z,t) \tag{A.1}$$

where Z and F are n-dimensional vector fields. To determine the n Lyapunov exponents of the system, corresponding to some initial condition Z(o), we have to find the long term evolution of the axes of an infinitesimal sphere of states around Z(0). For this purpose, consider the tangent map given by the set of equations,

$$\frac{d\delta Z}{dt} = J.\delta Z \tag{A.2}$$

where J is the n×n Jacobian matrix with

$$J_{ij} = \frac{\partial F_i}{\partial Z_j} \tag{A.3}$$

A solution of (A.2) can be formally written as

$$\delta Z(t) = M\,(Z(t),t)\,\delta Z(0) \tag{A.4}$$

Where M (Z(t),t) is the tangent map whose evolution equation is easily seen to be

$$\frac{dM}{dt} = J \cdot M \tag{A.5}$$

Let Λ be an n×n matrix given by $\Lambda = \lim_{t\to\infty} (MM^T)^{1/2t}$, where M^T denotes the matrix transpose of M. The Lyapunov exponents then equal the logarithm of the eigen values of Λ [74].

In the standard method, one first chooses n orthogonal tangent vectors as initial conditions for (A.2). These vectors are orthonormalized using the Gram-Schmidt Reorthonormalization (GSR) procedure at discrete steps. Then n Lyapunov exponents are

determined from the rates of growth of these vectors. An explicit source code for the computation based on this procedure is given in [33]. In this method we have to integrate n(n+1) coupled equations, as there are n equations for the fiducial trajectory in (A.1) and n copies of the tangent map equations in (A.2).

The algorithm developed by Rangarajan et al.[34] evaluate the Lyapunov exponents without using the vectors δZ directly and consequently without using the associated reorthogonalization and rescaling. For this, one exploits the fact that M can be written as M = QR, a product of an orthogonal n×n matrix Q and an upper triangular matrix R with positive diagonal entries.

Substituting this in (A.5) we get

$$\dot{Q}R + Q\dot{R} = JQR \tag{A.6}$$

where the overdot denotes a time derivative. Multiplying the above equation by Q^T from left and R^{-1} from the right, we get

$$Q^T\dot{Q} + \dot{R}R^{-1} = Q^T JQ \tag{A.7}$$

here $Q^T\dot{Q}$ is a skew(anti)-symmetric matrix for any orthogonal matrix Q and $\dot{R}R^{-1}$ is still an upper triangular matrix.

The orthogonal matrix Q can be represented by the product of n(n-1)/2 orthogonal matrices, each of which corresponds to a simple rotation in the $(i - j)^{th}$ plane (i < j). Hence Q is parametrized by n(n-1)/2 angles which we denote by θ_i (i=1,2,....n(n-1)/2). These angles will be collectively denoted by θ.

And the upper triangular matrix R can be represented by (since it has positive diagonal entries)

$$R = \begin{bmatrix} e^{\lambda_1} & r_{12} & . & . & r_{1n} \\ 0 & e^{\lambda_2} & r_{23} & . & r_{2n} \\ 0 & 0 & e^{\lambda_3} & . & r_{3n} \\ . & . & . & . & . \\ 0 & 0 & . & . & e^{\lambda_n} \end{bmatrix} \qquad \text{(A.8)}$$

The quantities λ_i are closely related to the Lyapunov exponents.

Now (A.7) can be written as

$$\begin{bmatrix} \dot{\lambda}_1 & r''_{12} & . & . & r''_{1n} \\ f_1(\dot{\theta}) & \dot{\lambda}_2 & r''_{23} & . & r''_{2n} \\ . & . & . & . & . \\ . & . & . & . & . \\ f_{n-1}(\dot{\theta}) & . & . & f_{n(n-1)/2}(\dot{\theta}) & \dot{\lambda}_n \end{bmatrix} = Q^t \dot{J} Q \qquad \text{(A.9)}$$

Denoting the matrix $Q^T\dot{J}Q$ as S and comparing the diagonal elements on both sides of (A.9) we get

$$\dot{\lambda}_i = S_{ii}, i = 1.2.3.....n \qquad \text{(A.10)}$$

The Lyapunov exponents are equal to λ_i/t in the limit $t \to \infty$ [34]. In this method to solve for the first m Lyapunov exponents, one has to solve m(2n-m+1)/2 equations which is always less than n(n+1)/2 (the total number of equations) for m < n. So this method seems to be computationally more efficient than the standard or other methods.

References:

1. Hao Bai- Lin, *Chaos*, World Scientific, Singapore, 1985
2. S.Ushiki, *Chaotic Dynamical System*, World Scientific, Singapore, 1992
3. Bountis, *Chaotic Dynamics*, Plenum Press, New York, 1992
4. Leo P. Kadanoff, *From order to Chaos*, World Scientific, Singapore, 1993
5. Thomas Kapitanaih, *Controlling Chaos*, Academic Press 1996
6. Cvitanovic P, (Ed.), *Universality in Chaos*, Adam Hilger, Bristol, 1989.
7. R.M. May, *Simple mathematical models with very complicated dynamics*, Nature **261**,(1976) 459.
8. E.N. Lorenz, Universal behaviour in Nonlinear systems J.Atmos. Sci. **20**, (1963) 130
9. D. Ruelle , *Strange Attractors* Math. Intelligencer 2,(1980)126.
10. M.J. Fegenbaum, *Universal behaviour in non-linear systems* Los Almos Science**1**, (1980)4.
11. J.P. Eckmann, *Roads to turbulence in dissipative dynamical systems*, Rev. Mod. Phys. **53**, (1981)643.
12. A. Libchaber and J. Maurer, *A Rayleigh-Benard experiment- Helium in a small box.* Proc. Of NATO Advanced studies Institute on Nonlinear Phenomena at Phase Transitions and Instabilities, (1982) 259.
13. A. Libchaber, C. Larocha and S. Fauve, *Period doubling cascade in mercury, a quantitative measurement*, J.Phys.Lett. **43**, (1982)L211.
14. J P. Gollub and H.L. Swinney, *Onset of turbulence in a rotating fluid*, Phys.Rev.Lett. **35**, (1975) 927.
15. M. Giglio S. Musazzi and U. Perini, *Transitions to Chaotic behaviour via a reproducible sequence of period doubling bifurcations*, Phys.Rev.Lett. **47**,(1981)243.
16. P. Berge,M. Duboise,P. Manneville and Y. Pameaue, *Intermittency in Rayleigh-Benard convection*, J.Phys.Lett. **41**, (1980) L341.

17. J.L. Hudson and J.C. Mankin, *Chaos in the Belouzov-Zhabotinskii reaction*, J.Chem.Phys. **74**,1 (1981) 617.

18. Y. Pameau,J.C. Roux,A. Rossi, S. Bachelart and C. Vidal, *Intermittent behaviour in the Belouzov-Zhabotinskii reaction*, J.Phys.Lett. **42**, (1981) L271.

19. J. Testa, J. Perez and C. Jeffries, *Evidence for universal chaotic behaviour of a driven non-linear oscillator*, Phys.Rev.Lett. **48** ,(1982) 714.

20. M.R. Guevera,L. Glass and A. Shrier, *Phase locking, Period-doubling bifurcations, and irregular dynamics in periodically stimulated cardic cells*, Science **214**,(1981) 1350.

21. M.C. Valsakumar, S.V.M. Sathyanarayana and V. Sreedhar, *Signature of chaos in power spectrum*, Pramana **48**(1997)69.

22. Eward Ott - *Chaos in Dynamical Systems*, Cambridge University Press,1993.

23. Takeuchi Y. *Global Dynamical Properties of Lotka-Volterra System*. World Scientific, Singapore (1996).

24. M. Henon, *A two-Dimensional Mapping with a strange Attractor*, Communications in Math. Phys. **50** (1976) 69.

25. George M. Zaslavsky, *Physics of chaos in Hamiltonian systems*, Imperial College Press, 1998.

26. Henon M. and C. Heils, *The Applicability of the third integral of motion, some numerical experiments*, Astron. J. **69**(1964)73.

27. Hellman R.H.G., *Self Generated Chaotic behaviour in nonlinear mechanics*. in Fundamental problems in Statistical Mechanics. Vol.**5** (Ed. E.G.D. Cohen),(1980),165

28. M. C. Gutzwiller, *Chaos in Classical and Quantum Mechanics* Springer-Verlag, Berlin, 1990

29. K. Ganeshan and K. T. Taylor, *Rydberg states of the Hydrogen atom near a metal surface*. *J .Phys.***B29** (1996) 1293.

30. K. Ganesan and R. Gabarowski, *Chaos in hydrogen atom interacting with external*

*fields, Pramana, J.Phys.***48** (1997) 379.

31. Rajan Nambiar A., Valsakumar M.C. and Rameshan P. *Choas in Charged Particle motion in a medium with dielectric discontinuity*. Proceeding of !3th Kerala Science Congress, January 2001., Thrissur. Pp.97-99.
32. Fawwas T. Ulaby, *Applied Electromagnetics*, Prentice Hall Intl. Inc. (1997).
33. A. Wolf, J. B. Swift, H. L. Swinny and J. A. Vasatano, *Determining Lyapunov exponents from a time series, Physica* **16D** (1985) 285
34. G. Rangarajan, S. Habib and R. D. Ryne, *Lyapunov exponents without Rescaling and Reorthonormalization, Phys. Rev. Lett.* **80** (1998) 3747
35. Robert Gilmore, *Topological Analysis of Chaotic dynamical Systems*, Rev. of Mod. Phys. **70**(1998)1455
36. M. C. Vaisakumar, S. V. M. Sathyanarayana and V. Sreedhar, *Signature of chaos in power spectrum*, Pramana **48**(1997)69.
37. H. G. Schuster, *Deterministic Chaos- An Introduction (3rd edition*, Wiley, New York(1995).
38. McDonald S. W., and Kaufmann, A. N., *Spectrum and eigenfunctions for a Hamiltonian with stochastic trajectories*. Phys. Rev. Lett. 42,1189(1979).
39. Berry M. V., and Tabor M., *Level clustering in the Regular spectrum*, Proc. Roy. Soc. (London) A356, **375** (1977).
40. Berry M. V., in R. H. G. Hellman and G.Ioos (eds.), *Chaotic behaviour of Deterministic systems.*, Les Hauches Summer School 1981, North- Holland, Amsterdam.(1983).
41. Bohigas O., Giannoni, M. J., and Schmit, C., *Characterization of chaotic Quantum Spectra and Universality of Level Fluctuation laws.*, Phys. Rev. Lett. **52**, 1 (1984).
42. Zaslavsky G. M., *Stochasticity in Quantum systems.*, Phys. Rep. 80, **157** (1981).
43. David Bohm, *Quantum Theory*, Prentice-Hall, Inc., Englewood Cliffs, N.J. (1951).

44. P. R. Holland, *The quantum theory of motion*, Cambridge Univ. Press, Cambridge, (1993).

45. Bohm D., Physical Rev. **85**, (1952 a) 167.

46. Bohm D., Physical Rev. **85**, (1952 b) 180.

47. R. H. Parmenter and R. W. Valentine, *Deterministic chaos and causal interpretation of quantum mechanics*, Phys. Lett. A **201** (1995) 1.

48. Guglielmo Iacomelli and Marco Pettini, *Regular and chaotic quantum motions*, Phys. Lett. A **212** (1996) 29.

49. C. Dewdney and Z. Malik, *Measurement, decoherence and chaos in quantumpinball*, Phys. Lett. A **220** (1996)183.

50. R. H. Parmenter and R. W. Valentine, *Chaotic causal trajectories associated with a single stationary state of a system of noninteracting particles*, Phys. Lett. A **227** (1997) 5.

51. Adam J. Makowski and Michal Frackowiak, *The simplest non-trivial model of chaotic causal dynamics*, ACTA PHYSICA POLONICA B **32** (2001) 2831.

52. Sengupta S. and Chattaraj P. K., *The quantum theory of motion and signature of chaos in the quantum behaviour of a classically chaotic system.*, Physics Lett. A **215** (1996) 119

53. Valsakumar M. C., Rajan Nambiar A and Rameshan P. (under preperation).

54. Rajan Nambiar A., Valsakumar M. C. and Rameshan P. (under preparation)

55. Ying-cheng Lai and Raimond L. Winslow., *Riddled Parameter Space in Spatiotemperal Chaotic Dynamical systems.*, Phys. Rev. Lett. **72** (1994)1640.

56. Yu L. Maistrenko, V. L. Maistrenko, O. Popovych and E. Mosekilde, *Desynchronization of chaos in coupled logistic maps*. Physical Review E, **60**(1999)2817.

57. Mathias Woltering and Mario Markus, *Riddled-like Basins of Transient Chaos.*,Phys. Rev. Lett. **84**(2000)630.

58. H. L. Yang, *One-side riddled basin below and beyond the blowout bifurcation*, Physical Review E, **62**(2000)R4509.

59. Yang-Cheng lai, *Catastrophe of riddling*, Physical review E, **62**(2000)R4505.

60. Tomasz Kapitaniak, Yuri Maistrenko and Svitlana Popovych, *Chaos-hyperchaos transition*, Physical review E, **62**(2000)1972.

61. Sang-Toon Kim and Woochang Lim, *Mechanism for the riddling transition in coupled chaotic systems*, Physical Review E, **63**(2001)026217-1 to 7.

62. A. Krawiecki and S. Matyjaskiewicz, *Blowout bifurcation and stability of marginal synchronization of chaos*, Physical Review E, **64**(2001)036216-1 to 7.

63. Bernard Cazelles, *Blowout bifurcation with non-normal parameters in population dynamics*, Physical review E,**64**(2001)032901-1 to 3.

64. Ying-Cheng Lai and Victor Andrade, *Catastrophic bifurcation from riddled to fractal basins*, Physical Review E, **64**(2001)056228-1 to 16.

65. Alaxander B. madvinsky et al, *Patchy environment as a factor of complex plankton dynamics*, Physical Review E, **64**(2001)021915-1 to 7.

66. H. L. Yang, *Milnor strange non chaotic attractor with complex basin of attraction*,Physical review E, **63**(2001)036208-1 to 4.

67. Zang Fu and Jack Heidel, *Non-chaotic behaviour in three dimensional quadratic systems*, Nonlinearity, **10** (1997) 1289.

68. J. C. Sprott, *Some simple chaotic flows*, Phys. Rev. E, **50** (1994) R647.

69. J. C. Sprott, *Some simplest dissipative chaotic flow*, Phys. Lett. A, **228** (1997) 271.

70. Jack Heidel and Zang Fu, *Non chaotic behaviour in 3-D quadratic systems. II Conservative case*. Nonlinearity ,**12** (1999) 617.

71. P. Coulett, C. Tresser and A. Arneodo, *Transition to Stochasticity for a class of Forced oscillators*, Phys. Lett., **72** A (1979) 268.

72. A. Arneodo, P. H. Coulett, E. A. Spiegel and C. Tresser, *Assymtotic chaos.*, Physica D,

14(1985) 327.

73. Valsakumar M. C., Rajan Nambiar A. and Rameshan P., (under preparation.)

74. J. P. Eckman and D. Ruelle, Rev. Mod. Phys. **57**, (1995)617.

Conferences attended.

1. International Conference on Perspectives in Theoretical Physics, jan., 2001, P.R.L. Ahmedabad, India.
2. Kerala Science Congress, Jan 2001, Thrissur, Kerala.
3. National Seminar on Chaos and Fractals: Applications, Jan. 2002, Rajagiri School of Engineering & Technology, Kochi.

NB4536